

## Depositional Aspects of Pollutant Behavior in Fog and Intercepted Clouds

Jed M. Waldman<sup>1</sup> and Michael R. Hoffmann<sup>2</sup>

Environmental Engineering Science, W. M. Keck Laboratories, California Institute of Technology, Pasadena, CA 91125

*Droplet deposition during fog is shown to play an important role in the removal of anthropogenic pollutants from the atmosphere. Relevant theoretical principles are reviewed. The in-cloud scavenging of aerosols and soluble gases coupled with the small size of fog droplets results in higher chemical concentrations in fog water than in rainwater. In the urban regions of southern California and the southern San Joaquin Valley, fog water chemistry is dominated by sulfate, nitrate, and ammonium ions, which are measured at millimolar levels. The formation of fog is shown to accelerate deposition rates for water-scavenged atmospheric constituents. During stagnation episodes, pollutant removal by ventilation of valley air requires at least 5 days, while the enhancement of deposition by fog formation leads to pollutant lifetimes on the order of 6–12 h. Thus, in an environment characterized by flat, open landscape and low wind speed, droplet sedimentation can be the dominant removal mechanism of pollutants during prolonged stagnation episodes with fog.*

**T**HE REMOVAL OF ANTHROPOGENIC EMISSIONS and windblown material to ground surfaces occurs by processes known as wet and dry deposition. The deposition of airborne pollutants is essential for cleansing the

<sup>1</sup>Current address: Environmental and Community Medicine, University of Medicine & Dentistry of New Jersey—Robert Wood Johnson Medical School, Piscataway, NJ 08854

<sup>2</sup>To whom correspondence should be addressed

atmosphere, but some deposited pollutants may have the potential for significant environmental impact when they reach the surface. Key deposition pathways are shown schematically in Figure 1.

Scavenging and deposition of ambient gases and aerosols by raindrops is more rapid and efficient than removal under dry conditions. However, precipitation is an intermittent event. The dry flux of pollutants due to the cumulative effect of long dry periods may contribute a greater mass of material than rainfall. Liljestrand (1) found this situation to be the case in southern California. A small fraction of total  $\text{NO}_x$  and  $\text{SO}_2$  emissions in the region was accounted for by wet deposition monitoring; Liljestrand estimated a 10-fold greater removal by dry versus wet deposition, and the majority of emissions was advected away from the region. In contrast, the net deposition in the eastern United States has been associated primarily with precipitation. Bischoff et al. (2) have estimated that wet fluxes constitute 75% of  $\text{SO}_2$  and more than 90% of  $\text{NO}_x$  emissions.

In addition, the potential exists for appreciable deposition during fog episodes. Even though the occurrence of fog is often infrequent, fog-induced deposition may be important in several specific environments. In coastal regions, fogs often serve as a dominant source of moisture and nutrient input to local ecosystems (3). Similarly, many mountainous regions are frequently intercepted by clouds and the accompanying chemical input (4). Urban areas, subject to higher ambient pollutant concentrations, may have substantial fog-induced deposition as well.

In many respects, fog is simply a ground-level cloud in which processes such as nucleation, gas scavenging, and droplet growth are important. At the same time, fogs consist of discrete water droplets, and sedimentation and inertial impaction are dominant transport mechanisms because of the relatively large sizes of these particles. However, because fog droplets may change size continually, their transport behavior may be altered.

Fog may make important contributions to pollutant deposition or impacts in selected environments for the following reasons:

(1) Fog and cloud droplets are important chemical reactors (5) that can modify the nature of pollutant material in the atmosphere (6). They act as sinks for many gaseous pollutants such as nitric acid, ammonia, and sulfur dioxide that are appreciably soluble in aqueous solutions. Fog and cloud droplets are sufficiently small such that gas scavenging is not limited by mass transport in most cases (7). Their effect on pollutant speciation, in turn, will have impacts on the chemical balance of depositing components.

(2) Under dry conditions, much of the aerosol mass of pollutant species is found in the size range 0.1-1.0- $\mu\text{m}$  diameter. Deposition velocities ( $V_d$ ) of these small particles are extremely low (8). Scavenging of

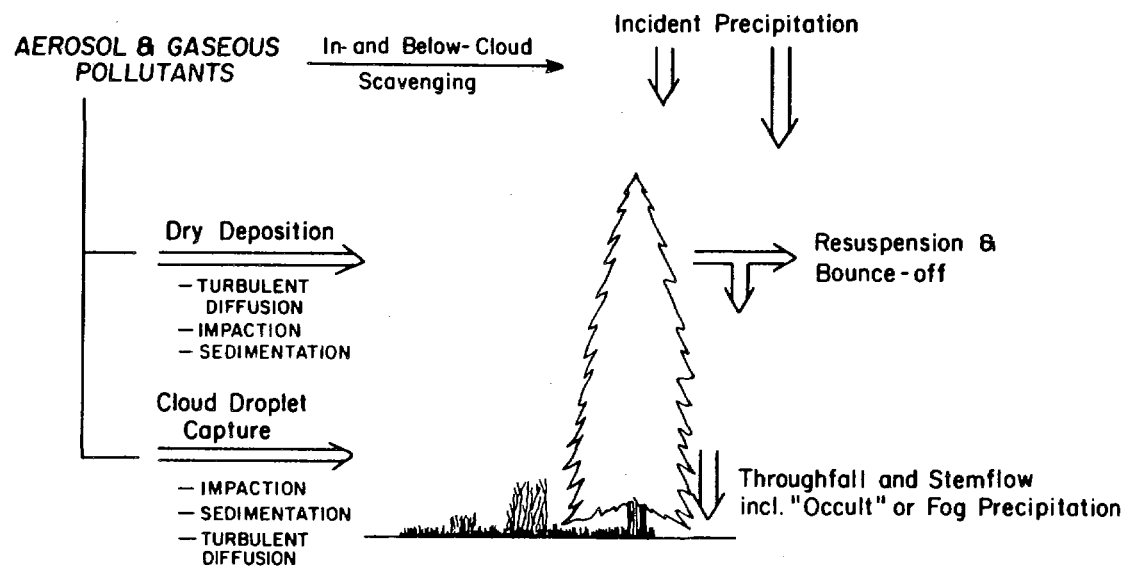


Figure 1. Pathways for pollutant deposition.

ambient aerosols by fog droplets leads to the association of solute mass with larger sized particles. Hence, when dissolved in fog droplets, solute species are more efficiently deposited by particle impaction and sedimentation.

(3) Surface moisture deposited by fog and dew can significantly increase the  $V_d$  of aerosols by reducing rebound and resuspension (9). In addition, moisture on surfaces also serves as a sink for soluble gases (10).

(4) The capture of fog droplets by foliar and ground surfaces can be a significant component of the water and nutrient fluxes to an ecosystem (3, 4). Lovett (11) reported water flux at rates of 0.1–0.3 mm h<sup>-1</sup> from advected clouds to a subalpine forest canopy. This range agreed with his numerical model, which indicated that sedimentation and inertial impaction, especially to the upper 3 m of the canopy, were the dominant deposition mechanisms.

(5) The analyses of fog and cloud water show at least an order-of-magnitude greater concentration for ambient solutes compared with rainwater. Therefore, droplets can make a greater contribution to pollutant flux per volume of water deposition.

(6) Intercepted fog and drizzle wet surfaces but do not necessarily flush them clean as does rain. Dissolution of previously accumulated material can lead to concentrated solutions of acids (12) and metals (13) at collection surfaces. Waldman et al. (14) found that droplets, after depositing on pine needles, were in general more concentrated than ambient cloud water except when the needles had been previously rinsed by measurable rainfall. The acidity of drops removed from foliar surface was as high as the ambient cloud water despite enrichment with calcareous material.

(7) Damage to sensitive receptor surfaces, as measured in field and laboratory studies (15–17), has been caused by the exposure to acidic fog droplets.

### ***Theoretical Considerations of the Chemistry and Microphysics of Fog***

**Fog Microphysics.** Fog and cloud droplets are formed by condensation of water vapor in saturated air. Droplets form with diameters between 2 and 100  $\mu\text{m}$ , although in nonprecipitating clouds and fog, the majority of droplet mass occurs in the range of 5–30  $\mu\text{m}$ . In contrast, raindrops are far larger, mostly in the range of 200–2000  $\mu\text{m}$ . The mass of liquid water is typically 0.01–0.5 g m<sup>-3</sup>; the number concentration of droplets is generally ten to hundreds per cubic centimeter. Droplet interactions, such as coagulation or differential settling, have negligible impact on their dynamics except when intensive convection leads to rain or drizzle (18).

Vertical motions lead to the formation of most clouds with the exception of fogs. Generally, extensive ground contact suppresses net vertical motion. Fogs are primarily classified as either advection- or radiation-type, depending on their mechanism of formation (19). Advection fogs are formed by large-scale, horizontal air movement. For example, in the case of marine fogs, a warm, moist air mass comes in contact with a cooler surface. Radiation fog forms by radiative cooling near the ground to a clear, nighttime sky. This cooling causes an intense thermal gradient within the ground layer that may lead to fog or dew formation. Turbulent eddy transfer of momentum and heat play important roles under these conditions. A high level of turbulence inhibits fog (20), but some eddy mixing is essential to fog formation (21). Finally, fogs also occur on mountain slopes by the interception with a mesoscale cloud deck or fog formed locally by the upward sloping wind component.

The presence of condensation nuclei, which are composed of both soluble and nonsoluble material, is essential to the formation of atmospheric water droplets. The effects of surface tension and the chemical potential of the aquated solutes are important processes that raise and lower the saturation vapor pressure near the droplet surface, respectively. Accretion or evaporation of water to the condensation nucleus or droplet is forced by the difference between the ambient and local (i.e., surface) humidities. Droplet growth equations have been derived by coupling microscale heat and mass transfer at the aerosol surface (18). The principal terms depend on atmospheric relative humidity, droplet surface tension, and solute activity. Condensation caused by the radiative cooling of water droplets may also be an important factor in the dynamics of radiation fog (22).

During growth, the droplet temperature differs from the ambient because of latent heat release, which in turn depends upon the instantaneous growth rate. Hence, the complete growth-rate equation takes an implicit form; however, simplifying assumptions can be applied for all but the very smallest nuclei (18). The equation for rate of change in droplet diameter ( $D_o$ ) is

$$D_o \frac{dD_o}{dt} = \frac{S_v - a_w e^{(B)}}{C + E (A - 1) a_w e^{(B)}} \quad (1)$$

where  $t$  is time;  $S_v$  is the ambient water vapor saturation ratio;  $a_w$  is the activity of water in a droplet; and  $A$ ,  $B$ ,  $C$ , and  $E$  are constants defined in the appendix at the end of this chapter.

Families of curves can be deduced by solving the growth equation for the equilibrium condition  $dD_o/dt = 0$  at various saturation ratios for different dry aerosol masses. An example of these families, known as the

Köhler curves, is shown in Figure 2. The maxima occur at points known as the critical supersaturation,  $SS_{cr}$ , and activation size,  $D_{act}$ . When the ambient water vapor supersaturation,  $SS_e$ , is less than  $SS_{cr}$ , nuclei achieve stable equilibrium sizes ( $D_{eq} < D_{act}$ , where  $D_{eq}$  is the equilibrium diameter). When  $SS_e$  is sustained at values greater than  $SS_{cr}$ , droplets will form and continue to grow.

**Fog Chemistry.** The study of fog has traditionally remained in the domain of atmospheric physicists principally concerned with its effect on visibility or the mechanisms of formation analogous to clouds. Yet, even the data of early investigations of fog indicated that fog water can be highly concentrated with respect to a variety of chemical components (Table I). Cloud water, sampled aloft, has been found to exhibit similar composition, although not with the same extreme values (23-25). On the other hand, rainwater compositions when compared with fog water are found to be far more dilute. Fog droplets are approximately 100 times smaller than raindrops, which form partially by the further condensation of water vapor. Hence, fog droplets should be more concentrated in solute derived from the condensation nuclei. Furthermore, fog forms in the ground layer where gases and aerosols are most concentrated.

The higher aqueous concentrations and extremes in acidity found in fog water are reason for concern. Fog-derived inputs have the potential to add substantially to the burden of acid deposition caused by precipitation. This input contribution can be disproportional to the sum of additional moisture because of its higher concentrations. Perhaps more importantly, deleterious effects of fog deposition may be associated with the intensity of solution acidity. For instance, appreciable nutrient leaching (26) and damage to leaf tissue (16) have been noted with application of acid fogs or mists. Finally, a historical correlation of fog with the most severe air pollution episodes provides additional cause for concern (41). Identification of a link between urban fog events and human health injury was made even before detailed measurements of fog composition were performed (42).

**Fog Scavenging Processes.** Fog droplets are highly effective at scavenging ambient materials present in the air. The overall fraction incorporated into fog droplets depends upon two processes: nucleation scavenging (i.e., activation of aerosols) and gas dissolution. The speciation of pollutant components precursory to fog formation is therefore important. Furthermore, in situ chemical transformations may alter this speciation and the effectiveness of fog scavenging while the droplet phase is present.

The following notation has been adopted in this chapter: (C) is the

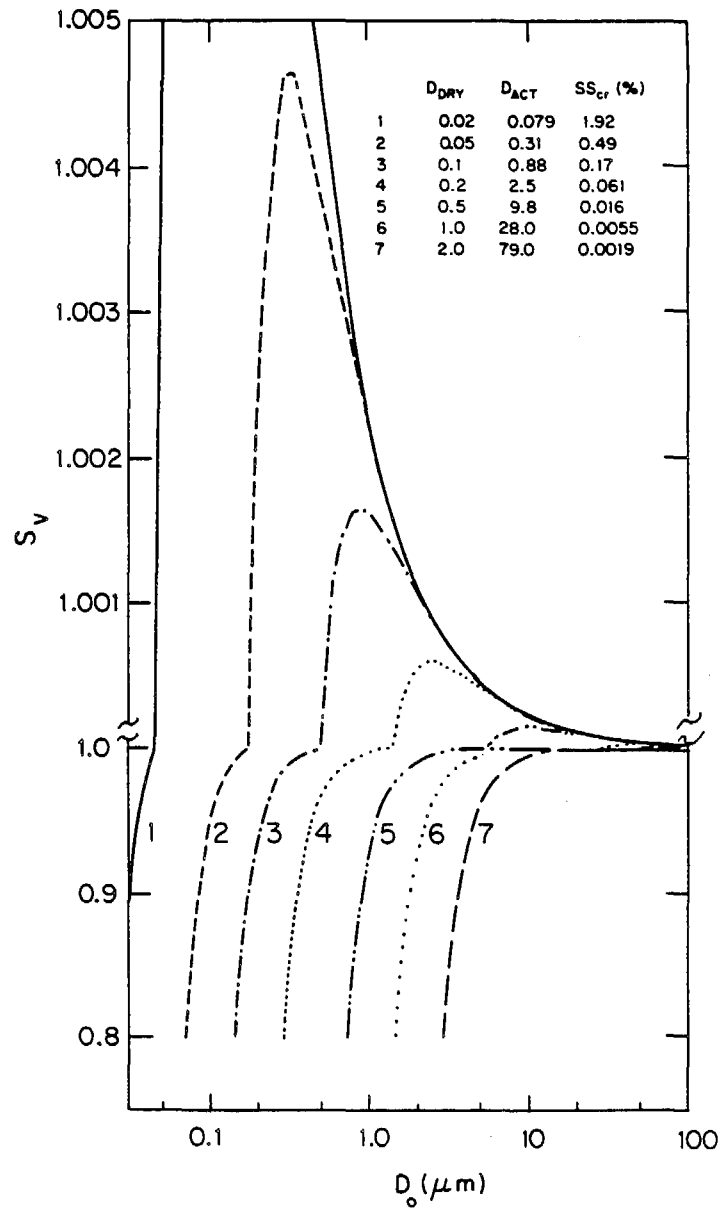


Figure 2. Equilibrium vapor pressure ( $S_v$ ) over aquated ammonium sulfate nuclei as a function of droplet diameter ( $D_0$ ). The dry diameter ( $D_{dry}$ ), activation diameter, ( $D_{act}$ ), and critical supersaturation ( $SS_{cr}$ ) were calculated from the equations given in the appendix.

Table I. Summary of Fog Water Composition Measurements

Location	Date	Type	Number of Samples	pH	Na <sup>+</sup>	NH <sub>4</sub> <sup>+</sup>	Ca <sup>2+</sup>	Mg <sup>2+</sup>	Cl <sup>-</sup>	NO <sub>3</sub> <sup>-</sup>	SO <sub>4</sub> <sup>2-</sup>	Ref.
Mt. Washington, NH (1900 m)	1930-1940	I	35*	4.5					4		150	27
Coastal MA and ME	1930-1940	M	37*	3.0-5.9					0-34		4-1100	
				4.7					940		380	
				3.5-6.3					0-5800		60-2600	
Germany												
Baltic Sea	1955-1965	M	42*	3.8	1500	2300	750		700	900	1900	28
Dresden	1955-1965	R	12*	4.2		2100	3200		590	450	780	
Harz Mtn. (1150 m)	1955-1965	I	18*	5.1	300	710	220		200			
Japan												
Mt. Noribura (3028 m)	July 1963	I	10 <sup>+</sup>	3.9	87	175			110	36	3300	29
				3.4-4.3	45-165	115-260			75-230	25-175	230-1250	
Mt. Tsukaba (876 m)	November 1963	I	5 <sup>+</sup>	5.9	290	880			800	17	1600	
				5.6-6.5	180-435	110-965			295-1290	5-37	360-2100	
Whiteface Mtn., NY (1500 m)	August 1976	I <sup>#</sup>	28*	3.7	11	89	17	6	31	90	140	30
	August 1980	I	50	3.2-4.0	1-7	1-200			1-14	7-190	32-800	31
Los Angeles, CA foothills (780 m)	Spring	I	120 <sup>+</sup>	2.9	240	580	140	80	190	1510	840	14
	1982 and 1983			2.1-3.9	135-8700	62-7400	5-3000	1-1800	15-9650	160-16300	130-9300	

Nova Scotia, Canada	August 1975	M	14°		1040	33	45	100	87		250	32
					600-1530	3-94	20-69	13-130	3-450		50-500	
California	Fall 1976	M	8°		320	190	55	68	400	115	200	33
Central Coast					80-950	0-580	9-100	23-175	95-1240	24-235	77-490	
Los Angeles area, CA	Fall-Winter 1980-1982	M, I	11 <sup>+</sup>	3.3	139	1580	168	54	223	110	584	34
				2.7-7.1	30-620	420-4260	0-460	22-310	68-423	580-2980	354-1875	
Los Angeles area, CA	Fall-Winter 1981-1982	M	24	2.3-5.8	12-2180	370-7960	190-4350	7-1380	56-1110	130-12000	62-5000	35
Pt. Reyes, CA	August 1982	M	17 <sup>+</sup>	4.5	190	64	10	36	215	23	186	36
				3.5-5.0	21-4700	28-330	0-240	5-1200	34-7000	2-526	36-1281	
San Nicholas Island, CA	August 1982	M	7 <sup>x</sup>	3.9	6100	450	450	1500	5300	1580	1080	37
San Diego Area, CA	January 1983	M	5 <sup>x</sup>	2.9	510	780	49	130		1850	470	
Albany, NY	October 1982	R	24 <sup>+</sup>	5.8	36	215	120	13	47	85	155	38
				4.3-6.4	10-100	70-350	65-350	6-47	18-175	11-220	21-1360	
Bakersfield, CA	Winter 1983	R	108 <sup>+</sup>	4.2	20	1440	47	6	47	850	1160	39
				2.6-7.0	1-325	490-1330	7-3500	1-430	1-980	200-6800	10-9400	
Po Valley, Italy	February and November 1984	R	5°	3.5-4.3	10-110	580-1620	60-130	10-50	20-120	290-1100	400-990	40

NOTE: All concentrations are in  $\mu\text{equiv L}^{-1}$ . Abbreviations are as follows: I is intercepted stratiform cloud, M is marine or coastal fog, and R is radiation fog. ° denotes average number of samples or events. + denotes median number of samples or events. # denotes nonprecipitating stratiform cloud data only. x denotes volume-weighted mean of  $n$  samples. ° denotes average, range, or both average and range of  $n$  events.

total concentration of species  $C$  in the atmosphere, and  $(C)_f$ ,  $(C)_g$ , and  $(C)_a$  are the concentrations of  $C$  corresponding to fog water, gas, and nonactivated aerosol phases expressed as moles per cubic meter of air. Aqueous concentrations in fog water are expressed in moles per liter with the notation  $[C]$ . Multiplication of these concentrations by the liquid water content (LWC) yields  $(C)_f = \text{LWC} [C]$ , where LWC is expressed as liters per cubic meter. For components in the gas phase, partial pressure ( $P_C$ ) values may be converted to give the same units. The mass balance may then be written as follows:

$$(C) = \text{LWC} [C] + P_C (RT)^{-1} + (C)_a \quad (2)$$

where  $R$  is the gas constant ( $\text{atm m}^3 \text{ mol}^{-1} \text{ K}^{-1}$ ) and  $T$  is absolute temperature (K). The components for which we are most concerned are sulfur dioxide, sulfuric acid, nitric acid, ammonia, and the neutralized salts of these compounds because of their abundance and effect on acidification in urban-impacted environments. The terms S(IV), S(VI), N(V), and N(-III) are used to refer to all species of that oxidation state in any phase.

**NUCLEATION SCAVENGING.** The pollutant species of concern are often present as hygroscopic aerosols (e.g., ammonium sulfate and ammonium nitrate). These aerosols will deliquesce to form aquated condensation nuclei at high relative humidity (RH), growing to larger equilibrium sizes as RH approaches 100%. The Köhler curves show the range of aerosols that can become activated into droplets. For soluble nuclei, the following proportionalities are valid:  $D_{\text{eq}} : D_{\text{dry}}^{1.5} : \text{SS}_{\text{cr}}^{-1}$ , where  $D_{\text{dry}}$  is the dry diameter for a hygroscopic aerosol. Achievement of greater  $\text{SS}_{\text{cr}}$  can lead progressively to activation of smaller nuclei. The presence of a nonsoluble fraction in particles of a given size can significantly raise their  $\text{SS}_{\text{cr}}$  (43). The chemical composition of nuclei also plays a role, although the differences between aerosols composed of pure solute species are minor, as shown here, where  $K$  is the proportionality coefficient (see equation A12 in the appendix at the end of this chapter).

<i>Solute</i>	<i>K for <math>D_{\text{dry}}</math> (<math>\mu\text{m}</math>) at <math>10^\circ\text{C}</math></i>
$(\text{NH}_4)_2\text{SO}_4$	$4.93 \times 10^{-5}$
$\text{NH}_4\text{HSO}_4$	$4.59 \times 10^{-5}$
$\text{NH}_4\text{NO}_3$	$4.82 \times 10^{-5}$
$\text{H}_2\text{SO}_4$	$4.21 \times 10^{-5}$
$\text{NaCl}$	$3.68 \times 10^{-5}$

Figure 3a shows three hypothetical particle size distributions formed by superimposing the two modes generally observed in the aerosol size spectra of sulfate (44). The smaller ( $0.05 \mu\text{m}$ ) mode corresponds to particles formed by condensation of gases; the larger ( $0.5 \mu\text{m}$ ) mode is known as the accumulation mode, which is formed primarily by coagulation and combustion. A third, coarser fraction is also routinely observed, although the contribution from anthropogenic sources may vary, especially with regard to nitrate aerosol (45, 46). The activation of these distributions, corresponding to  $(\text{NH}_4)_2\text{SO}_4$  particles, is shown in Figure 3b as a function of  $\text{SS}_v$ . The nonactivated fraction is expressed as  $f_c^a = (C)_a/(C)$ , and  $1 - f^a$  represents the aerosol scavenging efficiency in the fog.

Measurements of  $\text{SS}_v$  in the atmosphere are not widely available. Gerber (47) found that rapid oscillations of ambient humidities occurred

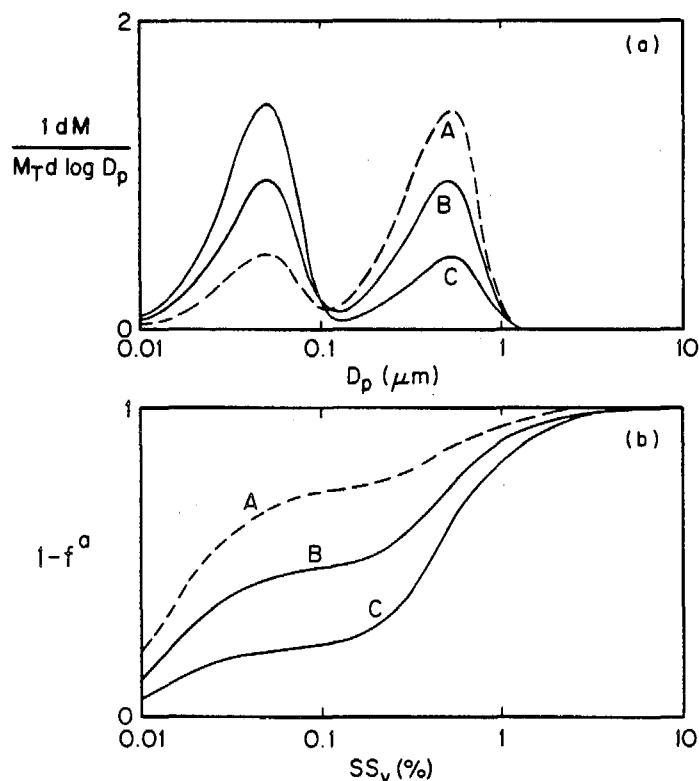


Figure 3. (a) Hypothetical fog nuclei size distributions and (b) scavenging efficiency ( $1 - f^a$ ) as a function of supersaturation ( $\text{SS}_v$ ). Curves A, B, and C represent 75%, 50%, and 25% of total mass in the larger size mode. Abbreviations are as follows:  $M$  is fog water mass,  $M_T$  is total mass, and  $f^a$  is the nonactivated fraction.

in radiation fog with excursions about a mean near to  $RH = 100\%$ ;  $SS_c$  rarely exceeded 0.1%–0.2%. Hudson (48) measured interstitial aerosol in fog and cloud environments; he found a systematic removal (i.e., activation) of larger nuclei. These cutoff values were used to calculate an effective supersaturation for the ambient atmosphere. In fogs and ground-based sampling of stratus clouds, Hudson's measurements indicated  $SS_c$  values were in the range of 0.03%–0.2%. Comparing these measured or calculated values to Figure 3b shows that little of the smaller size mode is likely to be scavenged in these environments. Conversely, solutes that are associated with a coarser ( $>1 \mu\text{m}$ ) fraction can be readily activated.

At the same time, the fraction of these nuclei (i.e.,  $D_{eq} > D_{act}$ ) that will be activated or the droplet size that they will achieve is not known. The relative increase in droplet size is faster for smaller diameters, and modeling would indicate that droplets of any size can grow from nuclei of any mass, depending upon the  $SS_c$  history they have experienced, mixing, and the aerosol size spectrum (49). Limited field data address this controversy. Measurements of solute mass for individual fog droplets have been attempted. On the Japanese coast, Naruse and Maruyama (50) found correlations between droplet size and nucleus mass, in which the biggest droplets generally had large sea salt nuclei, and the smaller droplets formed on smaller, ammonium sulfate aerosols. Hudson and Rogers (51) indirectly measured condensation nuclei within stratus cloud droplet spectra, selectively removing droplets above a certain size. They reported an increasing fraction of low  $SS_{cr}$  (i.e., large) nuclei in the larger droplets and a vanishing fraction of these nuclei in the interstitial aerosol spectrum. These relationships are at best qualitative. This area of fog microphysics—the size–composition relationship within droplet spectra—may strongly affect the chemistry and deposition of fog-borne material and remains in need of further research.

**EQUILIBRIUM DISSOLUTION OF SOLUBLE GASES.** Dissolution of gaseous species in fog water is dependent on gas–aqueous equilibria and the quantity of liquid water present. Temperature and pH are the most important parameters that affect phase equilibria (e.g., aqueous, gas–aqueous, etc.). Ionic strength effects are not as important for the aqueous concentrations generally found (*see* Table I). For highly soluble species, LWC may control the overall partitioning because the droplets can provide a sufficient solution volume to deplete the gas phase. Thermodynamic data for important gas–aqueous equilibria for  $\text{SO}_2$ ,  $\text{HNO}_3$ , and  $\text{NH}_3$  are given in Table II.

Sulfur dioxide is fairly insoluble at low pH. At higher pH (7 and above), dissociation of  $\text{SO}_2 \cdot \text{H}_2\text{O}$  to  $\text{HSO}_3^-$  and  $\text{SO}_3^{2-}$  can lead to much greater S(IV) solubility. With increasing LWC,  $(\text{S(IV)})_f$  rises and can

Table II. Thermodynamic Constants

Constant <sup>a</sup>	Reaction	pK	$\Delta H$ (kcal/ mol)	Ref.
$H_s$	$\text{SO}_2(\text{g}) + \text{H}_2\text{O} \rightleftharpoons \text{SO}_2 \cdot \text{H}_2\text{O}(\text{aq})$	-0.095	-6.25	52
$K_{s1}$	$\text{SO}_2 \cdot \text{H}_2\text{O}(\text{aq}) \rightleftharpoons \text{H}^+ + \text{HSO}_3^-$	1.89	-4.16	52
$K_{s2}$	$\text{HSO}_3^- \rightleftharpoons \text{H}^+ + \text{SO}_3^{2-}$	7.22	-2.23	52
$K_s$	$\text{HSO}_4^- \rightleftharpoons \text{H}^+ + \text{SO}_4^{2-}$	2.20	-4.91	52
$H_N^0$	$\text{HNO}_3(\text{g}) \rightleftharpoons \text{H}^+ + \text{NO}_3^-$	-6.51	-17.3	53
$H_A$	$\text{NH}_3(\text{g}) + \text{H}_2\text{O} \rightleftharpoons \text{NH}_3 \cdot \text{H}_2\text{O}(\text{aq})$	-1.77	-8.17	52
$K_B$	$\text{NH}_3 \cdot \text{H}_2\text{O}(\text{aq}) \rightleftharpoons \text{NH}_4^+ + \text{OH}^-$	4.77	0.9	52
$H_F$	$\text{CH}_2\text{O}(\text{g}) + \text{H}_2\text{O} \rightleftharpoons \text{CH}_2\text{O} \cdot \text{H}_2\text{O}(\text{aq})$	-3.8	-12.85	54
$K_F$	$\text{HMSA} \rightleftharpoons \text{CH}_2\text{O} + \text{HSO}_3^-$	-5.0		55
$K_w$	$\text{H}_2\text{O} \rightleftharpoons \text{H}^+ + \text{OH}^-$	14.00	13.35	52

<sup>a</sup>Abbreviations are as follows:  $H_s$ ,  $H_A$ , and  $H_F$  are the corresponding Henry's law constants for sulfur(IV), ammonia, and formaldehyde;  $K_{s1}$  and  $K_{s2}$ (M) are the first and second dissociation constants for  $\text{SO}_2(\text{aq})$ , respectively;  $H_N^0$ (M atm<sup>-1</sup>) is the modified Henry's law constant for nitrogen;  $K_B$  and  $K_w$ (M) are the dissociation constants for ammonia and water, respectively; and  $K_F$ (M) is the formation constant for HMSA.

lead to depletion of the gas phase (Figure 4a). The fraction of solute partitioning into the droplet phase is expressed as  $f_c = (C)_f / (C)_f + (C)_g$ . Appreciable  $[\text{S(IV)}]_{(\text{aq})}$  may be supported in the aqueous phase even at low  $P_{\text{SO}_2}$ , where  $P_{\text{SO}_2}$  is the partial pressure of  $\text{SO}_2$ . Figure 4b shows the aqueous concentration as a function of prefog  $P_{\text{SO}_2}$  at high and low LWC. Presence of gaseous aldehydes has been shown to substantially increase S(IV) solubility by the formation of stable bisulfite adducts (56).

Nitric acid is completely scavenged to droplets for fogs even at minimal LWC because it has such a high Henry's law coefficient [for  $\text{HNO}_3(\text{g}) + \text{H}_2\text{O} \rightleftharpoons \text{HNO}_3 \cdot \text{H}_2\text{O}(\text{aq})$ ,  $H_N = 2.1 \times 10^5 \text{ M atm}^{-1}$  (53)]. Ammonia scavenging is variable in the ranges of pH and LWC found. Similar to the case of  $\text{SO}_2(\text{g})$ , the atmosphere may exist as a reservoir for  $\text{NH}_3(\text{g})$  that can be dissolved or released from fog water as a function of the relative amount of atmospheric acidity and liquid water. Reservoirs of N(V) and N(-III), which also exist in the aerosol phase (e.g., ammonium nitrate), are discussed in the next section.

Gas transfer to fog-sized droplets by molecular diffusion is sufficiently rapid for phase equilibria to be achieved on the order of seconds or less under most conditions (57, 58). Greater time may be required in the cases where high solubility strongly favors gas-phase partitioning. The characteristic times required to supply the total amount of solute necessary to attain this equilibrium were evaluated by Schwartz and Freiberg (7). They found that times of the order 10 s were sufficient for

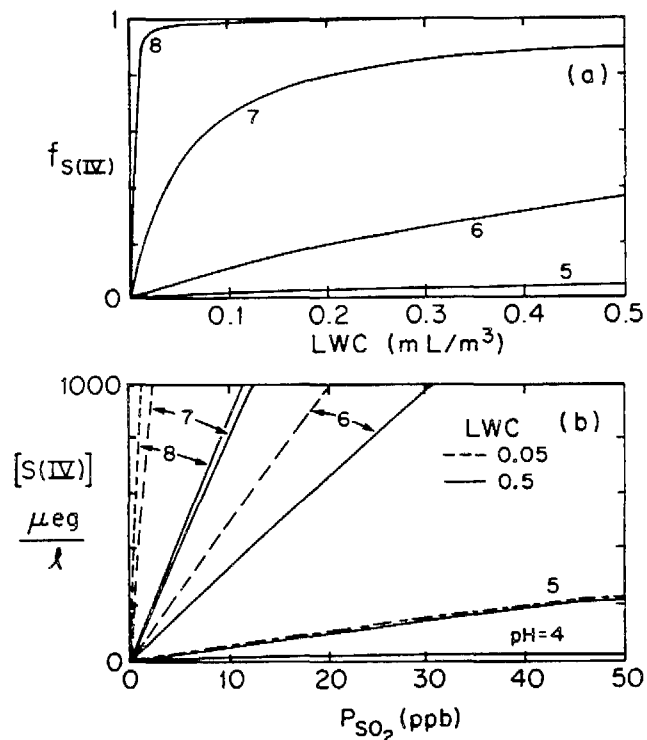


Figure 4. Effect of pH on SO<sub>2</sub> dissolution in fog: (a) fraction scavenged as function of LWC; (b) fog water concentration versus partial pressure of SO<sub>2</sub> ( $P_{SO_2}$ ).

SO<sub>2</sub>(g) to dissolve into droplets even at high pH. Similarly, the absorption of highly soluble gases such as HNO<sub>3</sub> and NH<sub>3</sub> in fog droplets is not instantaneous. However, phase equilibria are established relatively rapidly—times of the order 10–100 s (104)—compared to the lifetimes of droplets.

**OVERALL FOG SCAVENGING.** Nonactivated aerosol fractions of nitrate, sulfate, and ammonium coexist with fog water and gaseous constituents in the atmosphere. Solutes incorporated within the droplet spectrum are subject to gas-aqueous equilibria; nonactivated aerosols appear to remain inert in this regard. In the case of nonvolatile species such as sulfate, partitioning is exclusively between nonactivated aerosol and droplet phases. Applying mass balances for HNO<sub>3</sub>(g) and NH<sub>3</sub>(g), the overall fractions,  $F_C = (C)_f / (C)$ , may be calculated as functions of gas-aqueous equilibria and nonactivated aerosol fraction. The mass balances for S(VI), N(V), N(-III), and S(IV) are given by equations 3-6.

$$(S(VI)) = LWC [S(VI)] + (S(VI))_a \quad (3)$$

$$(N(V)) = \frac{P_{HNO_3}}{RT} + (LWC) [NO_3^-] + (N(V))_a \quad (4)$$

$$(N(-III)) = \frac{P_{NH_3}}{RT} + (LWC) ([NH_3 \cdot H_2O] + [NH_4^+]) + (N(-III))_a \quad (5)$$

$$(S(IV)) = \frac{P_{SO_2}}{RT} + (LWC) ([SO_2 \cdot H_2O] + [HSO_3^-] + [SO_3^-] + [HMSA]) \quad (6)$$

where HMSA is hydroxymethylsulfonic acid, and  $(S(IV))_a$  is assumed to be negligible. The resulting scavenging efficiencies ( $F$ ) for equations 3-6 are given by equations 7-10.

$$F_{S(VI)} = (S(VI))_f / (S(IV)) = 1 - f_{S(VI)}^g \quad (7)$$

$$F_{N(V)} = (N(V))_f / (N(V)) = \frac{H_N^g (LWC) RT}{H_N^g (LWC) RT + [H^+]} (1 - f_{N(V)}^g) \quad (8)$$

$$F_{N(-III)} = (N(-III))_f / (N(-III)) = \frac{H_A (LWC) RT (1 + K_B [H^+] / K_w)}{1 + H_A (LWC) RT (1 + K_B [H^+] / K_w)} (1 - f_{N(-III)}^g) \quad (9)$$

$$F_{S(IV)} = (S(IV))_f / (S(IV)) = 1 - \left[ 1 + (LWC) H_S RT \left( 1 + \frac{K_{s1}}{[H^+]} + \frac{K_{s1} K_{s2}}{[H^+]^2} + \frac{K_{s1} K_F H_F P_{CH_2O}}{[H^+]} \right) \right]^{-1} \quad (10)$$

where  $K_B$  is the base dissociation constant;  $K_w$  is the dissociation constant for water;  $H_A$ ,  $H_S$ ,  $H_N$ , and  $H_F$  are the corresponding Henry's law constants for ammonia, sulfur(IV), nitrogen, and formaldehyde;  $K_{s1}$  and  $K_{s2}$  are the first and second dissociation constants for  $SO_2(aq)$ , respectively;  $K_F$  is the formation constant for HMSA; and  $H_N^g$  is the modified Henry's law constant for nitrogen.

Without specific knowledge about solute size-composition relationships, a more general model of fog scavenging can be proposed based on solute speciation and the relative abundance of ambient acids and bases. Aerosols are generally found as neutral salts in the system dominated by  $H_2SO_4$ ,  $HNO_3$ , and  $NH_3$ . Nitrate and sulfate are counterbalanced by ammonium ion, while excess acids or bases reside in the gas

phase as  $\text{HNO}_3(\text{g})$  or  $\text{NH}_3(\text{g})$  (25, 59). Only for the cases where sulfate acidity exceeds the ambient ammonia [i.e.,  $(\text{S(VI)}) > (\text{N(-III)})$ ] would an acidic aerosol be thermodynamically stable in the dry atmosphere (60, 61). Consider two cases for these constituents:

$$\text{case i: } (\text{N(V)}) + 2 (\text{S(VI)}) = (\text{acids}) > (\text{N(-III)})$$

$$\text{case ii: } (\text{N(-III)}) > (\text{acids}).$$

where acids is the total amount of sulfuric and nitric acids.

Nucleation scavenging is assumed to depend on LWC. For example, a linear dependence to a maximum of  $F_{\text{S(VI)}} = 90\%$  at  $\text{LWC} = 0.3 \text{ mL m}^{-3}$  is assumed for sulfate in Figure 5a. This maximum approximates the progressive activation of a spectrum dominated by the large aerosol fraction. We also assume that scavenging of aerosol  $\text{N(V)}$  and  $\text{N(-III)}$  follows this same relationship. Solute-specific size spectra are not addressed at this point; actual differences in the proportion of fine versus coarse particles would be reflected in the nucleation scavenging efficiencies for each solute.

For case i, available  $\text{N(-III)}$  is immediately exhausted in neutralizing acidic sulfate and nitrate. In the atmosphere, the dissociation of ammonium nitrate aerosol [ $\text{NH}_4\text{NO}_3 \rightleftharpoons \text{NH}_3(\text{g}) + \text{HNO}_3(\text{g})$ ] is highly dependent upon ambient temperature and RH (60). Ammonium nitrate aerosol volatilizes at low RH and high temperature. However, at high RH, the formation of aerosols leads to equimolar depletion of the gases until one is present at a negligible level; essentially, the gases do not coexist. Hence,  $\text{N(V)}$  in excess of  $\text{N(-III)}$  remains in the gas phase. When a droplet phase forms,  $\text{HNO}_3(\text{g})$  is 100% scavenged, and only nonactivated  $\text{N(V)}$  aerosol is left outside the droplet spectrum. Figure 5b shows the effect of  $\text{N(-III)}/\text{acid}$  and  $\text{N(V)}/\text{acid}$  equivalent ratios based on the assumption that aerosol scavenging for nitrate proceeds similar to sulfate. Overall, ambient  $\text{N(V)}$  will be more efficiently scavenged when the total acids are in greater excess of  $\text{N(-III)}$  and other bases, and when  $\text{S(VI)}$  makes a greater contribution to the net acidity in the precursor atmosphere.

In case ii, we assume  $(\text{NH}_3(\text{g})) = (\text{N(-III)}) - (\text{acids})$  in the humid atmosphere, while the remaining material forms neutral ammonium aerosol. Furthermore, assuming ammonium aerosol nucleation proceeds as in Figure 5a, the total  $\text{N(-III)}$  scavenging depends on the gas-aqueous equilibrium, fog water pH, and LWC (Figure 5c). In the alkaline regime, the presence of soluble, weak-acid gases can play an important role in determining the resultant pH of fog water that forms, and this pH affects the scavenging of  $\text{N(-III)}$ . Dissolution of formic and acetic acids  $\text{p}K_a = 3.8$  and 4.8, respectively (62), for example, provides base-neutralizing capacity to the droplet. Also, the acidity of the droplet

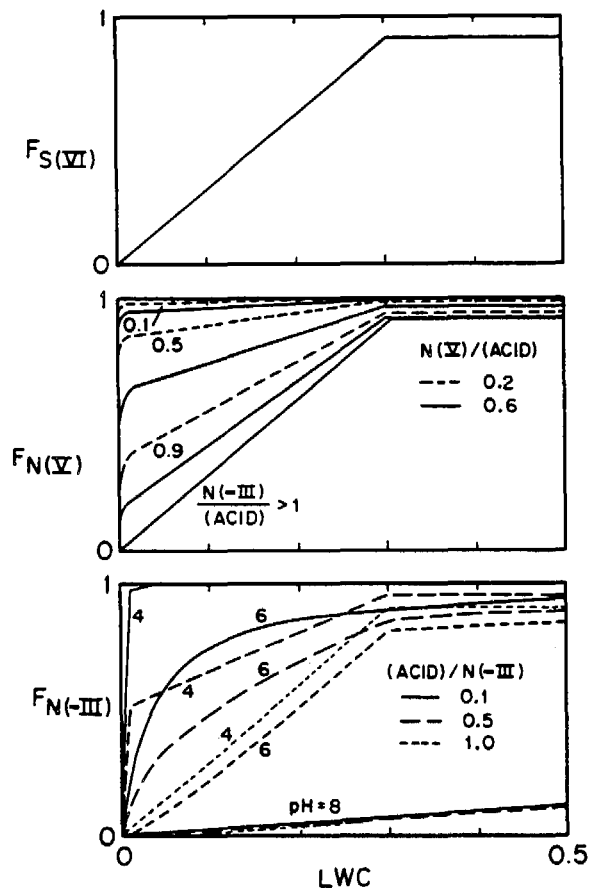


Figure 5. Fog scavenging ( $F$ ) for  $S(VI)$ ,  $N(V)$ , and  $N(-III)$  as a function of liquid water content ( $LWC$ ). Aerosol scavenging for  $N(V)$  and  $N(-III)$  is similar to the form shown for  $S(VI)$ . For  $F_{N(V)}$ , the 0.1, 0.5, and 0.9 values represent  $N(-III)/(ACID)$ .

can be increased by the formation of  $S(IV)$ -formaldehyde adducts (e.g., HMSA), which increase  $S(IV)$  solubility, or in situ  $S(VI)$  production. Each process will lead to  $N(-III)$  scavenging that can eventually deplete  $NH_3(g)$ .

Nitrate and sulfate aerosols may be found within different size fractions. In southern California, Appel et al. (63) reported that nitrate is found predominantly in a coarser fraction than sulfate. In the San Joaquin Valley, Heisler and Baskett (64) found a similar relationship except during the wintertime; a substantial increase in the coarse sulfate fraction ( $>2.5 \mu m$ ) was observed during wintertime stagnation. Ammonium was found to occur in the same fraction as nitrate. However, the measure-

ments of Heisler and Baskett did not include gaseous ammonia, which can be a sizeable portion of total N(-III) in the region. Therefore, the true partitioning was not determined. Differences in predominant sizes for these three major constituents can significantly alter results of the simplified model given above. Most significant would be the presence of a coarse particle fraction enriched with N(V) or S(VI) that would be readily scavenged. Simultaneous measurements of these components in the three phases have not been satisfactorily made in fog.

**Fog Deposition.** Early studies documented the hydrological and chemical importance of intercepted cloud and fog water inputs to mountain slope and coastal ecosystems (65). For instance, open collectors placed below trees exposed to fog-laden wind on the San Francisco peninsula measured an average water flux of 50 cm in one rainless month (66). Natural and artificial "fog-drip" collectors exposed for extended periods have shown that these "occult" inputs can have comparable magnitudes to annual precipitation values for water and nutrient capture (3, 4). However, the true relationship of these measurements to the capture by actual vegetation was uncertain.

Fog deposition from the ambient atmosphere to ground surfaces can be viewed as a two-step process (67). First, a droplet in the ambient atmosphere must be transported through an aerodynamic layer toward the ground. Next, once within a canopy layer, droplets must be deposited to canopy surfaces. The resistance to mass transport may reside in either layer, primarily depending on the geometry of the canopy and the degree of atmospheric turbulence. Research in the subject area of droplet or large particle deposition has addressed the specific mechanisms that can control their flux.

From measurements of droplet capture by monitored trees, Hori (68) and co-workers reported deposition rates on the order of 0.5 mm h<sup>-1</sup> for a forest intercepted by dense coastal fog. Yosida and Kuroiwa (69) found that momentum and droplet transport coefficients were of similar order of magnitude, based on measurements of wind force and droplet-capture rate by a small conifer tree. However, although the drag coefficient for the canopy elements decreased with increasing wind speed, the authors found that capture efficiency rose because of impaction. In the same field area, Oura (70) determined that interception near the leading edge of the forest was about 3 times more effective than for interior locations.

Lovett (11) adapted a resistance model to cloud droplet capture by a balsam fir forest canopy. He included turbulent transport and impaction to the canopy elements, conceived as a set of 1-m-thick height strata in a 10-m-high forest, and edge effects were not included. The model predicted a nearly linear correspondence between water flux and

canopy-top wind speeds greater than  $2 \text{ m s}^{-1}$ . Droplet impaction, primarily to the upper 3 m of strata, was the dominant deposition mechanism. Wind speeds between 2 and  $10 \text{ m s}^{-1}$  yielded water fluxes of  $0.2\text{--}1.1 \text{ mm h}^{-1}$  (equivalent to  $V_d = 10\text{--}70 \text{ cm s}^{-1}$  for the simulated conditions). For lesser wind speeds, Lovett found that sedimentation controlled the water capture.

Legg and Price (71) calculated that the sedimentation flux of large particles to vegetation with a large leaf-area index (i.e., total leaf area per surface area of ground) would also increase with wind speed. This increase would be caused by wind-driven turbulence bringing particles to the lower leaves where sedimentation would lead to additional removal. Their model did not account for a vertical profile caused by depletion of particles, especially by impaction to the top of the canopy. Lovett (11) showed that the depletion reduced the net sedimentation flux nearer to the ground as wind speeds increased; nonetheless, greater leaf-area index caused sedimentation fluxes slightly higher than by terminal fall velocities alone.

Davidson and Friedlander (67) identified particle size regimes where different transport mechanisms dominated for a short-grass canopy. Under moderate wind conditions, the filtration efficiencies in calculations for  $D_o > 10 \mu\text{m}$  were high enough that deposition was effectively limited by turbulent transport or sedimentation to the canopy from above.

Droplet precipitation measured to flat plates in radiation fog averaged  $0.03 \text{ mm h}^{-1}$ , and this value agreed with calculated terminal fall velocities; measured rates for grass-model collectors (<1 m high) indicated approximately a twofold greater deposition (72). In another field study of radiation fog, Roach et al. (21) calculated that sedimentation removed as much as 90% of water that condensed to droplets during fog. Brown and Roach (73) parameterized the fog deposition rate as a linear function of LWC in their companion modeling paper. However, Brown (74) later determined that the gravitational flux was overestimated by this relationship for higher LWC. Jiusto and Lala (75) also found a linear fit between sedimentation rate and LWC as measured from droplet size spectra in radiation fog. Corrandini and Tonna (76) evaluated this parameterization for droplet size spectra given in the literature for different types of fog and found it did not fit well for advection and valley fogs.

Dollard and Unsworth (77) made direct measurements of turbulent fluxes for wind-driven fog drops above a grass surface. Their technique relied on precise determinations of LWC and wind speed made simultaneously at several heights. From the gradient of these parameters, the authors calculated turbulent transport for droplets and momentum. Their experimental data gave values of turbulent droplet flux  $1.8 \pm 0.9$

times the sedimentation rate when wind speeds were 3–4 m s<sup>-1</sup>. At wind speeds less than 2 m s<sup>-1</sup>, their measurements showed that total fluxes were no more than 50% greater than by sedimentation alone.

**Transport Parameters and Processes.** The difference between deposition in dry and fog-laden air is primarily due to the increase in particle size for the latter case. Fog droplets are of the size where inertial impaction and sedimentation dominate their deposition to collection surfaces (78). In the general case, impaction to surface elements occurs when particles diverge, because of their inertia, from the airflow streamlines where they curve around the obstacle. The efficiency of impaction depends on the radius of curvature of the impaction surface ( $R_f$ ) and the particle inertia and is characterized by the Stokes number (St):

$$St = \frac{\rho_w D_o^2 U_s}{18 \mu R_f} \quad (11)$$

where  $\rho_w$  is the density of the particle (i.e., water for droplets);  $D_o$  is the droplet diameter;  $\mu$  is the dynamic viscosity of air; and  $U_s$  is the relative velocity between the particle and the obstacle. Fog and cloud droplet sedimentation or terminal fall velocity ( $V_s$ ) follows the form of Stokes law:

$$V_s = \frac{\rho_w g D_o^2}{18 \mu} \quad (12)$$

where  $g$  is the gravitational acceleration. At larger diameters, such as raindrops, Stokes law no longer holds because of viscosity and drop deformation effects (18).

**IMPACTION.** The droplet impaction to cylinders can be viewed as an idealized analog of particle capture by grasses or conifer leaves. Impaction efficiencies have been theoretically derived for potential flow as a function of Stokes number (79) and extended for higher Reynolds number ( $Re = \rho_a U_s D_o / \mu$ ) (80).

Experimental data have also been applied to calculations of particle or droplet flux to receptor surfaces. For example, Davidson and Friedlander (67) used a least-squares fit to data for impaction on cylinders. The efficiency,  $\eta$ , represented the fraction of particles that impact compared to the total number of particles passing through the projected area of the obstacle. For a single cylinder, the empirical expression was given as

$$\eta = \frac{St^3}{St^3 + 0.75 St^2 + 2.80 St - 0.20} \quad (13)$$

The flux by impaction to a canopy of cylinders of diameter  $d_f$  was calculated by integrating over the length of the cylinder and multiplying by the number of cylinders per unit area of ground ( $N$ ):

$$J = -d_f N \int_{z_s}^H \eta(z) U(z) C(z) dz \quad (14)$$

where  $J$  is the flux of particles per unit area of ground,  $z$  is the vertical scale,  $U$  is the horizontal wind speed,  $C$  is the concentration of particles,  $H$  is the canopy height, and  $z_s$  is the particle sink [i.e., the level at which either  $C$  or  $U$  is assumed to vanish to zero, and impaction no longer occurs (67)]. The convention is that  $J$  is positive for upward flux.

Alternatively, Lovett (11) used the experimental results of Thorne et al. (81). These results were measured specifically for components of the balsam fir canopy that they studied. The efficiency was given as

$$\eta = e^{(-1.84 + 0.90(\ln St) - 0.11(\ln St)^2 - 0.04(\ln St)^3)} \quad (15)$$

The needles were oriented randomly, and the effect of interferences in airflow caused by neighboring canopy elements was accounted for empirically. For 50% efficiency,  $St = 4$  according to Thorne et al. (81) and  $St = 2$  in equation 13. Lovett (11) calculated the matrix of boundary-layer resistances for droplet capture as a function of horizontal wind speed and canopy structure (e.g., leaf-area index) for the different levels within the canopy.

Because the wind speed and droplet concentration profiles are also strongly dependent on the canopy structure, solutions for fog deposition due to impaction are not readily generalized. Davidson et al. (78) showed that the range of large particle deposition rates was 1 order of magnitude among five wild grass canopies that were studied. As stated in the previous section, the overall efficiency was found to be limited by turbulent transport to the top of the canopy for large particles ( $\geq 10 \mu\text{m}$ ). In the case of the balsam fir canopy studied by Lovett (11), no such limitations were found to occur, and impaction led to very high deposition rates, also mentioned previously.

In practice, the collection efficiency of particles may be different from impaction efficiency. This difference largely depends on the surface properties of the collector element. In wind tunnel experiments (9, 82) and field measurements (83), particle deposition to dry surfaces was far below that to wet surfaces. As wind speeds increased, so did particle rebound. For wet surfaces, collection efficiencies of dry particles were more in accord with impaction theory. Experimental results for droplet collection efficiencies were generally in good agreement with theory

(84). The surface tension of water droplets was found to provide adequate adhesion to ensure near-perfect retention for  $D_o < 50 \mu\text{m}$  (85). Wind-induced shear may cause some droplet removal from foliar elements, and this removal was observed in wind tunnel tests with glycerol droplets when  $St > 10$  (81). Nonetheless, sheared drops will generally fall because of their large size rather than be resuspended. In the wind tunnel experiments of Merriam (86), LWC was found to be a more important factor in determining total droplet capture than variations in canopy element geometry.

**DEPOSITION VELOCITY.** Although an overall deposition may be modeled for a specific canopy geometry and elements, wind speed and turbulence profiles, and particle size distributions (11, 78, 87), the flux to the canopy can be parameterized by the quantity known as deposition velocity,  $V_d$ . In this approach, the depositional flux,  $J_d$ , is scaled to the ambient concentration of some component at a reference height,  $H$ , above the canopy:

$$J_d = -V_d C(H) \quad (15a)$$

The deposition velocity may be calculated in terms of droplet fluxes or the specific chemical elements contained within the droplets.

**TURBULENCE VERSUS SEDIMENTATION.** The flux of droplets through the aerodynamic layer ( $J_a$ ) can be expressed by

$$J_a = -K_p(z) \frac{dC}{dz} - V_s C \quad (16)$$

where  $K_p$  is the eddy diffusivity for particles, and  $V_s$  is the sedimentation velocity. In the steady state,  $J_a$  is constant with height, so  $C$  and  $dC/dz$  are functions of  $z$ .

The relative importance of turbulence versus sedimentation transport may be expressed by  $E = V_d/V_s$ , the ratio of deposition to sedimentation velocities. With substitution ( $J_a = J_d$ ), equation 16 becomes

$$K_p(z) \frac{dC}{dz} + V_s C = E V_s C(H) \quad (17)$$

This equation can be readily solved for  $C(z)$  to give the concentration profile:

$$\frac{C(z)/C(H) - E}{1 - E} = e^{\left[ - \int_H^{z_s} \frac{V_s}{K_p(z)} dz \right]} \quad (18)$$

For the momentum exchange between the air and the ground, a logarithmic wind profile can be assumed for thermally neutral conditions (88):

$$U(z) = \frac{U^*}{k} \ln \left( \frac{z}{z_0} \right) \quad (19)$$

where  $U^*$  is the friction velocity,  $k$  is von Karman's constant (0.4), and  $z_0$  is a roughness scale. In cases where an appreciable canopy structure exists, the profile will be displaced by some height,  $d$ , above the ground surface, and  $z$  is replaced by  $(z - d)$ . Above the canopy, an analogy between turbulent exchange of particles and momentum is often assumed for neutral atmospheric stability (9, 78, 88):

$$K_p(z) = k U^* z \quad (20)$$

Again, when displacement of the wind profile is observed,  $z - d$  replaces  $z$ . The presumption of neutral stability is not always warranted; with daytime heating, vertical motions are enhanced by buoyancy. However, fog occurs during periods where minimal isolation and thermal neutrality or slight stability predominate (21, 89).

The analogy between momentum and particle transport may sometimes be inappropriate. For example, in the viscous boundary layer, momentum transfer to the canopy elements is augmented by the bluff-body (or normal pressure) forces. There is no analogy in heat or mass transport. Hence, the resistance to momentum exchange is generally less than for the other entities (90). The failure of large particles to follow fluid streamlines will also reduce their effective turbulent diffusivity, although this reduction is only important for  $D_0 > 30 \mu\text{m}$ , based on the calculations of Csanady (91). However, for the conditions of fog, the analogy between momentum transfer with turbulent transport of particles has given satisfactory results (77).

In applying measurements made in radiation fog, we were interested in identifying the relative importance of sedimentation and turbulent transport for various degrees of turbulence (i.e.,  $U^*$ ) and sizes of particles ( $V_s$ ). We solved equation 18 by using equation 20 for eddy diffusivity and the boundary condition of  $C = 0$  at  $z = z_s$ , the particle sink (67). Figure 6 shows the results of calculations for  $z_s/H$  between 0.05 and 0.005 (e.g., for  $H = 3$  m, particle sink at 15 or 1.5 cm). This range corresponds to a shallow canopy where impaction is effective enough that transport is limited by turbulence or sedimentation (78). The enhancement of deposition by turbulent-driven droplet transport is seen to be rather limited for low and moderate wind speeds. The rea-

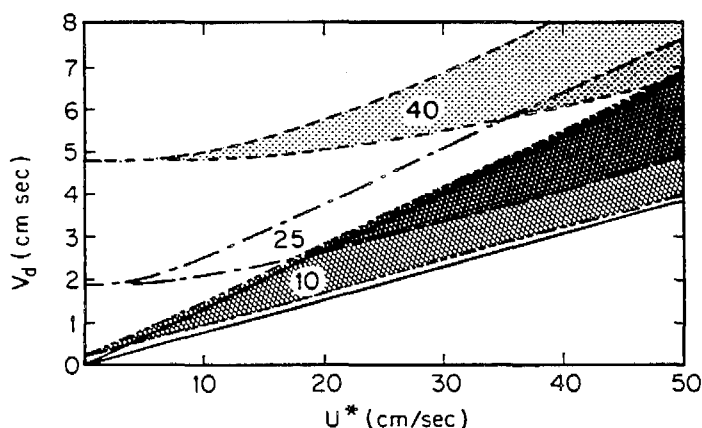


Figure 6. Fog deposition curves. Deposition velocity ( $V_d$ ) as a function of friction velocity of wind ( $U^*$ ) for the droplet diameters ( $\mu\text{m}$ ) indicated. The indicated range for  $z_s/H$  is between 0.05 (upper) and 0.005 (lower), where  $z_s$  is the particle sink and  $H$  is the reference height for  $V_d$ .

sions stated for less-effective turbulent exchange for particles vis-a-vis momentum would require that the indicated rates could be even lower. These calculations identified the same range of turbulent transport values given by Dollard and Unsworth (77).

**DROPLET LIFETIMES.** Changes in particle size will strongly affect depositional processes. The rate at which hygroscopic aerosols achieve equilibrium in the humid region over wet surfaces was recently studied in wind tunnel experiments by Jenkin (92). If equilibria were attained as particles approached the wet surface, an order-of-magnitude enhancement in deposition would be expected. Jenkin's experiments indicated that the growth rate was not sufficiently rapid; a twofold increase was the maximum observed. Hence, the residence of depositing particles within the humid region was not long enough for growth to equilibrium sizes.

An alternative concern is for the converse case in which fog droplets are exposed to lower humidity in the region near warmer-than-air surfaces. A rapid shift of the droplet distribution to smaller sizes would significantly alter both the chemistry and deposition rate. Even under nighttime, radiative conditions, the ground may remain warmer than the overlying air during fog because of the ground's high heat capacity. However, the vertical extent of conductive warming is limited to several centimeters in fog until insolation becomes important (75).

The lifetimes for fog droplets instantaneously exposed to drier air were calculated from the growth equation (equation 1) as a function of relative humidity and nucleus mass. These calculation results are shown

in Figure 7 for several initial diameters. Mature fog droplets ( $D_0 \geq 20 \mu\text{m}$ ) are very resistant to rapid evaporation until RH drops well below 100%. Solute concentration has little effect on the shrinkage rate for these larger droplets. On the other hand, the rates at which smaller droplets evaporate could be quite rapid; those with greater solute mass change size less rapidly. Because sedimentation alone will transport larger droplets downward at  $1\text{--}3 \text{ cm s}^{-1}$ , droplet evaporation would not be expected to alter size-dependent depositional processes until a drier region extends several meters above the canopy surface. This situation is what happens when a fog starts to "lift", generally within several hours after sunrise. Even before the fog dissipates, evaporation from wetted surfaces can be important to the net water flux (11), but until the atmosphere dries sufficiently, the flux of fog water solutes will continue.

**POLLUTANT SCAVENGING.** An essential facet of fog deposition is the scavenging of ambient aerosols and gaseous constituents into droplets. Partitioning of species between phases determines the relative importance of respective removal pathways. As particulates are incorporated into droplets, their deposition rate will increase with enhanced sedimentation and impaction efficiency. Simple models of fog deposition

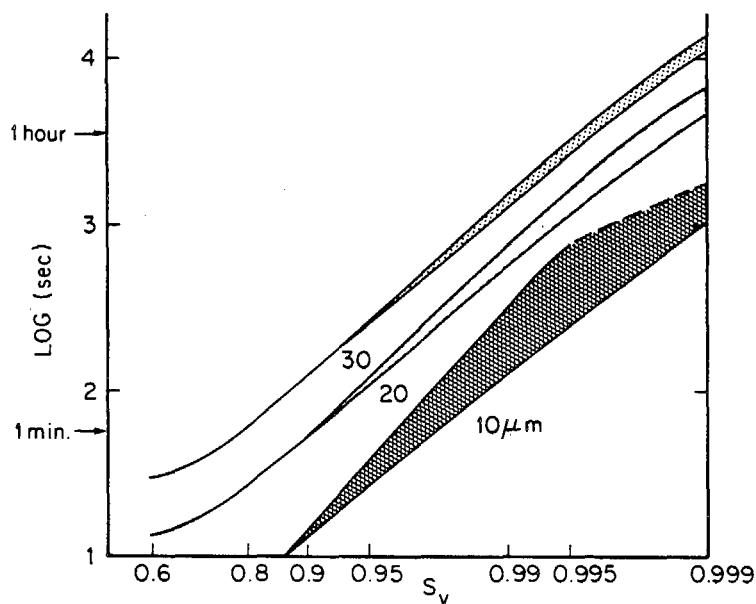


Figure 7. Droplet lifetimes are the times required for droplets of a given initial diameter to shrink to equilibrium size for the indicated humidity ( $S_v = RH/100$ ). The indicated range is from 0.1 (lower) to 1.0 (upper)  $\mu\text{m}$  for the nucleus diameter.

presume that fog leads to an increase for all particle sizes. However, when only a portion of aerosol mass achieves droplet sizes, the actual increase in deposition is reflected in this proportionality. Furthermore, fog may effectively scavenge important pollutant gases such as  $\text{SO}_2(\text{g})$ ,  $\text{HNO}_3(\text{g})$ , and  $\text{NH}_3(\text{g})$ . Turbulent diffusional processes are predominantly responsible for deposition of gases, and deposition velocities of about  $1 \text{ cm s}^{-1}$  have been reported for  $\text{SO}_2(\text{g})$  (93) and  $2 \text{ cm s}^{-1}$  for  $\text{HNO}_3(\text{g})$  (94). However, gas scavenging by droplets would cause removal of these species to be dominated by the sedimentation or impaction flux.

### **Field Experiments**

**Experimental Results.** Atmospheric pollutant behavior was studied in the southern San Joaquin Valley of California during periods of dense fog and stagnation (90). Fluxes to the ground of water-soluble species were determined by surrogate-surface collectors while simultaneous fog water and aerosol composition measurements were made. Repetitive, widespread fogs were observed only when the base of the temperature inversion was 150–400 m above the valley floor. Dense fogs (visual range < 200 m) lasted 10–17 h at sampling locations. Atmospheric loadings of water-soluble species in the droplet phase were composed almost entirely of  $\text{NH}_4^+$ ,  $\text{NO}_3^-$ , and  $\text{SO}_4^{2-}$  (Figure 8). Substantial concentrations of free acidity ( $\text{H}^+$ ) and S(IV) species were occasionally measured in fog water samples (Table III). Concurrent with fogs, appreciable gaseous ammonia was often present, but only when atmospheric acidity was absent. Gaseous nitric acid concentration was generally lower than detection limits during all fog periods. Deposition samples (Figure 9) were similarly dominated by the same major ions as fog water and aerosol phases, although slightly greater contributions were made by soil dust species. These contributions were still far lower than the major species.

Substantially higher deposition rates for aerosol species occurred during fogs compared to rates during nonfog periods. Rates for major ions were enhanced by factors of 5–20 as shown in Figure 9. Deposition velocities,  $V_d$  and  $V_{d,\text{fog}}$ , were calculated by normalizing measured deposition rates by the total and droplet-phase atmospheric loadings, respectively (Figure 10). The proportions of deposited solute for major ions were closely matched to the fog water composition. That is, despite large differences between  $V_d$  values, there was close agreement for  $V_{d,\text{fog}}$  values among major ions (Figure 11). The median value of  $V_{d,\text{fog}}$  was approximately  $2 \text{ cm s}^{-1}$ , and measurements were in the range of 1–5  $\text{cm s}^{-1}$ . Calculations of  $V_{d,\text{fog}}$  were sensitive to LWC data, which have large uncertainties ( $\pm 50\%$ ) for absolute values. An operationally defined

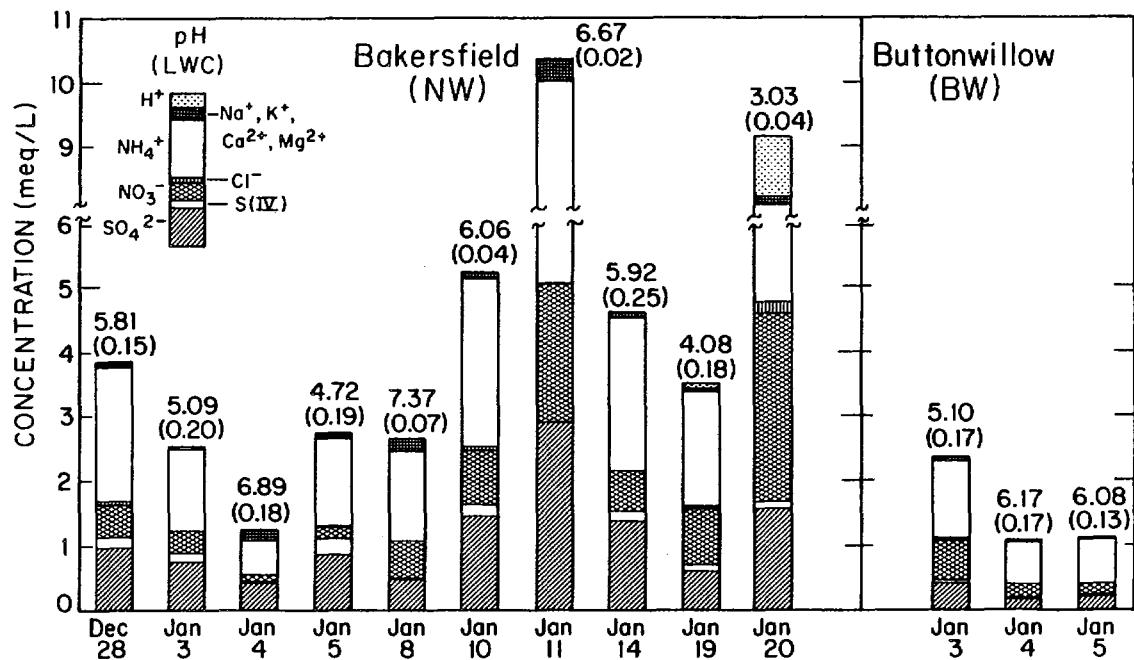


Figure 8. Summary of fog water compositions at San Joaquin Valley sites from winter 1984-1985. Volume-weighted concentrations, pH, and LWC ( $\text{g m}^{-3}$ ) for measurements ending on the morning of the date taken are given.

Table III. Fog Water Composition Summary

Location, Date, and Time	N	LWC	pH	Na <sup>+</sup> ( $\mu\text{equiv L}^{-1}$ )	K <sup>+</sup>	NH <sub>4</sub> <sup>+</sup>	Ca <sup>2+</sup>	Mg <sup>2+</sup>	Cl <sup>-</sup>	NO <sub>3</sub> <sup>-</sup>	SO <sub>4</sub> <sup>2-</sup>	S(IV) ( $\mu\text{mol L}^{-1}$ )	CH <sub>2</sub> O	-/+ <sup>a,b</sup>	$\Delta$	$\Sigma$
Bakersfield Airport																
December 28, 1984 00:35 to 08:35	6	0.149	5.81	14	4	2100	46	9	41	505	1004	153	98	0.81	+410	10
January 2-3, 1985 20:15 to 10:15	10	0.202	5.09	10	3	1260	25	3	13	335	764	128	78	0.95	+69	3
January 3-4, 1985 20:00 to 01:55	5	0.176	6.89	5	3	530	171	11	6	96	442	18	32	0.78	+156	12
January 4-5, 1985 20:10 to 09:15	13	0.191	4.72	21	4	1350	33	4	19	190	889	231 <sup>c</sup>	105	0.93	+102	4
January 8, 1985 09:00 to 10:00	1	0.070	7.37	57	8	1380	109	24	6	570	501	16	27	0.69	+483	18
January 10, 1985 07:15 to 08:50	2	0.035	6.06	25	9	2600	54	5	50	830	1619	180		0.99	+18	0
January 11, 1985 06:35 to 07:30	1	0.016	6.67	58	24	4920	248	9	20	2115	2920			0.96	+206	2
January 14, 1985 01:30 to 04:30	1	0.249	5.92	26	3	2350	37	5		630	1400	145	123	0.90	+246	5
January 18-19, 1985 20:05 to 09:00	10	0.182	4.08	7	7	1780	21	4	32	870	650	89	147	0.86	+263	7
January 20, 1985 07:15 to 09:30	3	0.040	3.03	26	17	3280	64	10	183	2900	1610	84	165	1.10	-461	5
Buttonwillow																
January 2-3, 1985 20:20 to 06:50	6	0.174	5.10	7	3	120	38	4	17	640	440	36	55	0.89	+135	6
January 3-4, 1985 17:25 to 10:30	7	0.173	6.17	5	2	600	27	3	40	225	195	9	28	0.73	+172	15
January 4-5, 1985 19:30 to 09:00	11	0.133	6.08	3	2	670	19	3	14	190	245	22	33	0.68	+224	19

NOTE: Concentration values are volume-weighted mean values collected for indicated time periods. Abbreviations are as follows: N is the number of individual fog water samples taken, LWC is liquid water content, -/+ =  $\Sigma$  anions/ $\Sigma$  cations,  $\Delta$  =  $\Sigma$  anions -  $\Sigma$  cations, and  $\Sigma$  is sum of all ions.

<sup>a</sup>S(IV) is assumed to be in monovalent form.

<sup>b</sup>Correction for bicarbonate is not included.

<sup>c</sup>The S(IV) concentration for six samples was  $>300 \mu\text{mol L}^{-1}$ , which is the upper limit for the colorimetric method.

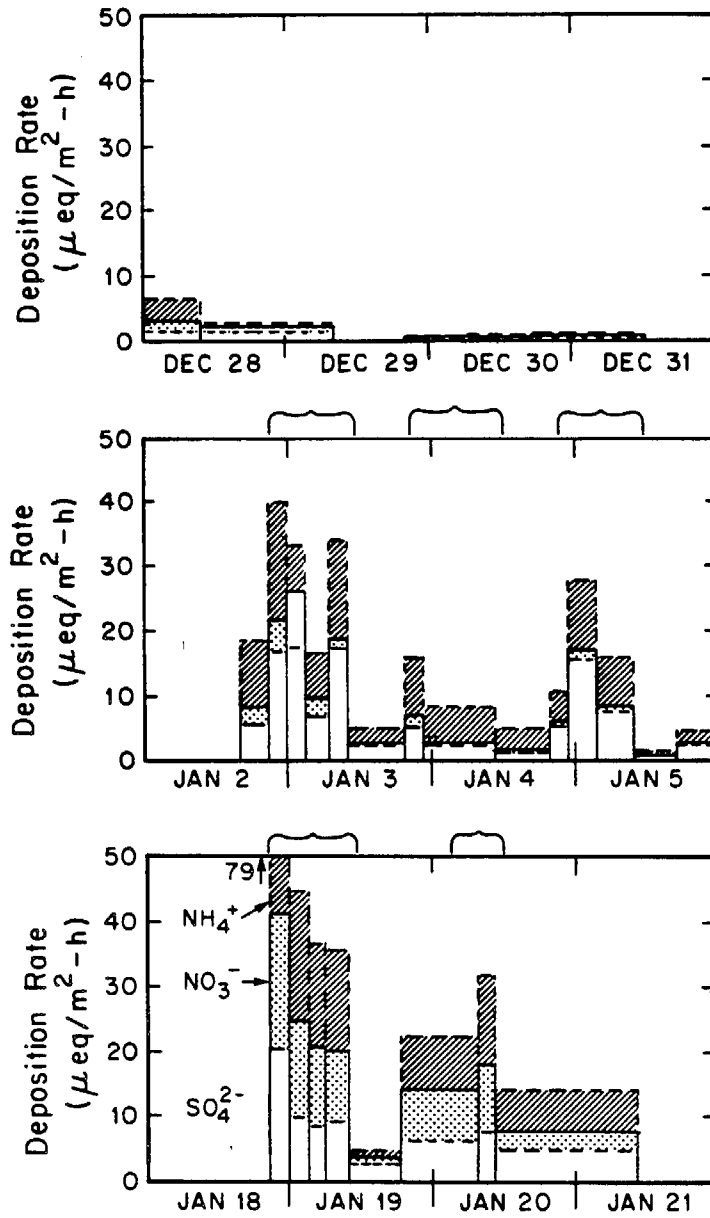


Figure 9. Deposition rates of major ions to Petri dish collectors at the Bakersfield Airport (NW) site. Braces above figures indicate periods of fog.

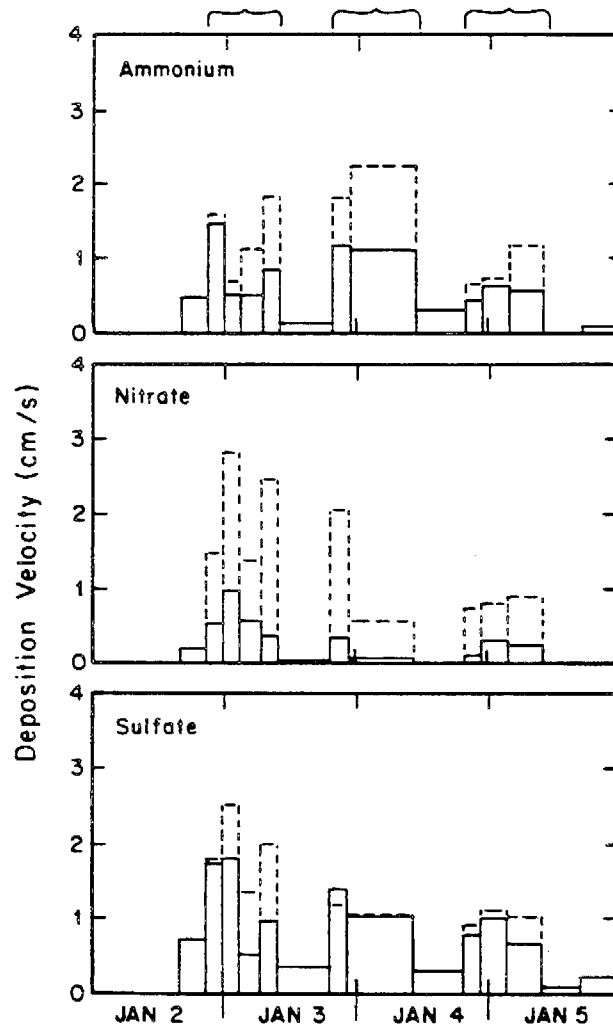


Figure 10. Deposition velocities for major ions measured to Petri dish collectors at NW site. Concurrent values of  $V_d$  and  $V_{d,fog}$  are shown as solid and dashed lines, respectively. Braces over figures indicate periods of fog.

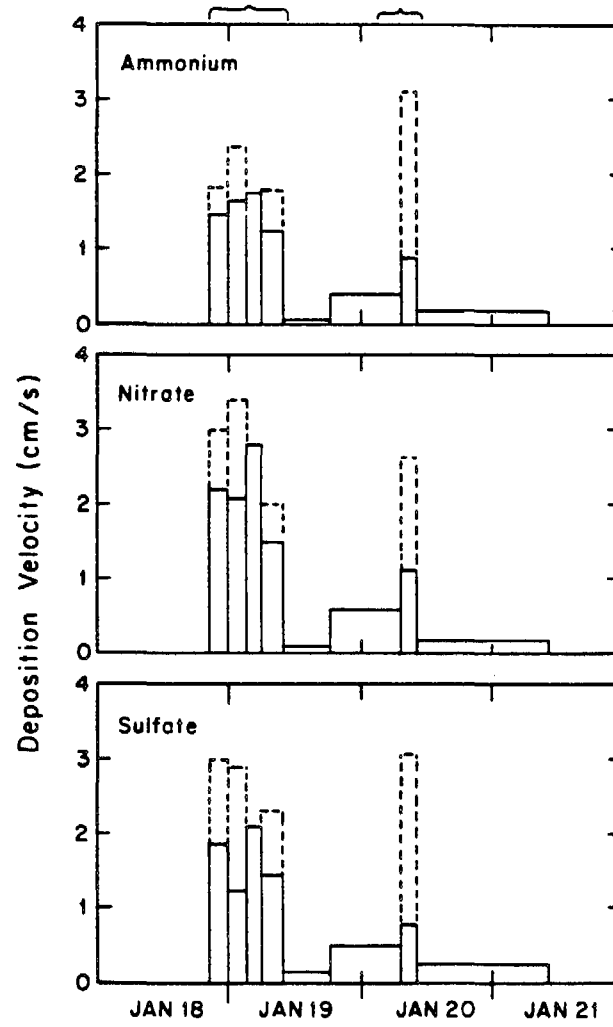


Figure 10.—Continued.

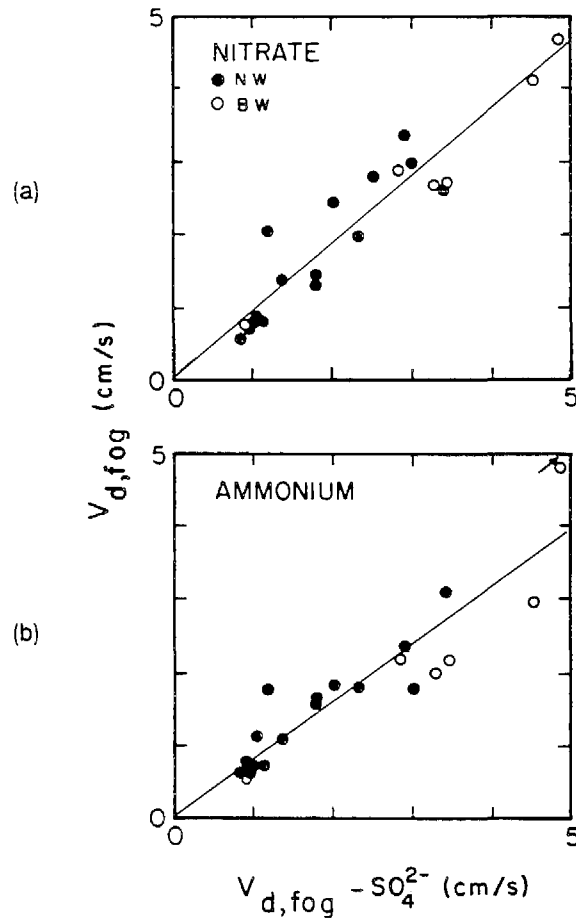


Figure 11. Fog deposition velocities ( $V_{d,fog}$ ) to Petri dish collectors at NW site. The graphs are (a) nitrate and (b) ammonium versus sulfate. Lines indicate best fit of data. Key: ● is Bakersfield Airport (NW) data, and ○ is Buttonwillow (BW) data.

LWC was used for which the relative error was less ( $\pm 20\%$ ). For the data, no correlation with LWC was found for droplet solute deposition. The rates were comparable to the terminal settling velocities of typical fog droplets.

Volatile loss of ammonium ion from the fog-wetted deposition surfaces was indicated. This loss may have been enhanced by the fallout of calcareous dust onto the hydrophobic collector surface. However, under normal conditions,  $NH_3$  loss via volatilization of fog-deposited ammonium aerosol can also be expected to some degree.

Substantially greater deposition rates ( $V_d$ ) for sulfate were found

compared with nitrate in nonacidic fogs. This difference has been attributed to more efficient scavenging of soluble sulfur species by fog droplets. Sulfate deposition during fog was in the range of 0.5–2.0 cm s<sup>-1</sup>, and had a median value of about 1 cm s<sup>-1</sup>; the nitrate rate was generally 50% less than that for sulfate. In nonacidic fogs, as on January 2–3 and 4–5 (Figures 12 and 13, respectively), nitrate scavenging was uniformly low, and the fraction of sulfate incorporated into the droplet phase rose with increasing LWC. For the acidic fog on January 18–19 (pH < 4), the fraction of ambient nitrate scavenged by the fog droplet was much higher and increased with LWC (Figure 14). On this later date, higher atmospheric acidity is believed to have altered N(V) partitioning prior to fog formation. Higher acidity would support higher HNO<sub>3</sub>(g) concentrations in the prefog air, followed by subsequent nitric acid scavenging once the fog formed. However, measured HNO<sub>3</sub>(g) was not as great as the observed enhancement of N(V) scavenging. Depletion of gaseous ammonia accompanied the period of higher atmospheric acidity and low pH fog, and this depletion is believed to have caused a reduction in the formation of the smaller NH<sub>4</sub>NO<sub>3</sub> aerosol. In the absence of detectable NH<sub>3</sub>(g), newly formed N(V) was apparently incorporated into a coarser aerosol fraction and readily scavenged in fog.

**Mass Balance Analysis.** When widespread stagnation suppresses convective transport out of the basin, the accumulation of pollutants may proceed. The processes that control the fates of primary emissions in the atmosphere are varied and complex (96). Nonetheless, profiles of concentrations versus time have been reasonably interpreted based on continuous-flow, stirred-tank considerations of pollutant inputs and removal pathways (97). This accumulation of atmospheric constituents is governed by primary emissions, in situ transformations (production or loss terms), intrabasin circulation, ventilation, and removal by deposition to ground surfaces. The mixing height,  $H$ , controls the volume in which these processes occur. For example, mass balances for S(IV) and S(VI) may be described by

$$\frac{d(\text{S(IV)})}{dt} = \frac{E_{\text{SO}_2}}{H} - k_s (\text{SO}_2) - \nabla \cdot ((\text{SO}_2)\vec{V}) - \frac{(\text{SO}_2)}{\tau_v} - V_d \frac{(\text{SO}_2)}{H} \quad (21)$$

(a)                      (b)                      (c)                      (d)                      (e)

$$\frac{d(\text{S(VI)})}{dt} = k_s (\text{SO}_2) - \nabla \cdot ((\text{SO}_4^{2-})\vec{V}) - \frac{(\text{SO}_4^{2-})}{\tau_v} - V_d \frac{(\text{SO}_4^{2-})}{H} \quad (22)$$

where  $E$  is an areal emission rate (mol m<sup>-2</sup> h<sup>-1</sup>);  $k_s$  is a pseudo-first-order rate constant for S(IV) oxidation (h<sup>-1</sup>);  $V$  is the horizontal transport vector (m h<sup>-1</sup>);  $\tau_v$  (h) is the characteristic time for vertical ventilation; and  $\nabla$  is

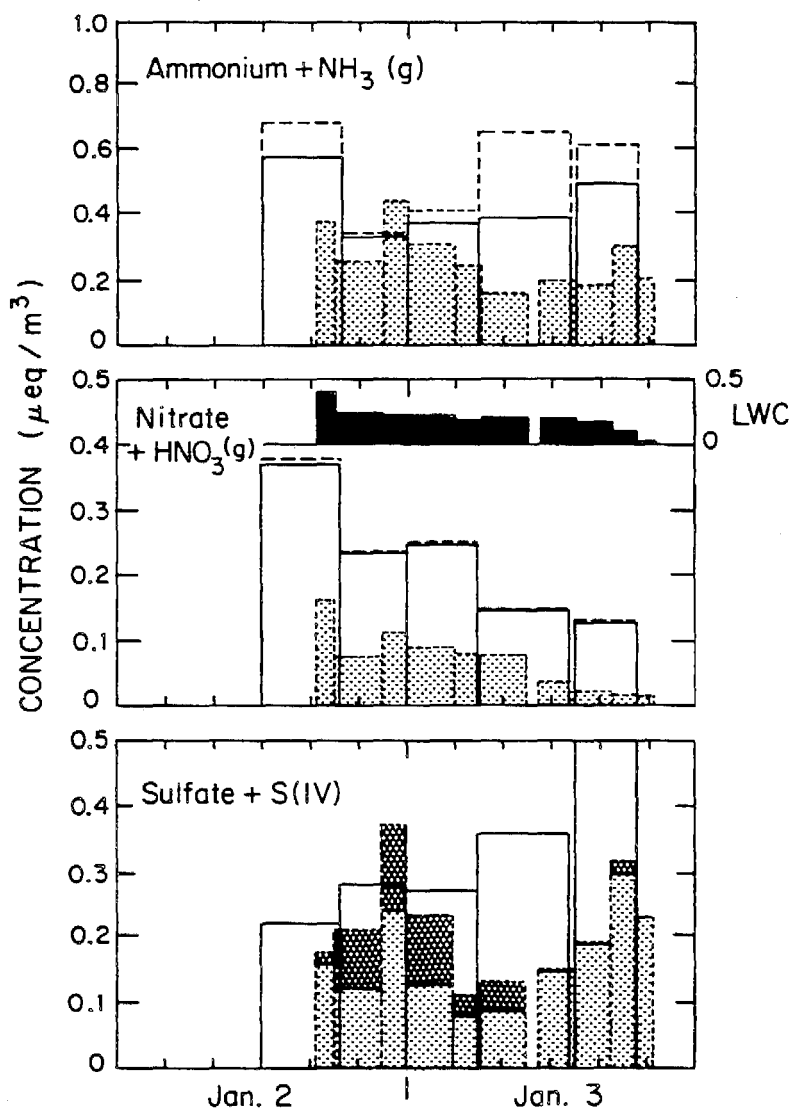


Figure 12. Total (line) and fog water (shaded) concentrations of  $\text{N}(-\text{III})$ ,  $\text{N}(\text{V})$ , and sulfur species at Bakersfield Airport site on January 2-3. Gaseous species (dashed line) and liquid water content (black) are also shown. Fog water  $\text{S}(\text{IV})$  is indicated by heavy shading.

the divergence vector operator. Deposition velocities ( $\text{m h}^{-1}$ ) will depend on the species and the phase: gas, aerosol, or droplet. Similar expressions may be formulated for nitrogen species, although the chemical transformations involving  $\text{NO}_x$  species are far more complex.

Under wintertime stagnation conditions in the southern San Joaquin

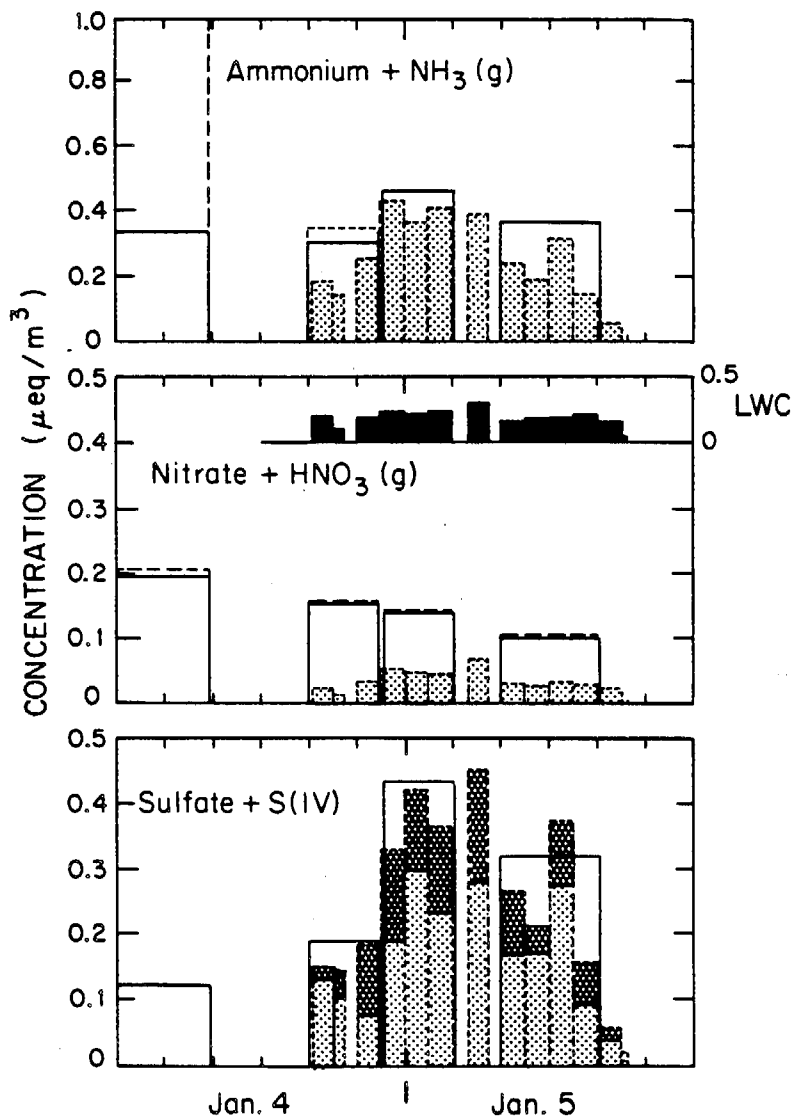


Figure 13. Same as Figure 12, but for January 4-5.

Valley,  $\tau_v = 3-5$  days or more (98). Time scales characteristic of emission and deposition rates are strongly dependent on mixing height. Mixing heights during stagnation episodes are generally 200-800 m above the valley floor. In the years we conducted studies, widespread fog occurred when the mixing height was  $\leq 400$  m (39, 97). For low wind speeds, deposition velocities can range from  $\sim 0.05$  cm  $s^{-1}$  for submicrometer aerosols to  $\sim 2$  cm  $s^{-1}$  for fog droplets or reactive gases. Hence,  $\tau_d$ , given

as  $H/V_d$ , can range from  $>3$  days to  $<3$  h. For sulfate aerosol, this range is largely dependent on the presence or absence of fog.

A characteristic time for S(IV) oxidation may be given as  $k_s^{-1}$ . In reality, in situ transformations are rarely simple first-order processes dependent on reactant concentration alone. These rates will depend on the nature and concentration of oxidants, metals, and other catalytic components, in addition to pH and LWC (99). The pseudo-first-order

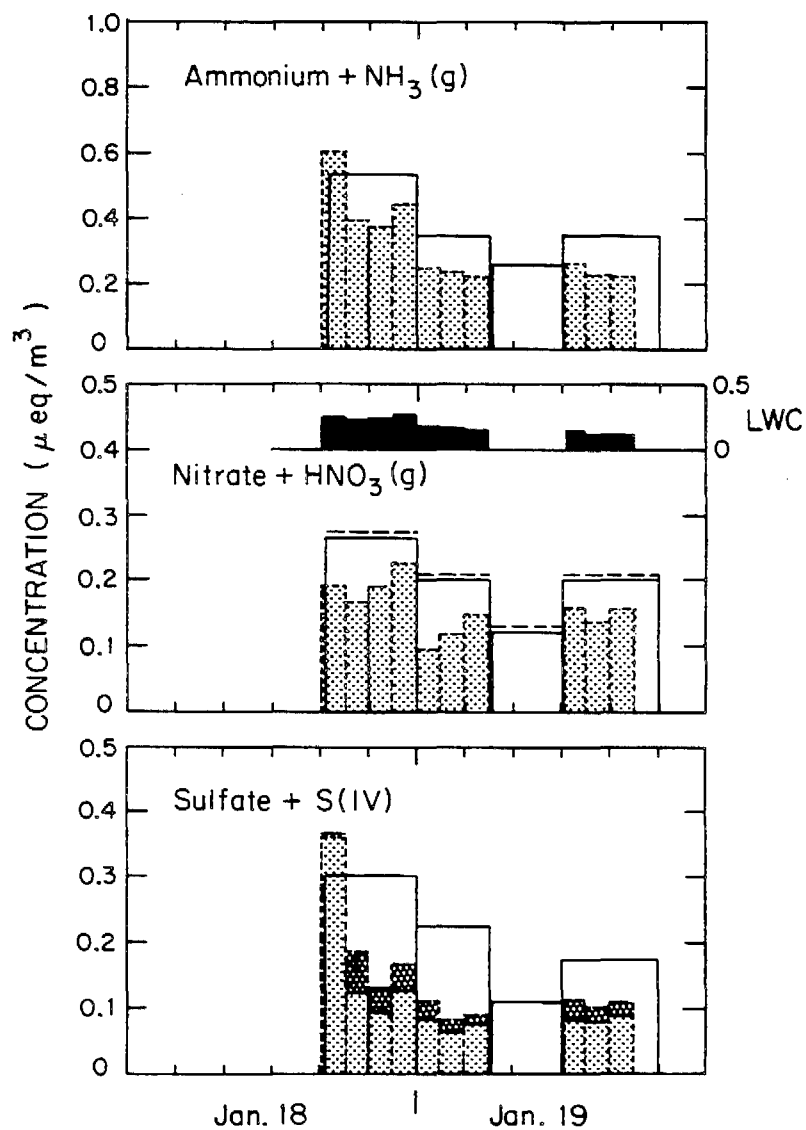


Figure 14. Same as Figure 12, but for January 18-19.

rate constant is a convenient means to parameterize the observed atmospheric kinetics. The oxidation reactions are thought to proceed more rapidly in fog, although interpretations of our prior San Joaquin Valley field measurements have not statistically verified this assertion (39, 97). Using values in a range given by Jacob et al. ( $1\% < k_s < 10\% \text{ h}^{-1}$ ), we estimated the time for S(IV) oxidation between 2 and 24 h (to lower the concentration by a factor of  $e$ ).

Emission inventories for  $\text{SO}_2$ ,  $\text{NO}_x$ , and  $\text{NH}_3$  have been determined by Jacob et al. (97) for the southern San Joaquin Valley as 192, 190, and 79 tons  $\text{day}^{-1}$ . These emissions translate to 29, 20, and 22  $\mu\text{equiv m}^{-2} \text{ h}^{-1}$  when expressed as area-wide averages. These units correspond to the secondary products; therefore,  $\text{SO}_2$  yields 2 equiv  $\text{mol}^{-1}$ . A characteristic time, taken here as the time required for emissions to replace a given atmospheric loading of pollutant  $C$ , would be expressed as  $\tau_E = (C)H/E$ . Given ( $\text{SO}_2$ )  $\sim 10$  ppb and  $H \sim 400$  m, the calculated  $\tau_E$  for  $\text{SO}_2$  is on the order of 12 h; for  $H \sim 200$  m,  $\tau_E$  is only half of this value. This term is useful to assess whether a balance of sources and sinks has been achieved. For example, when the time scales for loss terms are longer than  $\tau_E$ , atmospheric concentrations will increase. Higher concentrations of  $\text{NO}_x$  are a clear indication that  $\text{NO}_x$  depletion rates are slower than either  $\text{SO}_2$  or  $\text{NH}_3$ , because sources are comparable.

During dense fog, deposition becomes the predominant loss term for secondary aerosol species. Flux measurements to surrogate surfaces demonstrated that removal from the atmosphere can be very rapid. In Table IV, characteristic times have been calculated for deposition during dense fog. These values were determined from the total solute fluxes, mixing heights, and average aerosol concentrations measured during the individual events. The characteristic removal times were calculated to be 6–12 h for these periods with the exception of N(V). As discussed previously, during the sampling periods of acidic atmospheric condition (January 19 and 20), there was a distinct increase in the relative scavenging efficiency for nitrate species into fog water. The deposition rate for N(V) also increased for these events, and this can be seen in much lower  $\tau_d$  values for nitrate compared to the earlier fog events when  $\text{pH} \geq 5$ . Between the occurrences of fog, aerosol deposition was substantially reduced. Deposition velocities were generally an order of magnitude below in-fog values. Fogs persisted more than 50% of the time during January 2–5. In the absence of production terms, aerosol components would be more than 90% depleted during protracted fog episodes. However, such a net depletion was not observed. By inference, in situ production rates must have at least equaled the deposition rates.

Advection in this environment is difficult to assess. Wind directions are found to be erratic at valley stations during stagnation episodes (100). Resultant winds for the early January period were  $< 1 \text{ m s}^{-1}$  at all stations; therefore, net cross-valley transport would require  $\sim 1$  day. Before Jan-

Table IV. Characteristic Removal Times and Production Rates in San Joaquin Valley Fogs

Location and Date	Duration (h)	H (m)	$\tau_d$ (h)			Production Rate (ppb h <sup>-1</sup> )		
			NH <sub>4</sub> <sup>+</sup>	NO <sub>3</sub> <sup>-</sup>	SO <sub>4</sub> <sup>2-</sup>	E <sub>A</sub>	E <sub>N</sub>	E <sub>S</sub>
Bakersfield Airport (NW)								
Dec. 28, 1984	4	200	6	15	6	1.5	0.3	0.5
Jan. 2-3, 1985	14	240	6	10	6	1.5	0.4	0.7
Jan. 3-4, 1985	12	210	6	42	6	0.6	0.1	0.2
Jan. 4-5, 1985	12	230	11	27	7	0.8	0.1	0.5
Jan. 14, 1985	3	500	12	22	7	0.7	0.2	0.4
Jan. 18-19, 1985	14	300	6	4	5	1.5	1.1	0.5
Jan. 20, 1985	7	350	11	9	12	0.9	0.7	0.3
Buttonwillow (BW)								
Jan. 2-3, 1985	17	290	7	6	7	2.3	1.4	0.3
Jan. 3-4, 1985	17	260	10	17	9	0.5	0.2	0.1
Jan. 4-5, 1985	15	230	7	18	6	0.9	0.2	0.2

NOTE: The characteristic time for pollutant removal ( $\tau_d$ ) was calculated from the equation  $\tau_d = H/V_d$ , where  $V_d$  is the flux divided by the ambient concentration. The production or emission rate ( $E_A$ ,  $E_N$ , or  $E_S$ ) was determined as the deposition divided by the product of duration and height above ground level ( $H$ ).

uary 1, the concentrations of sulfate were uniformly low on both sides of the valley; after January 1, higher sulfate values were monitored in Bakersfield than in areas to the west or north. The spatial gradient for sulfate across the valley indicated that advection of sulfate aerosol was a less prominent term during January 2-5. Clearly, deposition of sulfate was more rapid than its transport away from the source region.

However, nitrate aerosol concentrations were uniform throughout the sampling network at that same time. Similar temporal variations were also observed at all valley sites except McKittrick, which was above the inversion base throughout that period. Because the deposition rates measured for nitrate were much lower than for sulfate during that period, more complete mixing could have occurred. This uniformity was probably aided by more widely dispersed emissions of  $\text{NO}_x$ .

For the two sites in the Bakersfield area, Bakersfield Airport (NW) and downtown Bakersfield (BA), concurrently measured aerosol concentrations agreed within 20% in most cases (12 for  $\text{NO}_3^-$  and 10 for  $\text{SO}_4^{2-}$  for 13 sampling periods), even though temporal variations spanned a factor of 5. Simultaneous peaks in  $\text{NH}_3$  concentrations were further indication of the spatial homogeneity at the two sites. However, it is impossible to state unequivocally that short-term changes at a particular site were due to in situ transportation rather than localized transport. Without a network of greater spatial resolution, the interpretation of sequential S(VI) or N(V) concentrations in terms of a generalized continuity-equation analysis would be moot. Nonetheless, advection of pollutant species away from this source region must represent a sink over longer time scales.

As a lower limit, we calculated production rates necessary to balance removal rates of aerosol species measured during fog (i.e., the production rate is proportionate to the deposition flux divided by  $H$ ). Essentially, this calculation equates terms (b) and (e) in equation 22 and neglects the rest. Production rates have been calculated in units of the primary emissions,  $\text{NH}_3$ ,  $\text{NO}_x$ , and  $\text{SO}_2$  (Table IV). Sulfur dioxide values measured at the fog study sites were mostly  $\leq 10$  ppb, although spatial variability of  $\text{SO}_2$ , especially near the oil fields, makes the calculation of an areal average concentration questionable. Assuming 10 ppb for the gaseous concentration, the pseudo-first-order S(IV) oxidation rates were calculated to be 2%-7%  $\text{h}^{-1}$ . Considering that advection represented a loss term for the Bakersfield area, the total sinks were likely to have been even greater than measured by deposition alone. The calculated S(IV) oxidation rates at Buttonwillow (BW) were not as great; assuming that  $\text{SO}_2$  concentrations were a factor of 2 less at the BW site compared with Bakersfield, the rates of S(IV) oxidation at the two locations in dense fog were similar. The S(VI) production and deposition rates should have been comparable at these sites because the meteorological conditions were similar (i.e., widespread nighttime fog and afternoon haze).

**Caveats.** Fog deposition as measured to flat surfaces or buckets represented a lower limit to rates occurring in the southern San Joaquin Valley. The NW site was chosen for its open and featureless terrain. In many ways, this site was characteristic of wintertime land use in this region. The majority of the southern San Joaquin Valley is cropland (43%) or rangeland (44%), and the remaining portions of the valley are orchard (8%), residential-commercial (4%), or forest (1%). In areas of tall (dense or sparse) canopy or buildings, wind profiles would be more turbulent, and canopy-top wind speeds would be closer to the National Weather Service sensor (10 m) values rather than to the low values measured close to the open field. Simply the presence of bare trees would substantially increase the surface area for pollutant deposition. Droplet impaction becomes important under these circumstances (11). In such cases,  $V_{d,fog}$ , and hence,  $V_d$ , would be adjusted upwards. Fog deposition may therefore lead to even greater pollutant influx to these areas. Although this influx may be of significance for certain receptor areas, we believe the effect is relatively unimportant to the conclusion regarding the dominance of sedimentation and the range of deposition values we have reported.

Finally, these measurements were specific to particles and droplets. Although we are convinced that dry deposition of  $SO_2$ , for example, did not significantly contribute to our measurements, this sink for S(IV) may itself be substantial. Moreover, scavenging of  $SO_2$  by droplets aided in its deposition during fog. In addition to the chemical transformations of S(IV), the removal of  $SO_2$  to surfaces, although not studied here, is an important term in the overall sulfur budget. Also,  $HNO_3$  deposition may have an important role in N(V) removal under certain circumstances.

**Precipitation Scavenging.** In the case of the rainfall event, the total amount of material brought to the ground was 2-5 times greater than the overburden of pollutants in the air (i.e., the product of ambient concentration and mixing height) prior to the rain (Figure 15). After the initial loading of accumulated pollutants was washed (or ventilated) out of the air mass, additional nitrate and sulfate must come from the transformation of primary emissions. Low  $SO_2$  concentrations were measured during the rainfall period; simultaneously, sulfate deposition was large. This measurement clearly indicated a period in which rapid S(IV) oxidation must have occurred in the presence of an aqueous phase. The smaller fluxes of nitrate suggested either a slower rate of N(V) formation for the same period or less efficient precipitation scavenging of secondary nitrate. However, without a detailed knowledge of atmospheric mixing and below-cloud processes, in situ oxidation rates cannot be determined from these rainfall measurements.

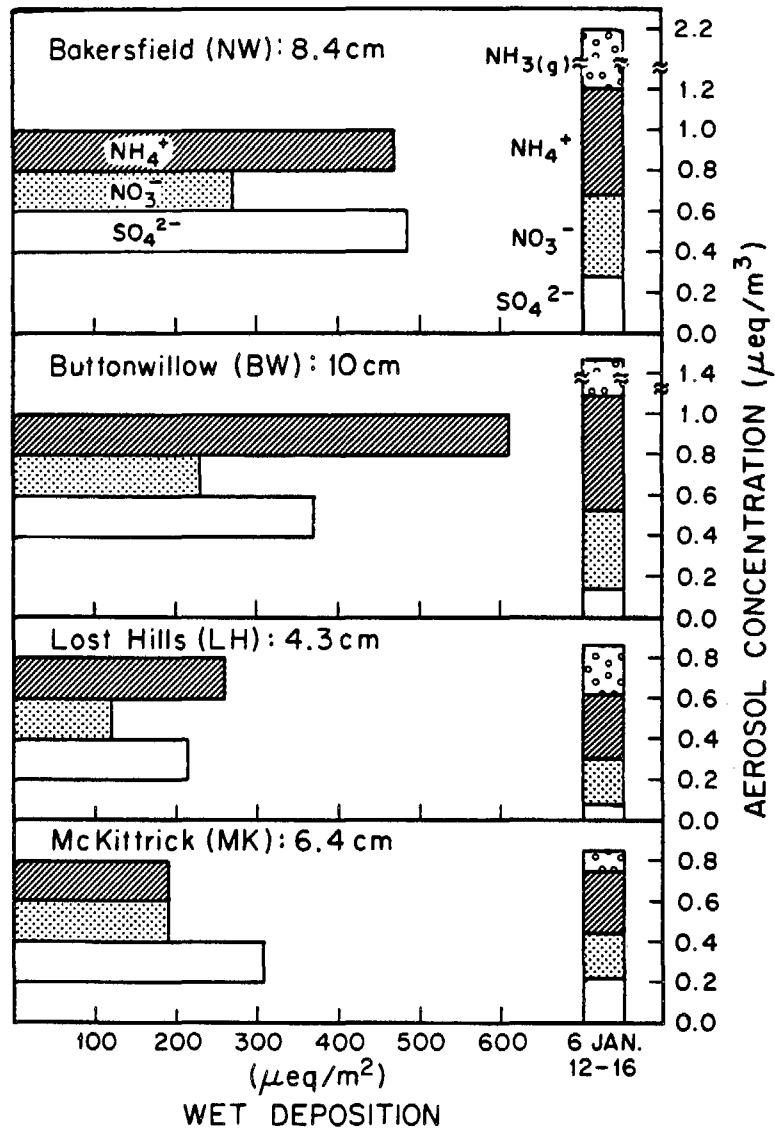


Figure 15. Wet deposition of major ions for four San Joaquin Valley sites measured on January 6-8, 1985. Filter data for the sampling interval immediately preceding rainfall are also shown.

### Discussion

The efficacy of fog in scavenging gaseous and aerosol species and enhancing their removal can cause the fog to be the dominant factor controlling ambient levels reached by pollutants during wintertime stag-

nation episodes. The measurements of depositional flux during the stagnation periods in the winter of 1985 illustrated the differences between episodes with dense fog and those when fog was absent. Detailed fog water and air quality data were also collected for the winters of 1983 and 1984 as part of our earlier field programs. These former studies included periods with and without dense, widespread fog. Concentrations of the major species in the fog water, aerosols, and gas phases are compared in Table V. The comparison is limited to parameters measured in the Bakersfield area. The values presented were for periods of stagnation when mixing heights were low and concentrations in the air had achieved apparent steady-state levels. Given the characteristic time for fog deposition and the emission rates of sulfur species, a steady state for sulfate could be attained in less than 1 day. Nonfoggy intervals require much longer times, and true steady-state levels may not have been fully reached before a change in meteorological conditions occurred. This type of comparison is readily acknowledged to be far from conclusive because other factors (e.g., daytime insolation, oxidant concentrations, and wind trajectories) have not been evaluated. We used this comparison primarily to point out the relationships that these unique data sets have provided.

Mixing heights were comparable during the six episodes. A disparity between two regimes is readily apparent with respect to aerosol nitrate and sulfate concentrations. The highest values were associated with January 2-6, 1983, and January 2-6, 1984. These were periods of low clouds when fog was absent. Average concentrations of particulate sulfate exceeding California air quality standards ( $25 \mu\text{g m}^{-3}$  or  $520 \text{ nequiv m}^{-3}$ ) were monitored during both episodes. Periods of dense fog led to lower concentrations of particulate loading, which leads to air of better quality despite lesser visibility.

The January 2-5, 1985 samples complemented a data set of pre-

Table V. Fog Water and Air Quality

Date	H (m)	pH	Fog Water			
			$\text{NH}_4^-$ (mequiv $\text{L}^{-1}$ )	$\text{NO}_3^-$ (mequiv $\text{L}^{-1}$ )	$\text{SO}_4^{2-}$ (mequiv $\text{L}^{-1}$ )	%S(IV)
Dec. 30-31, 1982 <sup>a</sup>	200	4.1	1600	850	800	62
Jan. 2-6, 1983 <sup>a</sup>	400					
Jan. 6-8, 1983 <sup>a</sup>	350	3.9	2600	900	1600	38
Jan. 11-15, 1983 <sup>a</sup>	300	3.6	1400	700	900	57
Jan. 2-6, 1984 <sup>a</sup>	350					
Jan. 2-5, 1985 <sup>b</sup>	200	4.9	1200	250	800	32
Jan. 18-20, 1985 <sup>b</sup>	300	3.9	1900	1000	600	22

<sup>a</sup>Measurements made at downtown Bakersfield (BA) site.

<sup>b</sup>Measurements made at Bakersfield Airport (NW) site. Parentheses denote BA values for same time period.

dominantly acidic fogs measured in January 1983. Simultaneous fog water and aerosol measurements were not made during the 1982-1983 study, but the ionic ratios indicate that N(V) scavenging was as great or greater than for sulfate during these low pH fogs. Both N(V) and S(VI) production were important sources of atmospheric acidity. Emission inventories for all producers during the selected periods are not available, but data on the east side support an assumption that year-to-year differences in primary emitter operations were not a factor (D. Anderson, Texaco, Inc., private communication). No obvious effect of acidity on SO<sub>2</sub> levels was observed; gaseous concentrations were uniformly low for both years. Interestingly, dissolution of S(IV) in fog water was not reduced in the acidic regime of the earlier year (Table V), as might be expected from gas-aqueous equilibria.

The primary determinant for acidity is most likely the relative N(-III) abundance as discussed in Jacob et al. (97) with respect to spatial patterns in the region. In an ammonia source region, factors can suppress or accelerate NH<sub>3</sub> release. Temperature, moisture, and land cover may be primary factors. Dawson (101) showed that there are strong dependencies for soil release of ammonia; release increases with temperature and with soil moisture until 20% saturation and then decreases. Uptake by vegetation can drastically reduce the net release of ammonia (102). Hutchinson et al. (103) measured ammonia release from a large cattle feedlot and found lower fluxes when the surface was wet from rain. However, this lowering was offset by greater-than-average rates while the surface dried.

The January 2-5, 1985 episode distinguished itself in one important regard. During other episodes, no daytime clearing occurred. Heavy overcast generally continued after the fog lifted. On the afternoons of the early January 1985 episode, there were periods of hazy sunshine and appreciable warming. This warming would promote ammonia release,

during Winter Stagnation Episodes

Aerosol			Gas			Dense Fog	Ref.
NH <sub>4</sub> <sup>+</sup> (nequiv m <sup>3</sup> )	NO <sub>3</sub> <sup>-</sup> (nequiv m <sup>3</sup> )	SO <sub>4</sub> <sup>2-</sup> (nequiv m <sup>3</sup> )	NH <sub>3</sub> (ppb)	NO <sub>x</sub> (ppb)	SO <sub>2</sub> (ppb)		
600	280	280		100	20	Yes	39
900	300	900		100	25	No	39
600	150	450		150	20	Yes	39
300	40	200		200	40	Yes	39
1000	400	700	1	100	20	No	97
350	190	210	9	25	10	Yes	this study
(380)	(210)	(270)	(6)	(100)	(10)		
510	280	320	<0.5	(50)	(10)	Yes	this study

especially from feedlots and agricultural soils. Despite this cooling, the ground would maintain higher temperature at nighttime as well. On the other hand, the acidification of the San Joaquin Valley atmosphere would be promoted by cooler and steady overcast conditions. Ammonia release also may be reduced in postrainfall periods. At the same time, this moisture is often important in sustaining widespread fog.

### Summary

The shallow and poorly ventilated mixed layer of the San Joaquin Valley under the intense temperature inversion represented a reactor of limited volume. A comparison was made between the mass deposited and the overburden of pollutants (i.e., the product of mixing height and ambient loading). For S(VI) and N(-III) species, 2-3 times the apparent overburden was deposited during prolonged fogs. This deposition should have caused substantial depletion of atmospheric concentrations; however, this depletion was not observed. Steady aerosol sulfate concentrations required S(IV) oxidation to proceed rapidly. A pseudo-first-order constant for SO<sub>2</sub> oxidation was calculated to be in the range of 2%-7% h<sup>-1</sup>. The true rate may be several times higher because (a) the reactant concentrations were frequently below the value (10 ppb) used to make the calculation, (b) the depositional flux measurements tacitly neglected the sink due to droplet impaction, and (c) advective loss terms in the mass balance equation were neglected in the source region. In similar fashion, ammonia emissions were calculated to be approximately 1 ppb h<sup>-1</sup> in order to balance solute removal in fog.

The two processes important for the determination of ambient sulfate concentration were removal by deposition and production by S(IV) oxidation. Measurements made during three wintertime fog-aerosol studies were summarized to consider the overall mass balance during stagnation episodes. This data set supported the hypothesis that fog deposition lowered the ambient concentrations of aerosol sulfate and nitrate during stagnation periods compared with periods of no fog. However, the importance of dry deposition of SO<sub>2</sub>, sulfate production in haze aerosol, and the contribution of impaction to droplet fluxes needs to be more fully investigated. Finally, the conditions under which fog water acidity was high were related to factors favoring ammonia release from sources (e.g., higher soil moisture and temperature).

### Appendix—The Droplet Growth Equation

The droplet growth equation is

$$D_o \frac{dD_o}{dt} = \frac{S_v - a_w e^B}{C + E (A-1) a_w e^B} \quad (\text{A1})$$

where

$$A = \frac{M_w L}{RT} \quad (\text{A2})$$

$$B = \frac{4M_w \sigma}{\rho_w D_o RT} \quad (\text{A3})$$

$$C = \frac{\rho_s RT}{4D_m M_w e_s(T)} \quad (\text{A4})$$

$$E = \frac{\rho_s L}{4kT} \quad (\text{A5})$$

$$a_w = e^{\left(-\phi \frac{n_s}{n_w}\right)} \quad (\text{A6})$$

For the activation point,

$$\frac{dD_o}{dt} = 0 \quad (\text{A7})$$

$$D_o = D_{\text{act}} \quad (\text{A8})$$

$$S_v = 1 + SS_{\text{cr}} \quad (\text{A9})$$

These equations yield

$$D_{\text{act}} = \left(\frac{3 \text{LNA}}{B}\right)^{1/2} \quad (\text{A10})$$

$$SS_{\text{cr}} = \frac{2}{3\sqrt{3}} \left(\frac{B^3}{\text{LNA}}\right)^{1/2} \quad (\text{A11})$$

$$= K D_{\text{dry}}^{-3/2} \quad (\text{A12})$$

In equation A10, LNA is defined as

$$\text{LNA} = \frac{M_w \rho_s}{M_s \rho_w} D_{\text{dry}}^3 \quad (\text{A13})$$

Parameters for these equations are defined as follows:

$D_o, D_{\text{act}}$	droplet diameter and diameter at activation point, respectively
$D_{\text{dry}}$	dry diameter for hygroscopic aerosol
$e, e_s(T)$	ambient and saturation water vapor pressure at $T$ , respectively

$S_v$	ambient water vapor saturation ratio, $e/e_s(T)$
$SS_{cr}$	critical supersaturation
$\rho_w, \rho_s$	density of pure water and solute salt, respectively
$R$	gas constant
$T$	temperature (K)
$L$	latent heat of evaporation
$D_m$	molecular diffusivity of water vapor in air
$k$	heat conductivity of air
$\sigma$	surface tension of water
$M_w, M_s$	molecular weight of water and dissociated solute ions, respectively
$n_w, n_s$	number of moles of water and dissociated solute in droplet, respectively
$a_w$	activity of water in droplet
$\phi$	osmotic coefficient of water in solution (assumed to equal 1)

### *Abbreviations and Symbols*

$\nabla$	gradient
$\mu$	dynamic viscosity of air
$\eta$	fraction of particles that impact receptor surface
$\rho_s$	density of solute salt
$\rho_w$	density of pure water
$\sigma$	surface tension of water
$\tau_E$	time for emissions to replace a given atmospheric loading of pollutant $C$
$\tau_v$	characteristic time for vertical ventilation
$\phi$	osmotic coefficient of water in solution
$a_w$	activity of water in a droplet
$A$	constant
$B$	constant
$C$	concentration of particles; constant
$(C)$	total concentration of species $C$ in the atmosphere
$[C]$	aqueous concentration of species $C$ in fog water
$(C)_a$	concentration of species $C$ in the nonactivated aerosol phase
$(C)_f$	concentration of species $C$ in the fog water phase
$(C)_g$	concentration of species $C$ in the gas phase
$d$	height
$d_f$	diameter of cylinder
$D_{act}$	activation size (diameter)
$D_{dry}$	dry diameter
$D_{eq}$	equilibrium diameter
$D_m$	molecular diffusivity of water vapor in air

$D_o$	droplet diameter
$e$	the exponential; ambient water vapor pressure
$e_s$	saturation water vapor pressure
$E$	ratio of deposition to sedimentation velocities; areal emission rate
$f^a$	nonactivated fraction
$f_c$	fraction of solute partitioning into the droplet phase
$F_c$	overall fraction of species $C$
$g$	gravitational acceleration
$H$	canopy height
$H_A$	Henry's law constant for ammonia
$H_F$	Henry's law constant for formaldehyde
$H_N^*$	modified Henry's law constant for nitrogen
$H_S$	Henry's law constant for sulfur (IV)
$J$	flux of particles per unit area of aerosol
$J_a$	aerodynamic layer flux
$J_d$	depositional flux
$k$	heat conductivity of air; von Karman's constant
$K$	proportionality coefficient
$K_B$	dissociation constant for ammonia
$K_F$	formation constant for HMSA
$K_p$	eddy diffusivity
$K_s$	dissociation constant for sulfur
$K_{s1}$	first dissociation constant for $SO_2$ (aq)
$K_{s2}$	second dissociation constant for $SO_2$ (aq)
$K_w$	dissociation constant for water
$L$	latent heat of evaporation
LWC	liquid water content
$M$	fog water mass
$M_s$	molecular weight of dissociated solute ions
$M_T$	total mass
$M_w$	molecular weight of water
$n_s$	number of moles of solute in droplet
$n_w$	number of moles of water in droplet
$N$	number of cylinders per unit area of ground
pK	- log dissociation constant
$P_c$	partial pressure of species $C$
$R$	gas constant
$R_f$	radius of cylinder
Re	Reynolds number
RH	relative humidity
St	Stokes number
$S_v$	ambient water vapor saturation ratio
$SS_{cr}$	critical supersaturation

$t$	time
$T$	temperature
$U$	horizontal wind speed
$U^*$	frictional velocity
$U_s$	relative velocity between particle and obstacle
$V$	horizontal transport vector
$V_d$	depositional velocity
$V_{d,fog}$	depositional velocity due to fog
$V_s$	sedimentation velocity
$Z_o$	roughness scale
$z_s$	particle sink

### Acknowledgments

We are grateful to the California Air Resources Board (CARB) for their financial support (CARB A4-075-32) and their assistance in the field aspects of this project. We appreciate the guidance and assistance provided by the program manager, Eric Fujita. We are also indebted to our colleagues, Daniel Jacob and J. William Munger, who spent many long hours in the field working on aspects of this research.

### References

1. Liljestrand, H. M. Ph.D. Thesis, California Institute of Technology, Pasadena, 1980.
2. Bischoff, W. D.; Paterson, V. L.; Mackenzie, F. T. In *Geological Aspects of Acid Deposition*; Bricker, O. P., Ed.; Acid Precipitation Series; Butterworth: Boston, 1984; Vol. 7, pp 1-21.
3. Azevedo, J.; Morgan, D. L. *Ecology* 1974, 55, 1135-1141.
4. Schlesinger, W. H.; Reiners, W. A. *Ecology* 1974, 55, 378-386.
5. Peterson, T. W.; Seinfeld, J. H. In *Advances in Environmental Science and Technology*; Pitts, J. N.; Metcalf, R. L., Eds.; Wiley: New York, 1980; Vol. 10, pp 125-180.
6. Barrett, E.; Parungo, F. P.; Pueschl, R. F. *Meteorol. Res.* 1979, 32, 136-149.
7. Schwartz, S. E.; Freiberg, J. E. *Atmos. Environ.* 1981, 15, 1129-1144.
8. Slinn, W. G. N. *Atmos. Environ.* 1981, 16, 1785-1794.
9. Chamberlain, A. C. *Proc. R. Soc.* 1967, 296, 45-70.
10. Brimblecombe, P. *Tellus* 1978, 30, 151-157.
11. Lovett, G. M. *Atmos. Environ.* 1984, 18, 361-371.
12. Wisniewski, J. *Water, Air, Soil Pollut.* 1982, 17, 361-377.
13. Lindberg, S. E.; Harriss, R. C.; Turner, R. R. *Science (Washington, D.C.)* 1982, 215, 1609-1611.
14. Waldman, J. M.; Munger, J. W.; Jacob, D. J.; Hoffmann, M. R. *Tellus* 1985, 37B, 91-108.
15. Thomas, M. D.; Hendricks, R. H.; Hill, G. R. In *Air Pollution: Proceedings of U.S. Technical Conference*; McCabe, L., Ed.; McGraw-Hill: New York, 1952; pp 41-47.
16. Haines, B.; Stefani, M.; Hendrix, F. *Water, Air, Soil Pollut.* 1980, 14, 403-407.

17. Granett, A. L.; Musselman, R. C. *Atmos. Environ.* 1984, 18, 887-891.
18. Pruppacher, H. R.; Klett, J. D. In *Microphysics of Clouds and Precipitation*; Reidel: Amsterdam, 1978; pp 9-27, 136-148, 412-421.
19. Myers, J. N. *Sci. Am.* 1968, 219, 75-82.
20. Taylor, G. I. *Q. J. R. Meteorol. Soc.* 1917, 43, 241-268.
21. Roach, W. T.; Brown, R.; Caughey, S. J.; Garland, J. A.; Readiness, C. J. *Q. J. R. Meteorol. Soc.* 1976, 102, 313-333.
22. Roach, W. T. *Q. J. R. Meteorol. Soc.* 1976, 102, 361-372.
23. Oddie, B. C. V. *Q. J. R. Meteorol. Soc.* 1962, 88, 535-538.
24. Hegg, D. A.; Hobbs, P. V. *Atmos. Environ.* 1982, 16, 2663-2668.
25. Daum, P. H.; Schwartz, S. E.; Newman, L. *J. Geophys. Res.* 1984, 89, 1447-1458.
26. Scherbatskoy, T.; Klein, R. M. *J. Environ. Qual.* 1983, 12, 189-195.
27. Houghton, H. G. *J. Meteorol.* 1955, 12, 355-357.
28. Mrose, H. *Tellus* 1966, 18, 266-270.
29. Okita, T. *J. Meteorol. Soc. Jpn.* 1968, 46, 120-126.
30. Castillo, R. A.; Jiuso, J. E.; McLaren, E. *Atmos. Environ.* 1983, 17, 1497-1505.
31. *Cloud Chemistry and Meteorological Research at Whiteface Mountain: Summer 1980*; Falconer, P. D., Ed.; Publication No. 806; Atmospheric Sciences Research Center, State University of New York: Albany, 1981.
32. Mack, E. J.; Katz, U. "The Characteristics of Marine Fog Occurring off the Coast of Nova Scotia"; Report CJ-5756-M-1; Calspan: Buffalo, NY, 1976.
33. Mack, E. J. et al. "An Investigation of the Meteorology, Physics and Chemistry of Marine Boundary Layer Processes"; Report CJ-6017-M-1; Calspan: Buffalo, NY, 1977.
34. Brewer, R. L.; Ellis, E. C.; Gordon, R. J.; Shepard, L. S. *Atmos. Environ.* 1983, 17, 2267-2271.
35. Munger, J. W.; Jacob, D. J.; Waldman, J. W.; Hoffmann, M. R. *J. Geophys. Res.* 1983, 88C, 5109-5121.
36. Jacob, D. J. Ph.D. Thesis, California Institute of Technology, Pasadena, 1985.
37. Jacob, D. J.; Waldman, J. M.; Munger, J. W.; Hoffmann, M. R. *Environ. Sci. Technol.* 1985c, 19, 730-735.
38. Fuzzi, S.; Castillo, R. A.; Jiusto, J. E.; Lala, G. G. *J. Geophys. Res.* 1984, 89D, 7159-7164.
39. Jacob, D. J.; Waldman, J. M.; Munger, J. W.; Hoffmann, M. R. *Tellus* 1984b, 36B, 272-285.
40. Fuzzi, S., unpublished manuscript.
41. Hoffmann, M. R. *Environ. Sci. Technol.* 1984, 18, 61-64.
42. Firket, J. *Trans. Faraday Soc.* 1936, 32, 1192-1197.
43. Saxena, V. K.; Fisher, G. F. *Aerosol Sci. Technol.* 1984, 3, 335-344.
44. Whitby, K. T. *J. Aerosol Sci.* 1978, 12, 135-159.
45. Wolfe, G. T. *Atmos. Environ.* 1984, 18, 977-981.
46. Manane, Y.; Noll, K. E. *Atmos. Environ.* 1985, 19, 611-622.
47. Gerber, H. E. *J. Atmos. Sci.* 1981, 38, 454-458.
48. Hudson, J. G. *J. Clim. Appl. Meteorol.* 1984, 23, 42-51.
49. Lee, I-Y.; Pruppacher, H. R. *Pure Appl. Geophys.* 1977, 115, 523-545.
50. Naruse, H.; Maruyama, H. *Pap. Meteorol. Geophys.* 1971, 22, 1-21.
51. Hudson, J. G.; Rogers, C. F. *Proc. 9th Int. Cloud Phys. Conf.* 1984.
52. Smith, R. M.; Martell, A. E. *Critical Stability Constants*; Plenum: New York, 1976; Vol. 4.
53. Schwartz, S. E.; White, W. H. In *Advances in Environmental Science and*

- Engineering*; Pfafflin, J. R.; Ziegler, E. N., Eds.; Wiley-Interscience: New York, 1981; pp 1-45.
54. Ledbury, W.; Blair, E. W. *J. Am. Chem. Soc.* **1925**, *127*, 2832-2839.
  55. Dasgupta, P. K.; DeCesare, K.; Ullrey, J. C. *Anal. Chem.* **1980**, *52*, 1912-1922.
  56. Munger, J. W.; Jacob, D. J.; Hoffmann, M. R. *J. Atmos. Chem.* **1984**, *1*, 335-350.
  57. Baboolal, B.; Pruppacher, H. R.; Topalian, J. H. *J. Atmos. Sci.* **1981**, *38*, 856-870.
  58. Schwartz, S. E. In *SO<sub>2</sub>, NO and NO<sub>2</sub> Oxidation Mechanisms: Atmospheric Considerations*; Calvert, J. G., Ed.; Acid Precipitation Series; Butterworth: Boston, 1984; Vol. 3, pp 173-208.
  59. Jacob, D. J.; Waldman, J. M.; Munger, J. W.; Hoffmann, M. R. *J. Geophys. Res.* **1986**, *91*, 1089-1096.
  60. Stelson, A. W.; Seinfeld, J. H. *Atmos. Environ.* **1982**, *16*, 983-992.
  61. Bassett, M. E.; Seinfeld, J. H. *Atmos. Environ.* **1983**, *17*, 2237-2252.
  62. Martell, A. E.; Smith, R. M. *Critical Stability Constants*; Plenum: New York, 1977; Vol. 3.
  63. Appel, B. R.; Kothny, E. L.; Hoffer, E. M.; Hidy, G. M.; Wesolowski, J. J. *Environ. Sci. Technol.* **1978**, *12*, 418-425.
  64. Heisler, S.; Baskett, R. "Particle Sampling and Analysis in the California San Joaquin Valley"; Report CARB-RR-81-14; California Air Resources Board: Sacramento, 1981.
  65. Kerfoot, O. *For. Abstr.* **1968**, *29*, 8-20.
  66. Oberlander, G. T. *Ecology* **1956**, *37*, 851-852.
  67. Davidson, C. I.; Friedlander, S. K. *J. Geophys. Res.* **1978**, *83*, 2342-2352.
  68. *Studies on Fog in Relation to Fog-Preventing Forest*; Hori, T., Ed.; Tanne Trading: Sapporo, Japan, 1953; p 399.
  69. Yosida, Z.; Kuroiwa, D. *Ibid.*, pp 261-278.
  70. Oura, H. *Ibid.*, pp 239-252.
  71. Legg, B. J.; Price, R. I. *Atmos. Environ.* **1980**, *14*, 305-309.
  72. Wattle, B. J.; Mack, E. J.; Pilie, R. J.; Harley, J. T. "The Role of Vegetation in the Low-Level Water Budget in Fog"; Report 7096-M-1; Arvin/Calspan Advanced Technology Center: Buffalo, NY, 1984.
  73. Brown, R.; Roach, W. T. *Q. J. R. Meteorol. Soc.* **1976**, *102*, 335-354.
  74. Brown, R. *Q. J. R. Meteorol. Soc.* **1980**, *106*, 781-802.
  75. Jiusto, J. E.; Lala, G. G. *Radiation Fog Field Programs—Recent Studies*; Publication No. 869; Atmospheric Sciences Research Center, State University of New York: Albany, 1983.
  76. Corrandini, C.; Tonna, G. *J. Atmos. Sci.* **1980**, *37*, 2535-2539.
  77. Dollard, G. J.; Unsworth, M. H. *Atmos. Environ.* **1983**, *17*, 775-780.
  78. Davidson, C. I.; Miller, J. M.; Pleskow, M. A. *Water, Air, Soil Pollut.* **1982**, *18*, 25-43.
  79. Brun, R. J.; Lewis, W.; Perkins, P. J.; Serafini, J. S. "Impingement of Cloud Droplets on a Cylinder and Procedure for Measuring Liquid Water Content and Droplet Sizes in Supercooled Clouds by Rotating Multicylinder Method"; Report 1215; National Agricultural Chemicals Association: Washington, DC, 1955.
  80. Israel, R.; Rosner, D. E. *Aerosol Sci. Technol.* **1983**, *2*, 45-51.
  81. Thorne, P. G.; Lovett, G. M.; Reiners, W. A. *J. Appl. Meteorol.* **1982**, *21*, 1413-1416.
  82. Chamberlain, A. C.; Chadwick, R. C. *Ann. Appl. Biol.* **1972**, *71*, 141-158.

83. Davidson, C. I. Ph.D. Thesis, California Institute of Technology, Pasadena, 1977.
84. May, K. R.; Clifford, R. *Ann. Occup. Hyg.* 1967, 10, 83-95.
85. Hartley, G. S.; Brunskill, R. T. In *Surface Phenomena in Chemistry and Biology*; Danielli, S. F. et al., Eds.; Pergamon: Oxford, 1958.
86. Merriam, R. A. *Water Resour. Res.* 1973, 9, 1591-1598.
87. Bache, D. H. *Atmos. Environ.* 1979, 13, 1681-1687.
88. Thom, A. S. In *Vegetation and the Atmosphere*; Monteith, J. L., Ed.; Academic: London, 1975; pp 57-110.
89. Pilie, R. J.; Mack, E. J.; Kolmund, W. C.; Eadie, W. J.; Rogers, C. W. *J. Appl. Meteorol.* 1975, 14, 364-374.
90. Chamberlain, A. C. In *Vegetation and the Atmosphere*; Monteith, J. L., Ed.; Academic: London, 1975; pp 155-203.
91. Csanady, G. T. *J. Atmos. Sci.* 1963, 20, 201-208.
92. Jenkin, M. E. *Atmos. Environ.* 1984, 18, 1017-1024.
93. Sehmel, G. A. *Atmos. Environ.* 1980, 14, 883-1011.
94. Huebert, B. J.; Robert, C. H. *J. Geophys. Res.* 1985, 90D, 2085-2090.
95. Waldman, J. M. Ph.D. Thesis, California Institute of Technology, Pasadena, 1986.
96. McRae, G. J. Ph.D. Thesis, California Institute of Technology, Pasadena, 1981.
97. Jacob, D. J.; Munger, J. W.; Waldman, J. M.; Hoffmann, M. R. *J. Geophys. Res.* 1986, 91, 1073-1088.
98. Reible, D. D. Ph.D. Thesis, California Institute of Technology, Pasadena, 1982.
99. Hoffmann, M. R.; Jacob, D. J. In *SO<sub>2</sub>, NO and NO<sub>2</sub> Oxidation Mechanisms: Atmospheric Considerations*; Calvert, J. G., Ed.; Acid Precipitation Series; Butterworth: Boston, 1984; Vol. 3, pp 101-172.
100. Aerovironment Report AV-FR-80/603R; Aerovironment: Pasadena, CA, 1982.
101. Dawson, G. A. *J. Geophys. Res.* 1977, 82, 3125-3133.
102. Denmead, O. T.; Freney, J. R.; Simpson, J. R. *Soc. Biol. Chem.* 1976, 8, 161-164.
103. Hutchinson, G. L.; Mosier, A. R.; Andre, C. E. *J. Environ. Qual.* 1982, 11, 288-293.
104. Jacob, D. J. *J. Geophys. Res.* 1985, 90D, 5864.

RECEIVED for review May 6, 1986. ACCEPTED October 10, 1986.

Reprinted from ADVANCES IN CHEMISTRY SERIES No. 216  
*Sources and Fates of Aquatic Pollutants*  
Ronald A. Hites and S. J. Eisenreich, Editors  
Copyright © 1987 by the American Chemical Society  
Reprinted by permission of the copyright owner



# CHAPTER 8

## CHAPTER 8

### THE CHEMISTRY AND PHYSICS OF ACID FOGS, CLOUDS AND HAZE AEROSOL

Michael R. Hoffmann, Jed M. Waldman, J. William Munger and Daniel J. Jacob

Environmental Engineering Science  
California Institute of Technology  
Pasadena, California  
U.S.A.

#### FIELD OBSERVATIONS OF FOG AND CLOUD CHEMISTRY

##### Introduction

The chemistry of fogs, clouds, dew and rain at selected locations in California<sup>1-5</sup> has been observed over the last several years. Fog and cloud water in southern California often has extremely low pH values (i.e.,  $1.7 \leq \text{pH} \leq 4$ ) and extremely high concentrations of sulfate, nitrate, ammonium ion and trace metals. A representative set of values reported by Waldman et al.<sup>2</sup> and Munger et al.<sup>3</sup> are given in Table I along with values reported for other sites around the world. Of special interest are the high values observed for  $\text{SO}_4^{2-}$ ,  $\text{NO}_3^-$ , S(IV), CH<sub>2</sub>O, Fe, Mn, Pb and Cu in fog water. These values and their time-dependent changes<sup>1</sup> as shown in Figures 1 and 2 indicate that fogs provide a very reactive environment for the accumulation of HNO<sub>3</sub> and H<sub>2</sub>SO<sub>4</sub>. Concomitant incorporation of NH<sub>3</sub> gas and calcareous dust into the droplet phase neutralizes some of the acidity.

Because of their similarity to clouds with respect to physical characteristics, fogs are likely to reflect the same chemical processes occurring in clouds and, to some degree, in aqueous microdroplets. Cloud and fog water droplets are in the size range of 2  $\mu\text{m}$  to 50  $\mu\text{m}$  whereas deliquescent haze aerosol will be in the range of 0.01  $\mu\text{m}$  to 1.0  $\mu\text{m}$ . On the other hand, raindrops are approximately 100 times larger than cloud and fog water droplets (e.g., 0.1 mm to 3.0 mm). In Los Angeles, fog water was found to be more concentrated in the primary constituents than the overlying cloud water which was in turn more concentrated than rain water during overlapping periods of time.<sup>3</sup>

Before this research was initiated, few attempts had been made to collect fog water for chemical analysis. Houghton<sup>6</sup> observed pH values in the range 3.5-7.4 in coastal fogs of New England and Canada, and large concentrations of chloride and sulfate. Mrose<sup>7</sup> sampled coastal and urban fogs in East Germany, and reported pH values in the range 3.8-4.2. Mack et al.<sup>8</sup> found high sulfate and nitrate concentrations in fog water collected off the shore of California. A few other investigators collected cloud water intercepting mountain slopes.<sup>9,10</sup> These data sets have been summarized in Table I.

Table I. Summary of Fogwater Composition Measurements

Location	Date	Type <sup>(b)</sup>	N <sup>(c)</sup>	pH	Na <sup>+</sup> (a)	NH <sub>4</sub> <sup>+</sup>	Ca <sup>2+</sup>	Mg <sup>2+</sup>	Cl <sup>-</sup>	NO <sub>3</sub> <sup>-</sup>	SO <sub>4</sub> <sup>2-</sup>	Ref.
Mt. Washington, NH (1900 m)	1930-1940	I	35 <sup>*</sup>	4.5 3.0-5.9					4 0-34		150 4-1100	(76)
Coastal MA & ME	"	M	37 <sup>*</sup>	4.7 3.5-6.3					940 0-5800		380 60-2600	
Germany, Baltic Sea nr. Dresden	1955-65	M	42 <sup>*</sup>	3.8	1500	2300	750		700	900	1900	(7)
Harz Mtn. (1150 m)	"	R	12 <sup>°</sup>	4.2		2100	3200		590	450	780	
	"	I	18 <sup>°</sup>	5.1	300	710	220		200			
Japan, Mt. Noribura (3026 m)	July 1963	I	10 <sup>+</sup>	3.9 3.4-4.3	87 45-165	175 115-260			110 75-230	36 25-175	3300 230-1250	(9)
Mt. Tsukaha (876 m)	Nov. 1963	I	5 <sup>+</sup>	3.9 5.6-6.5	880 180-435			800	17 295-1290	1600	360-2100	
Whitface Mtn., NY (1500 m)	Aug. 1976	I <sup>d</sup>	28 <sup>*</sup>	3.7	11	89	17	6	31	90	140	(100)
	Aug. 1980	"	50	3.2-4.0	1-7	1-200			1-14	7-190	32-800	(101)
Los Angeles foothills (780 m)	Spring 1982 & 83	I	120 <sup>+</sup>	2.9 2.1-3.9	240 135-8700	580 62-7400	140 5-3000	80 1-1800	190 15-9650	1510 160-16300	840 130-9300	(5)
Nova Scotia	Aug. 1975	M	14 <sup>°</sup>		1040 600-1530	33 3-94	45 20-69	100 13-130	87 3-450		250 50-500	(102)
California, Central Coast	Fall 1976	M	8 <sup>°</sup>		320 80-950	190 0-580	55 9-100	68 23-175	400 95-1240	115 24-235	200 77-490	(8)
Los Angeles area	Fall-Winter 1980-82	M & I	11 <sup>+</sup>	3.3 2.7-7.1	132 30-620	1580 420-4260	168 0-460	54 22-310	223 68-423	110 580-2980	584 354-1875	(103)
Los Angeles area	Fall-Winter 1981-82	M	24	2.3-5.8	12-2180	370-7960	190-4350	7-1380	56-1110	130-12000	62-5000	(3)
Pt. Reyes, CA	Aug. 1982	M	17 <sup>+</sup>	4.5 3.5-5.0	190 21-4700	64 28-330	10 0-240	36 5-1200	215 34-7000	23 2-528	188 36-1281	(90)
San Nicholas Is., CA	Aug. 1982	M	7 <sup>x</sup>	3.9	6100	450	450	1500	5300	1580	1080	(4)
San Diego Area, CA	Jan. 1983	M	5 <sup>x</sup>	2.9	510	780	49	130		1850	470	
Albany, NY	Oct. 1982	R	24 <sup>+</sup>	5.8 4.3-6.4	36 10-100	215 70-350	120 65-350	13 6-47	47 18-175	85 11-220	155 21-1360	(104)
Bakersfield, CA	Winter 1983	R	108 <sup>+</sup>	4.2 2.6-7.0	20 1-325	1440 490-1330	47 7-3500	6 1-430	47 1-980	850 200-8800	1160 10-9400	(41)
Italy, Po Valley	Feb. & Nov.	R	5 <sup>°</sup>	3.5-4.3	10-110	580-1620	60-130	10-50	20-120	290-1100	400-990	(105)

a. Concentrations in micro-equiv L<sup>-1</sup>.

b. Fog type: I = intercepted stratiform cloud;

M = marine or coastal fog;

R = radiation fog

c. Number of samples or events: (•) = average, (+) = median,

(x) = volume-weighted mean of n samples;

(o) = average and/or range of n events

d. Non-precipitating stratiform cloud data only.

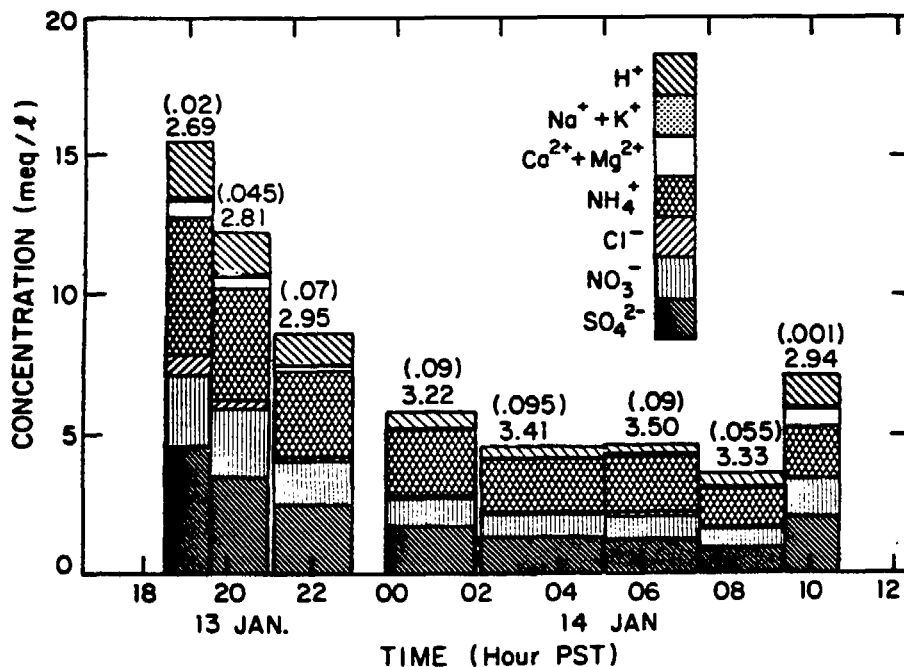


Figure 1. Evolution of fog water concentrations over the course of a fog event at Bakersfield during the winter of 1983. Fog water pH and the average liquid water content (LWC) in  $\text{g m}^{-3}$  is given on the top of each bar.

The paucity of data on the chemical composition of fog water is somewhat surprising since fogs have been associated with major health-threatening air pollution episodes;<sup>11</sup> significant examples are the fogs of London,<sup>12</sup> the Meuse valley<sup>13</sup> and Donora, Pennsylvania.<sup>14</sup> Furthermore, deposition of acid fog water has been shown to damage crops<sup>15,16</sup> and forests.<sup>17</sup>

A likely reason for the sparseness of data is that collecting fog water is not a trivial matter. Fog droplets range in size from  $1 \mu\text{m}$  to  $100 \mu\text{m}$ , with a mass median diameter typically in the  $10 \mu\text{m}$ – $30 \mu\text{m}$  range.<sup>18</sup> Droplets of this size are difficult to collect efficiently because of their inertia. A fog water sampling device must efficiently collect droplets of up to at least  $100 \mu\text{m}$ ; at the same time, it must exclude nonactivated submicron particles which have physical and chemical properties different from those of the fog droplets. Further, large amounts of water must be provided for wet chemical analysis while minimizing evaporation and condensation during the sampling process. These requirements cannot be satisfied by standard techniques for aerosol sampling.

#### Experimental Methods

##### Fog Water Collection

Fog water samples for chemical analysis were collected with a rotating arm collector (RAC). The Caltech RAC, which was based on an earlier design by Mack and Pilié,<sup>19</sup> was modified by application of current aerosol collection design criteria.<sup>20</sup> In essence, the RAC was a rapidly rotating ( $1700 \text{ rpm}$ ) narrow rod with slots on the leading edges and collection bottles on both ends; its steel surfaces were coated with Teflon. Prior to each field use, it was acid-soaked and carefully cleaned with distilled, deionized water ( $\text{D}_2\text{-H}_2\text{O}$ ). Calibration of a scale-model instrument was performed with chemically tagged solid particles. This calibration indicated a lower size cut (i.e., diameter for 50% collection efficiency) of  $20 \mu\text{m}$ .<sup>1</sup>

At most sites (listed in Table II), the RAC was placed on top of buildings. At several remote or rural sampling sites, the apparatus was situated on the ground in an open area. During sampling, the collection bottles (Nalgene, presoaked in  $\text{D}_2\text{-H}_2\text{O}$ ) were manually exchanged at the end of each

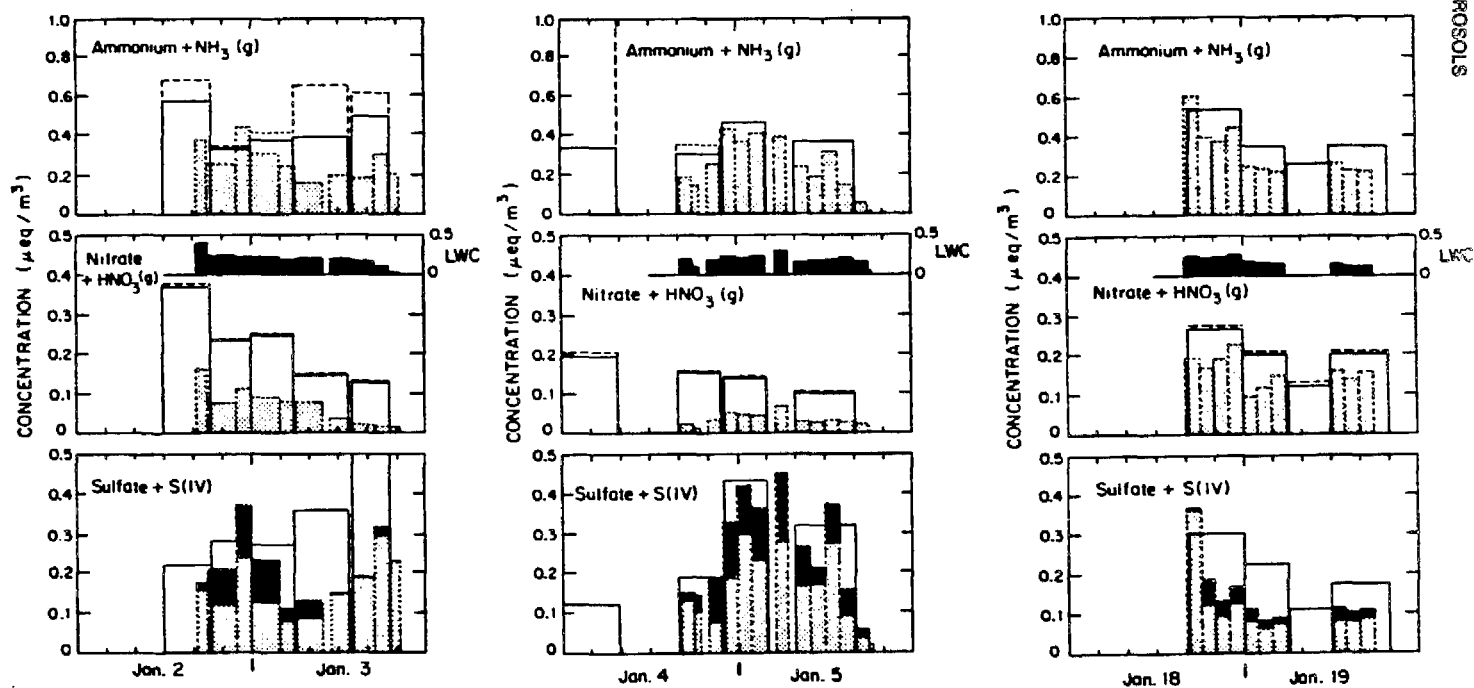


Figure 2. Total and fog water concentrations of N(-III), N(V), and sulfur species at the Bakersfield Airport site: (a) 2-3, (b) 4-5 and (c) 18-19 January 1985.

Table II. Summary of Fog Sampling Sites 1981 to 1985

Site Location	Reference
<i>Southern California</i>	
1. Pasadena (Keck roof at Caltech)	3
2. Long Beach (downtown Harbor)	4
3. Lennox (SCAQMD air monitoring station)	3
4. Corona del Mar (Kerkoff Marine Laboratory)	4
5. Del Mar (County fire station at fairgrounds)	"
6. San Marcos Pass (County fire station)	"
7. Henninger Flats (Nursery)	5
8. San Nicolas Island (U.S. Navy base)	4
9. Upland (CARB air monitoring station)	3
10. Ontario (CARB air monitoring station)	
<i>San Joaquin Valley</i>	
11. Oildale (CARB monitoring station)	3
12. Bakersfield (CARB air monitoring station)	41
13. Bakersfield (Meadows Field Airport)	42
14. Buttonwillow (Parks and Recreation building)	62
15. McKittrick (WOGA air monitoring station)	"
16. Visalia (CARB monitoring station)	"
<i>Central California Coast</i>	
17. Point Reyes (National Monument)	4
18. San Francisco (Mt. Sutro tower)	"
19. Morro Bay	"
20. San Luis Obispo (3 km off-shore aboard RV Acania)	"
<i>New York</i>	
21. Albany, NY (County airport).	61

interval. Between 30 to 120 min were generally adequate to provide sample volumes of 10 mL–60 mL, depending on fog density. Samples as small as 1 mL were collected in light fogs and subsequently analyzed. Aliquots for certain analyses (pH, formaldehyde, S(IV) and trace metals) were separated immediately following collection. The remaining volume was stored in the collection bottle and refrigerated.

#### *Aerosol and Gaseous Nitric Acid and Ammonia Concentrations*

Ambient aerosol concentrations were measured on 47 mm Teflon filter medium using open-faced filter holders. At the flow rate of 10 L/min<sup>-1</sup>, the holder inlet was large enough that anisokinetic bias should not have affected the collection of even large particles or fog droplets. For example, the Stokes number based on the inlet dimension and velocity ( $ST_{inlet}$ ; see Eq. 2.2) for a 50  $\mu$ m diameter droplet is 0.02; this value is below the point where an inlet bias will be important.<sup>21</sup>

A dual filter technique was used to measure gaseous HNO<sub>3</sub> and NH<sub>3</sub> in the atmosphere.<sup>22-24</sup> Nylon (for nitric acid) and oxalic acid-impregnated glass fiber (for ammonia) filters were placed in the back-up position of polycarbonate filter holders; each was immediately behind a Teflon filter. On several occasions, simultaneous filter samples were collected behind a cyclone separator to give the aerosol concentrations in the fine ( $\leq 3 \mu$ m) fraction.<sup>25</sup> Filters were extracted in water with a reciprocating shaker for at least 1 hour. Previously, concern had been raised that aqueous extraction may have been insufficient to fully wet the Teflon medium and dissolve trapped particles.<sup>26</sup> This possibility was tested by wetting extracted filters with methanol; less than 5% additional solute was recovered.

#### *Surrogate-Surface Deposition Measurement Methods*

Polyethylene buckets and polystyrene petri dishes were used to measure deposition of water-soluble material in fog environments. Collectors were generally placed at the same level as the aerosol sampler inlets ( $\geq 3$  m AGL). Deposition rates were measured over 3 h to 7 d intervals. Petri dish exposures in fog were usually 3 to 4 h. Water extractions were done for both containers which were rotated or tilted by hand to wet the bottom and sides. This method gave consistently good recovery of water soluble species, i.e., better than 90% when compared to subsequent extractions.

*Sample Analyses*

Major ions were determined in fog water, aerosol and deposition samples using similar techniques. Specific protocols were refined over the course of the research program. Due to the high aqueous concentration in most fog water samples, detection limitations were rarely a problem. Quantitative dilutions (5:1 to 50:1) were often necessary to bring major constituents within analytical range. The methods are summarized below.

Hydrogen ion activity (*pH*) was determined with a Radiometer Model PHM80 or PHM82 with combination electrode (Model GK2401C). Measurements were made in 0.5 mL–1.0 mL without agitation immediately after each fog water sample was collected. Stable values were found comparing field with laboratory *pH* measured days later when *pH* < 4. Neutral and alkaline samples occasionally showed a shift in *pH* after storage.

*Anions* ( $\text{Cl}^-$ ,  $\text{NO}_3^-$ ,  $\text{SO}_4^{2-}$ ). concentrations were determined by ion chromatography (IC) (Dionex Model 10 or 2000 with anion columns AS1, AS3, or AS4). We used  $\text{Na}_2\text{CO}_3/\text{NaHCO}_3$  eluents for strong acid anions in accordance with the manufacturer's recommendations.<sup>27</sup> The eluent strength used after 1983 (2.7/2.16 mM) was 10% lower than reported in earlier work,<sup>2,3</sup> and was found to give better ion separation with the newer columns.

Weak organic acids eluted very quickly during strong anion determinations given above. These interfered in the fluoride peak for fog water samples which were found to contain appreciable amounts of these acids. The high  $[\text{F}^-]$  reported in our earlier papers has now been recognized to be due to these interferences. In some samples with relatively high organic acid concentrations, these interfered with the chloride determination as well.<sup>4</sup>

Although a sulfite peak could be measured by IC, there was no way to be certain that this represented the *in situ* concentration, since oxidation in storage would cause an increase in measured sulfate. When appreciable S(IV) was found (> 5% total S), aliquots were dosed with  $\text{H}_2\text{O}_2$  to 0.06% prior to IC injection. This was done to determine a total sulfur value. Complete conversion of reduced sulfur to sulfate was verified with sulfite standards. Using S(IV) values (see below), sulfate was calculated by difference.

Analytical uncertainties were <  $\pm$  5% for nitrate and sulfate and  $\pm$  10% for chloride; when interference was observed for  $\text{Cl}^-$ , the value was not reported.

*Ammonium ion* was determined by the phenol-hypochlorite method of Solorzano<sup>28</sup> with colorimetric determination of indophenol blue at 640 nm. Oxalic acid filter extracts were analyzed for  $\text{NH}_4^+$  with a variation of this method described by Russell.<sup>29</sup> Analytical uncertainty for  $\text{NH}_4^+$  determinations was <  $\pm$  10%.

*Cations* ( $\text{Na}^+$ ,  $\text{K}^+$ ,  $\text{Ca}^{2+}$ ,  $\text{Mg}^{2+}$ ) were determined by atomic absorption spectrophotometry (AAS) using an air/acetylene flame (Varian Model AA5 or AA6). Aliquots were spiked with lanthanum (to 0.025%  $\text{La}^{3+}$  and 20 mM HCl) to release chelated calcium or magnesium ions. Analytical uncertainties were < + 5% for cations by AAS.

*S(IV) preservation* in separated fog water aliquots was done by the addition of excess formaldehyde at *pH* 4, and the pararosaniline method and colorimetric detection at 580 nm were used for subsequent S(IV) analyses.<sup>30</sup> Some samples before 1984 were preserved by addition of EDTA and phosphate buffer at *pH* 7 and analyzed by the colorimetric method given by Humphrey et al.<sup>31</sup>; see Munger et al.<sup>32</sup> for details.

*Formaldehyde* was determined by the formation of 3,5-diacetyl-1,4-dihydrolutidin through the addition of acetyl acetone in the presence of  $\text{NH}_4^+$ <sup>33</sup> and detection at 412 nm. High S(IV) concentrations caused interference with the  $\text{CH}_2\text{O}$  determination, presumably due to formation of hydroxymethanesulfonate (HMSA). Addition of  $\text{I}_2$  to aliquots, to oxidize S(IV), eliminated this interference.<sup>34</sup> This was verified by comparing  $\text{CH}_2\text{O}$  response in HMSA standards with  $\text{I}_2$  added; see Munger et al.<sup>32</sup>

*Trace Metals* (Fe, Mn, Pb, Cu, Ni) were determined by flameless AAS with graphite furnace (Perkin-Elmer 360 equipped with a HGA 2100 or Varian AA6 with CRA 90). Aliquots were stabilized with a 1% spike of Ultrex-grade  $\text{HNO}_3$  and stored in acid-washed Nalgene containers. Analytical uncertainties depended upon the element and concentration range;  $\pm$  20% may be taken as an average.

*Liquid Water Content Measurement (LWC) Techniques*

Four separate methods were used at field sites during this research; including (a) estimation by fog water collection rate; (b) mass determination with high-volume sampler and paper filter; (c) infrared (IR) extinction with a carbon-dioxide, laser transmissometer; and (d) droplet sizing with an optical particle counter. Additional details of field measurements have been given in Section 2.3 (*vide infra*).

**Fog Water Collection Rate (RAC) Method.** The RAC ideally sampled air at a rate of  $5 \text{ m}^3 \text{ min}^{-1}$ , given its rotational speed and dimensions. The air in the wake of the collection surface would need to be renewed in the time required for each half-rotation. While this was not verified experimentally, the RAC motion caused a fan effect which, along with the turbulence, induced air motion sufficient to satisfy this requirement. Besides incomplete renewal of sampled air, another factor which could decrease the overall water collection efficiency was the omission of smaller droplets. The size-cut indicated for the collector,  $20 \mu\text{m}$ ,<sup>20</sup> was comparable to droplet mass-median diameter measured in fog.<sup>35-37</sup> Hence, a nontrivial fraction of the droplet spectrum may have been omitted. Taking these factors into consideration, the value calculated from the nominal RAC collection rate represented a lower limit for LWC.

**High-Volume (Hi-Vol) Sampler Method.** A known volume of fog-laden air was drawn through a paper filter, and the amount of water collected was determined by mass difference. Standard high-volume (hi-vol) samplers were used with the flow rate maintained by a flow controller and/or checked with flow orifice. Short (5–20 min) intervals were used. Before each sample, the filter paper was briefly run or “primed” to saturate it with respect to water vapor. For the inlet dimension (20 cm),  $St_{inlet} < 0.1$  for  $50 \mu\text{m}$  droplets, hence anisokinetic sampling biases were not a problem.<sup>21</sup>

**Carbon-Dioxide Laser Transmissometer (CO<sub>2</sub>LT) Method.** An infrared transmissometer to operate in fog was designed and built at the Jet Propulsion Laboratory. Background theory is given later in the section on infrared extinction. The instrument was successfully tested at Henninger Flats during June 1983. Similar attempts were made at Albany, New York in October 1982 and in Bakersfield, California during 1984 and 1985 field studies. Laser power failures prevented successful field operation in these cases.

The instrument design is given in Figure 3. A CO<sub>2</sub> wave-guide laser (Hughes Model 3820-HGBD) emitted coherent infrared radiation at  $9.4 \mu\text{m}$  wavelength. The laser beam was split into a reference signal and a transmitted signal (1:2.8). The ZnSe beam splitter was constructed with a 7 degree wedge angle. This was done after we found that the fraction of transmitted laser radiation changed with minor wavelength variations, multiply reflected by the beam splitter surfaces, without this wedge. The optical path was folded with a total length 20 m at 1.5 m above the ground. A mirror (15 cm diameter) with a 10 m radius of curvature focused the transmitted beam back to the instrument. The emitted beam diameter (86% power) was 1.4 mm with 10 mrad divergence; focused by the mirror, the return beam diameter was approximately as small.

Two disk (2.5 cm diameter) calorimeters (Scientech Model 360) were used to thermally sense laser radiation. One was used as a reference for laser output and the other to monitor the return signal. Laser output changed slowly with small-amplitude, low-frequency oscillation, indicating some instability of the laser emission line. The ratio of signals was formed directly by using an analog ratiometer (Princeton Applied Research Model 188). Thus, transmission measurements were largely independent of these minor laser power fluctuations. The clear air ratio was stable before and after fog was monitored. For the data reported herein, both the signal ratio and laser output were recorded with a dual-channel strip chart and later digitized.

**Optical Particle Counter (CSASP) Method.** Droplet size spectra were measured in the fog with Classical Scattering Aerosol Spectrometer Probe manufactured by Particle Measuring Systems, Inc. (Model PMS CSASP-100HV). The instrument provided counts of droplets passing through a HeNe laser beam and classified them according to the intensity of light scattered onto photodetectors; further details of the principles of operation have been describe by Knollenberg<sup>38</sup> and others. Particles can be classified into 15 size intervals for four different ranges. In fog, droplet spectra were taken in Range 0 (2–47  $\mu\text{m}$  diameter) which had size intervals of  $3 \mu\text{m}$ . Sizing calibration and activity corrections provided by the manufacturer were used.

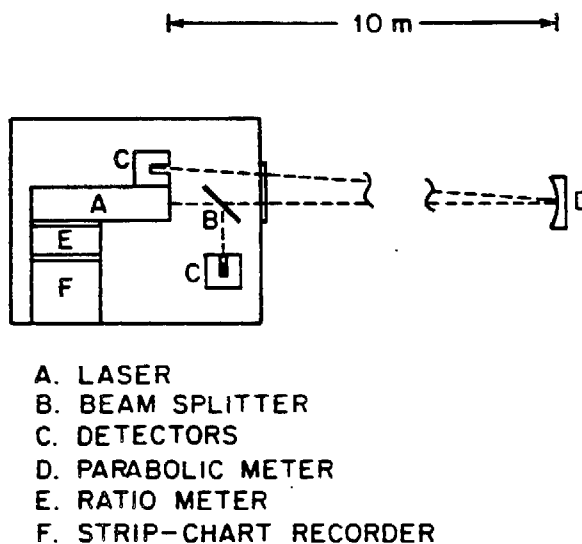


Figure 3. CO<sub>2</sub> laser transmissometer (CO<sub>2</sub>LT).

#### *Meteorological Measurements*

Most fog sampling sites were collocated where meteorological instrumentation was available. At more remote locations, temperature was measured with a glass-bulb thermometer, and wind speeds and directions were periodically assessed by observation. At Henninger Flats, Los Angeles County Fire Department records of precipitation, cloud cover, temperature and relative humidity were used to supplement field measurements. In the spring of 1983, supplementary wind data were provided by mechanical weather stations reported in Hering and Blumenthal.<sup>39,40</sup>

Wind and temperature data were recorded at the Bakersfield Airport fog sampling site with sensors (Qualimetrics, Inc., Sacramento, California) and data acquisition equipment specifically deployed for this research. Cup anemometers (Model 2005) and temperature sensors (Model 4480-A) were positioned on a 3m tower. Sensor signals were conditioned with manufacturer-designed modules. Analog outputs were continuously logged with an A/D converter and an IBM personal computer. Additional data from that period were also taken from National Weather Service observations. Relative humidity and ambient temperature were recorded with hygrothermographs located at other valley sites. Parameters aloft (wind speed, direction, temperature, and relative humidity) were measured by a tethersonde at Buttonwillow. Mixing height data for that period were also provided from acoustic radar located at Kernridge and cloud top observations at Bakersfield Airport by flight tower personnel.

#### **Field Results**

##### *Coastal Fogs*

The rotating arm collector was used in fog water sampling programs at several locations in California. Fog water samples collected along the California coast<sup>4</sup> were found to be consistently acidic, even in rural areas as shown in Table III. Extremely high acidities (pH down to 1.69) were observed at sites in the Los Angeles basin and downwind. The main contributors to strong acidity were sulfuric and nitric acid; coastal urban activities and oil production operations are important sources of SO<sub>2</sub> and NO<sub>x</sub>, precursors of these acids. Coastal atmospheres were found to have low acid-neutralizing capacities, and thus, to be very sensitive to acid inputs.

##### *Valley Fogs*

Fog water acidity may be neutralized if a sufficient amount of base is present in the atmosphere. Neutralization of fog water acidity by ammonia as illustrated in Figure 4 was investigated in two

**Table III. Liquid Water-Weighted Average Fogwater Concentrations.**

Site	Date <sup>(a)</sup>	n	pH	$\mu\text{eq l}^{-1}$									$\mu\text{M}^{-1}$		
				H <sup>+</sup>	Na <sup>+</sup>	K <sup>+</sup>	NH <sub>4</sub> <sup>+</sup>	Ca <sup>2+</sup>	Mg <sup>2+</sup>	Cl <sup>-</sup>	NO <sub>3</sub> <sup>-</sup>	SO <sub>4</sub> <sup>2-</sup>	S(IV) <sup>(d)</sup>	CH <sub>2</sub> O <sup>(d)</sup>	L <sup>(b)</sup>
Del Mar	9 Jan. 83 1840-2300	5	2.85	1410	511	9	781	49	130	614 <sup>(d)</sup>	1850	469	66	78	0.24
Corona del Mar	7 Dec. 82 2100-2300	1	2.16	6920	725	71	2860	197	188	1050	7900	1290	NA	NA	0.11
Long Beach	8 Jan. 83 0400-0500	2	4.90	12.7	82	12	759	45	26	221 <sup>(d)</sup>	252	487	NA	71	0.25
Lennox	7 Dec. 81 2305-0840	8	2.98	1100	65	12	1610	111	42	178 <sup>(d)</sup>	2210	926	80	196	0.30
	18 Dec. 81 2315-0045	3	2.66	2190	131	30	1280	127	48	150 <sup>(d)</sup>	2780	1280	NA	178	0.14
	6 Jan. 83	5	3.63	237	41	8	464	39	18	88 <sup>(d)</sup>	365	126	34	68	0.17
San Nicholas Island	26 Aug. 82 2115-0755	7	3.86	138	6060	148	452	450	1500	5490	1580	2080	11	15	0.052
San Marcos Pass (e)	20 Aug. 83 2340-1200	14	4.49	32.1	10	3	97	3	4	19	74	55	2	8	0.43
Morro Bay	14 Jul. 82 0500-0900	2	6.17	0.67	748	64	107	120	221	1200	114	214	6	7	0.14
Mt. Sutro	13 Aug. 82 2125-2225	1	3.99	102	648	52	183	93	170	851	87	319	NA	NA	0.056
Pt. Reyes	9 Aug. 82 2200-0000	1	3.60	251	3520	91	327	242	890	3040	526	1280	10	19	0.054
	10 Aug. 82 0230-1115	3	4.48	33.4	3150	72	95	153	782	4580	38	463	4	2	0.081
	11 Aug. 82 0200-1155	7	3.88	132	498	12	59	27	118	645	36	208	5	3	0.13
	12 Aug. 82 0340-0815	6	4.69	20	42	2	43	3	10	57	6	54	5	3	0.19

NA: not analyzed.

(a) date is that of the a.m. samples, or that of the morning following the fog. Time is local time.

(b) average liquid water content ( $\text{g m}^{-3}$ ), calculated from the total volume collected.

(c) number of samples analyzed for metals.

(d) [Cl<sup>-</sup>] may be overestimated due to interference from organic acids during analysis. At Del Mar, this uncertainty is significant only for the last three samples (see text).

(e) stratus cloud.

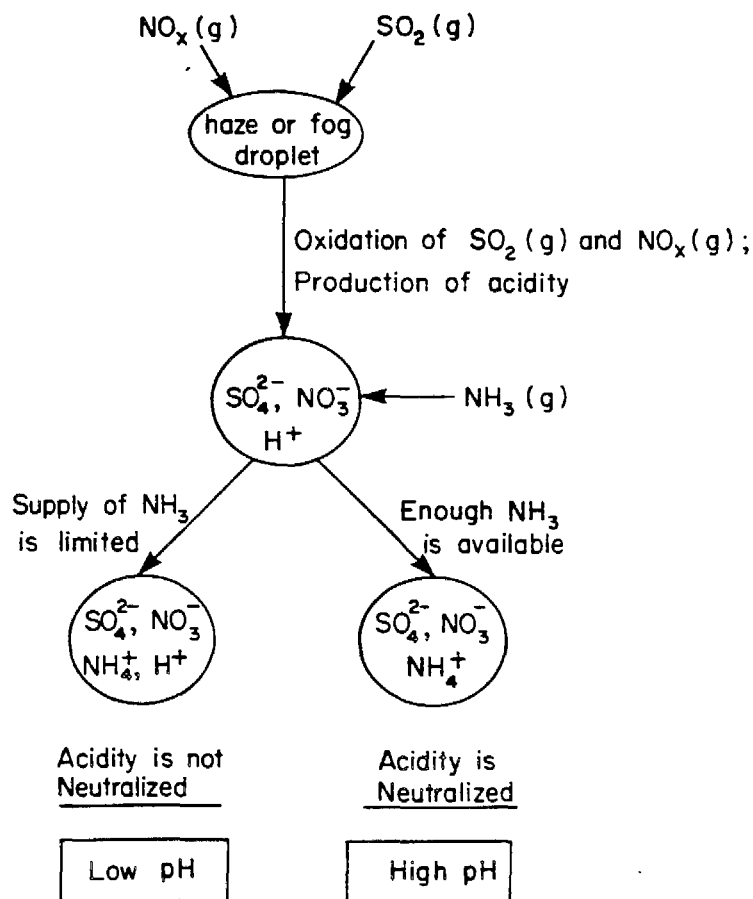


Figure 4. Schematic diagram that illustrates the dominant chemistry involved in the formation of acidic fogs and the role of  $\text{NH}_3$  with respect to pH control.

field experiments conducted in the San Joaquin Valley of California, where large inputs of strong acids are provided by oil and gas production ( $\text{SO}_2$ ,  $\text{NO}_x$ ), and large quantities of  $\text{NH}_3$  are released by industrial farming and livestock feeding operations.<sup>41,42</sup> The  $\text{H}_2\text{SO}_4$ - $\text{HNO}_3$ - $\text{NH}_3$  system contributed over 90% of the inorganic aerosol and fog water ionic loading, and the fog water alkalinity/mineral acidity could be correctly predicted from the local balance of sulfuric acid, nitric acid and ammonia in the atmosphere. Fog water acidity directly reflected the relative proximities of oil fields and confined feeding operations.

Most of the fogs sampled in the San Joaquin Valley formed over the course of extended stagnation episodes. Progressive pollutant accumulation under stagnant conditions was documented under nonfoggy stagnant conditions, and decreases in aerosol concentrations were observed following fogs. These trends are illustrated in Figure 5. It is suggested that deposition of fog droplets provides a rapid sink of suspended pollutants so that the occurrence of fogs limits pollutant accumulation in a stagnant atmosphere.

Deposition was the principal means of removal for S(VI), N(V), and N(-III); the patterns of pollutant accumulation were consistent with deposition velocities  $< 0.1 \text{ cm sec}^{-1}$  for secondary ( $\text{SO}_4^{2-}$ ,  $\text{NO}_3^-$ ,  $\text{NH}_4^+$ ,  $\text{H}^+$ ) aerosol, and deposition velocities  $> 1 \text{ cm sec}^{-1}$  for  $\text{HNO}_3(\text{g})$ . Slow scavenging of  $\text{SO}_2$  by fog was documented, and an average  $\text{SO}_2$  conversion rate of  $2\% \text{ h}^{-1}$  was

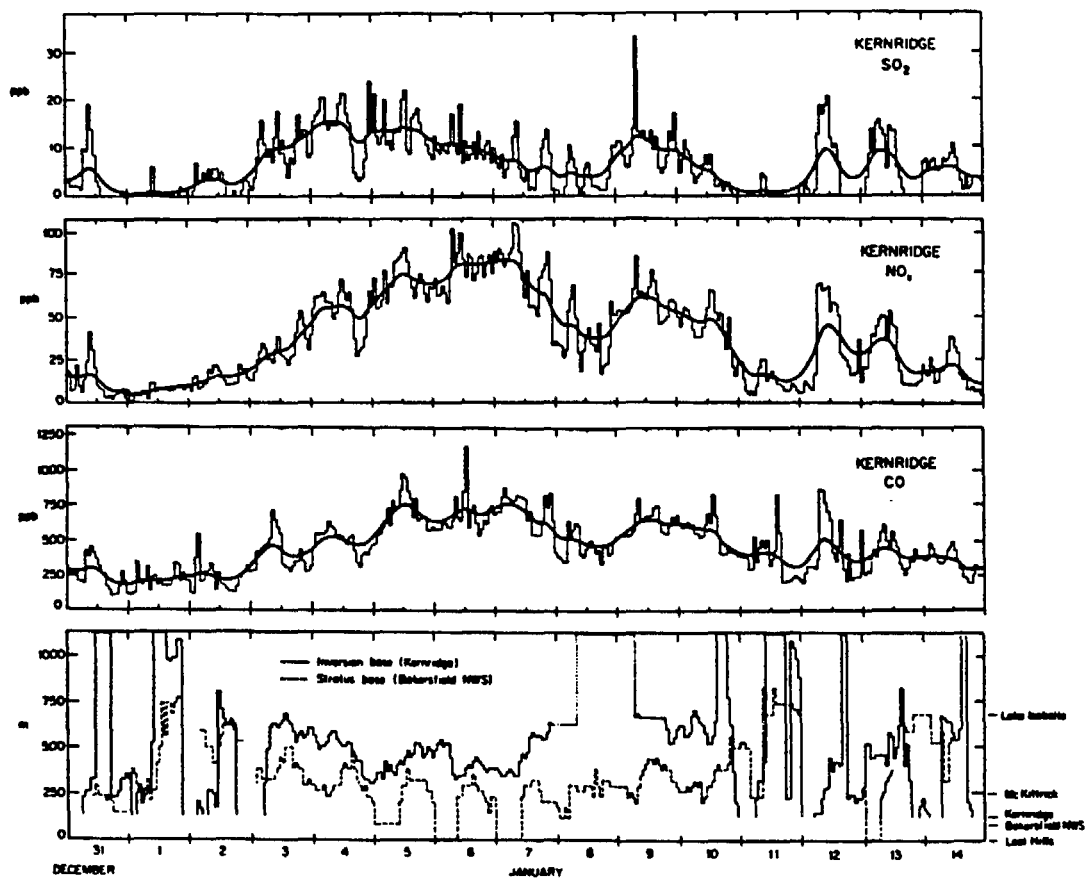


Figure 5. Variation of gas-phase components, mixing heights and stratus base during a prolonged stagnation episode in the southern San Joaquin Valley at Kernridge.

determined in an overcast boundary layer. Production of  $\text{HNO}_3$  was observed at the beginning of the stagnation episode, but was limited by the availability of gas-phase oxidants.  $\text{NO}_x$  was found not to be significantly scavenged by fog water. Overall, accumulation of strong acids  $\text{H}_2\text{SO}_4$  and  $\text{HNO}_3$  over the course of a stagnation episode resulted in a decrease of alkalinities at all sites in the southern San Joaquin Valley, and production of mineral acidities at the sites most distant from  $\text{NH}_3$  emissions.

The San Joaquin Valley experiment provided simultaneous measurements of S(VI), N(V) and N(III) concentrations in the gas phase, the aerosol and the fog water. These data were used to test the applicability of thermodynamic models for the  $\text{H}_2\text{SO}_4$ - $\text{HNO}_3$ - $\text{NH}_3$ - $\text{H}_2\text{O}$  system at high humidities and in fogs.<sup>43</sup> Under nonfoggy alkaline conditions the aerosol was a neutralized mixture, alkalinity remained in the gas phase as  $\text{NH}_3(\text{g})$ , and  $\text{HNO}_3(\text{g})$  concentrations were very low. Under nonfoggy acidic conditions  $\text{NH}_3(\text{g})$  concentrations were very low, and the acidity was present both in the gas phase as  $\text{HNO}_3(\text{g})$  and in the aerosol phase as partly neutralized sulfuric acid. These findings are in qualitative agreement with the model results of Bassett and Seinfeld.<sup>44</sup> The dissociation constants  $K = P_{\text{NH}_3} P_{\text{HNO}_3}$  predicted by Bassett and Seinfeld agreed to within one order of magnitude with the products of concentrations observed in the field although they were systematically too low.

In fog, concentrations of  $\text{HNO}_3(\text{g})$  were at or below the detection limit of  $4 \text{ neq m}^{-3}$  under nonacidic conditions and were very low (although generally nonzero) under acidic conditions. The observation of detectable  $\text{HNO}_3(\text{g})$  in acidic fog was attributed to the presence of unsaturated air parcels within the fog, and to the slow rate of diffusion of  $\text{HNO}_3(\text{g})$  to the fog droplets. No detectable  $\text{NH}_3(\text{g})$  was found under foggy acidic conditions, but substantial amounts were found under foggy nonacidic conditions. The observed  $\text{NH}_3(\text{g})$  concentrations were of the same magnitude as those predicted at equilibrium with fog water.

#### *S(IV) Adducts in Fog*

Carbonyl compounds, aldehydes and ketones influence liquid-phase sulfur dioxide chemistry through their reactions with  $\text{SO}_2$  to form stable  $\alpha$ -hydroxyalkanesulfonates. Aldehydes are ubiquitous contaminants in the atmosphere. They exist at especially high concentrations ( $24\text{--}58 \mu\text{g}/\text{m}^3$ ) in urban environments where vehicular emissions are a significant or even dominant source.<sup>45,46</sup> In addition, aldehydes are generated via numerous pathways from a variety of precursors present in both clean and polluted atmospheres. These include the oxidation of alkanes and alkenes by  $\text{OH}^\bullet$  and  $\text{O}_3$ . Aldehydes are highly reactive species that decompose rapidly through photolytic and free-radical reactions. For example, the half-life of gaseous formaldehyde,  $\text{CH}_2\text{O}(\text{g})$ , in the atmosphere is fairly short (2-3 h). However, dissolution of  $\text{CH}_2\text{O}$  and hydration to form methylene glycol,  $\text{CH}_2(\text{OH})_2$ , protects it from photochemical decomposition. Consequently, atmospheric droplets offer an ideal environment for sulfonic acid production.

Field measurements have detected formaldehyde at concentrations of greater than  $100 \mu\text{M}$  in fog and cloud water samples collected in Southern California.<sup>3,32,47,48</sup> The concentrations of acetaldehyde, propionaldehyde, propenal (acrolein), n-butanal, n-pentanal, n-hexanal and benzaldehyde occasionally approached or exceeded that of  $\text{CH}_2\text{O}$ .<sup>47</sup> We have also shown that formaldehyde, acetaldehyde and propanol are present in urban fog water samples at substantial concentrations.<sup>32</sup> In addition, we have shown that for each one of the aldehydes present, the corresponding carboxylic acid is also present and that the aldehydes may be slowly oxidized to their respective carboxylic acids upon storage. Furthermore, the presence of  $\text{CH}_2\text{O}$  and  $\text{H}_2\text{O}_2$  in conjunction with S(IV) at levels higher than those predicted by gas/liquid solubility equilibria suggests that hydroxymethanesulfonate (HMSA) production stabilizes a fraction of S(IV) with respect to oxidation.<sup>48</sup> Our equilibrium calculations using available thermodynamic and kinetic data for the reaction of  $\text{SO}_2$  and  $\text{CH}_2\text{O}$  demonstrate that elevated concentrations of S(IV) in fog water cannot be achieved without consideration of sulfonic acid production,  $\text{HORHSO}_3^-$ <sup>32</sup> (See Figures 6, 7). Recently, Munger et al.<sup>49</sup> identified and quantified HMSA using ion-pairing chromatography.

Carbonyl-bisulfite addition products are highly stable in aqueous solution at low pH, but they undergo facile dissociation under alkaline conditions. The kinetics of hydroxymethanesulfonate production under pH conditions characteristic of fog and cloud water has been studied in our laboratory. Boyce and Hoffmann<sup>50</sup> found that the formation of HMSA over the pH range 0.0 to 3.5 occurs by parallel reaction pathways involving nucleophilic addition of  $\text{HSO}_3^-$  and  $\text{SO}_3^{2-}$  to the carbonyl C-atom of formaldehyde. The formation constant for adduct formation has been determined recently by Deister et al.<sup>51</sup> and Kok et al.<sup>52</sup> to be  $10^7 \text{ M}^{-1}$ . This number is in agreement with

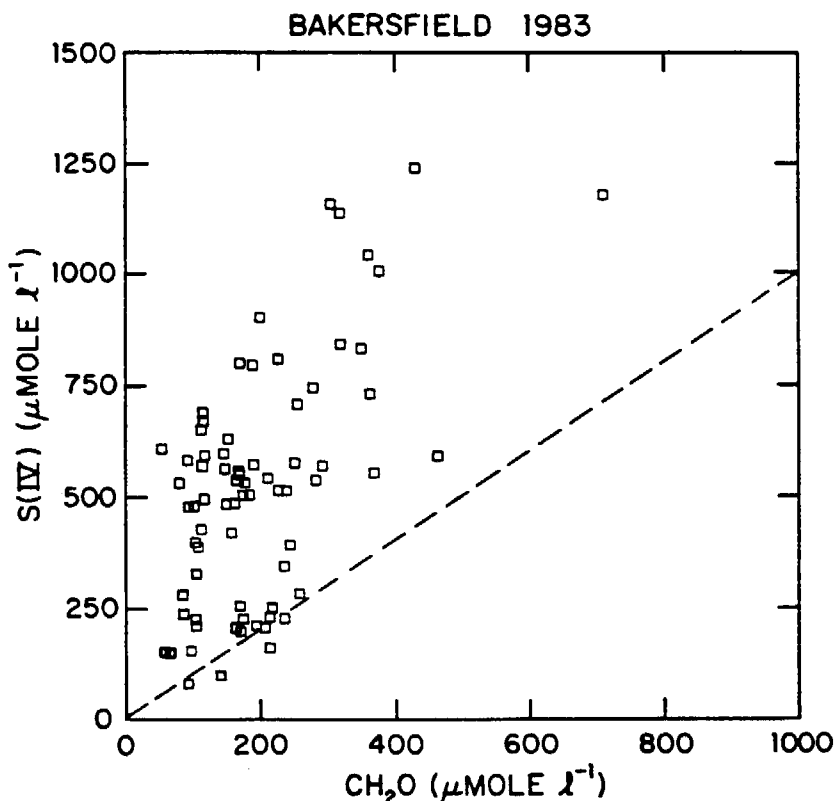


Figure 6. Plot of the observed aqueous-phase S(IV) concentrations versus observed HCHO concentrations in fog water in Bakersfield, California.

those reported previously by Kerp<sup>53</sup> and Donally.<sup>54</sup> Under more weakly acidic conditions ( $\text{pH} > 4$ ), the dehydration of methylene glycol (equation  $K_d$ ) may become rate-determining.<sup>55</sup> Application of the rate constants and activation energy parameters obtained in the laboratory to the analysis of the field measurements discussed above indicates that HMSA formation may account for the occurrence of S(IV) at elevated concentrations.<sup>32</sup> Kinetic data obtained for other aldehyde/sulfur(IV) reaction systems suggests that the mechanism outlined above can be generalized to describe the formation of a wide variety of  $\alpha$ -hydroxyalkanesulfonates.<sup>56</sup>

#### Stratus Clouds

Waldman et al.<sup>5</sup> have studied the chemistry and microphysics of intercepted cloud water on Los Angeles area mountain slopes. From 1982 to 1985, the observed pH values of the cloud water ranged from 2.06 to 3.87 with the median value below pH 3. The equivalent ratio of nitrate to sulfate in cloud water at Henninger Flats (MSL = 2,520 ft) was close to 2, while at the same site the  $[\text{NO}_3^-]/[\text{SO}_4^{2-}]$  ratio in rainwater was  $\sim 1$ . However, the nitrate/sulfate ratio observed in dry aerosol was significantly lower than that observed in cloud water; the additional nitrate found in cloud water appears to be derived from the scavenging of gaseous nitric acid. In addition, a higher fraction of nitrate aerosol appears to be scavenged by cloud droplets. This observation is consistent with current theories of homogeneous versus heterogeneous gas-to-particle pathways open to sulfur dioxide versus nitrogen oxides.

Cloud droplet capture in the form of intercepted fog appears to be a seasonably important sink for pollutant emissions in the Los Angeles basin. At Henninger Flats, up to 50% of the total wet

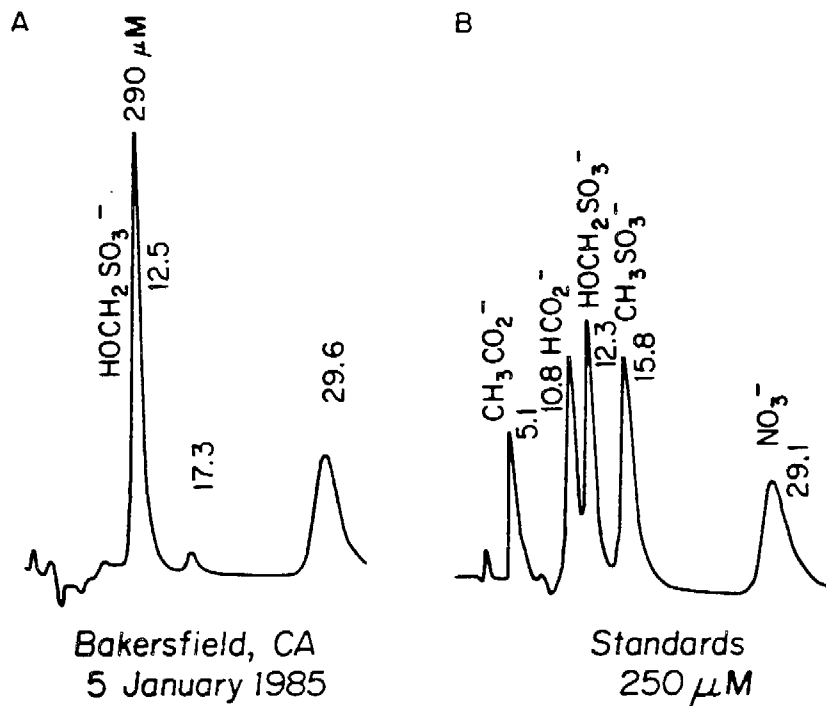
MOBILE PHASE ION CHROMATOGRAPHY

Figure 7. A representative chromatogram for the separation and identification of  $\alpha$ -hydroxymethanesulfonate in fog water collected in Bakersfield, California.

deposition of  $H^+$ ,  $NO_3^-$  and  $SO_4^{2-}$  may be due to cloud interception; low-intensity springtime drizzle accounted for 20% of the deposition measured in precipitation. The intercepted cloud water that deposited on pine needles was collected and analyzed. The acidity of the water dripping from trees was very similar to that of the suspended cloud water. The concentrations of major chemical components were found to be significantly greater than in the overlying cloud water. The additional solute in the drippings is thought to be derived from previously deposited material and the evaporated residue of intercepted cloud water. Even after sufficient rainfall had removed most of the accumulated residue, the concentrations of major cations such as  $Ca^{2+}$ ,  $Mg^{2+}$  and  $K^+$  showed relative increases compared to suspended cloud water samples. These increases may be attributed in part to ion exchange of  $H^+$  for  $K^+$ ,  $Mg^{2+}$  and  $Ca^{2+}$  from the pine needles.<sup>37</sup> The potential for harm to sensitive plant tissue appears to be high given prolonged exposure to the severe microenvironments observed on the slopes of the San Gabriel Mountains and in the Los Angeles National Forest.

#### FIELD INTERCOMPARISON OF FOG COMPOSITION AND LIQUID WATER CONTENT

##### Background

Sampling techniques for early research of fog and cloud water chemistry were not widely used or standardized. Reproducibility of results was seldom verified by intercomparison of available

methods. Since interest in this area has grown in recent years, many fog and cloud water collectors have been developed. However, few have been evaluated thoroughly.

Collector performance must be evaluated because droplets in the size range encountered in fogs and clouds are sensitive to anisokinetic sampling biases.<sup>38</sup> The important design considerations for fog water collectors have been enumerated by Jacob et al.<sup>20</sup> These are: (a) a sharp lower size cut which effectively excludes interstitial aerosol; (b) representative collection of all droplet sizes; and (c) preservation of physical and chemical integrity of sample volumes.

Calibration of a scale model of the Caltech rotating arm collector (RAC) indicated a lower size cut of 20  $\mu\text{m}$ . That is, at this diameter, 50% collection efficiency is attained while higher efficiencies are achieved for larger sizes.<sup>20</sup> This lower size cut is approximately twice as large as that determined for impaction to a rod of similar dimension without slots.<sup>39</sup> Since fog droplet size distributions have mass median diameters close to 20  $\mu\text{m}$ ,<sup>35-37,60,61</sup> field measurements made with the RAC may be subject to an unknown bias due to omission of smaller droplets. In order to properly interpret fog chemistry based on RAC samples, it was essential to determine if a collector bias existed.

During our study of stratus cloud water at Henninger Flats, the performance of several fog collection techniques were evaluated. In June 1983, a fog sampler intercomparison was performed using the Caltech RAC and four other collectors of various designs.<sup>39,40</sup> In addition, this provided an opportunity to compare our analytical protocol to that of an independent laboratory.

Interpretation of fog water chemistry is highly dependent on a knowledge of liquid water content (LWC) in the fog environment. This requires that the total droplet mass within a volume of air be measured. Water droplets are in a tenuous thermodynamic state with air at very low supersaturation and a large reservoir of water vapor. For example, saturated air at 10° C contains 12 g-H<sub>2</sub>O(g) m<sup>-3</sup> which can be compared to  $\leq 0.5$  g-H<sub>2</sub>O(l) m<sup>-3</sup> in dense fog. As a consequence, evaporation or condensation can easily bias measurements. Furthermore, the relatively large inertia of fog droplets increases the difficulty of representative sampling with an inlet.<sup>21,54</sup> A comparison of LWC methods was also performed at several sites. The presentation of the data is intended to underscore the uncertainties in LWC measurements made in the field and to assess the reliability of the RAC collection rate to estimate LWC.

#### Fog Water Composition Comparisons

In the following section, various data sets have been compared to determine their statistical relationships. Linear least-squares regressions and correlation coefficients have been determined by Waldman.<sup>62</sup> However, since neither measurement in data pairs represented an "error-free" independent parameter, least-squares analysis was not strictly applicable.<sup>63</sup> As an alternative, we have also calculated standard errors for sets of paired data ( $X_i, Y_i$ ) based on their relative difference with respect to the mean of the pair:

$$\Delta_i = \frac{2(Y_i - X_i)}{X_i + Y_i} \quad (1)$$

Since the values of many of the parameters ranged over several orders of magnitude, this statistical treatment was advantageous because it avoided an overemphasis on data pairs of the highest concentrations. Major constituents were normally present at levels far above the limits of detection. The samples which had greatest analytical error were frequently the most concentrated ones. These had the smallest volumes plus required substantial dilution. The mean and standard deviation of  $\Delta$  were compared with the  $t$  test to determine whether a nonzero mean had significance.<sup>63</sup>

#### Caltech Fog Collector (RAC) Reproducibility

Two identical RAC instruments were operated in fogs at Henninger Flats<sup>5</sup> during seven separate events in June 1983. During one event (June 11), samples were taken while the collectors were situated adjacent to each other (3 m apart). The remainder of simultaneous samples were taken with the RAC's located 30 m apart at opposite corners of the nursery area. Sample handling and analytical protocols were identical, and sampling intervals were generally 60 min.

Comparisons for simultaneous RAC samples are summarized in Table IV. Plots and addition statistical parameters have been presented by Waldman.<sup>62</sup> Despite wide ranges of ambient concentrations, the agreement between samples was remarkably good. Samples collected apart did not show statistically greater compositional variability than those collected side-by-side. For the dominant ions (H<sup>+</sup>, NH<sub>4</sub><sup>+</sup>, NO<sub>3</sub><sup>-</sup> and SO<sub>4</sub><sup>2-</sup>), the standard errors ( $\sigma_{\Delta}$ ) were  $\leq 10\%$ . With the exception of calcium, the remainder of measured ions had standard errors between 10%-15%.

Table IV. Rotating Arm Collector (RAC) Sampling Reproducibility

Parameter	Side-by-Side <sup>(a)</sup>		Separated <sup>(a)</sup>		Time-Averaged <sup>(b)</sup>	
	n <sup>(c)</sup>	$\sigma(\Delta)$ <sup>(d)</sup>	n	$\sigma(\Delta)$	n	$\sigma(\Delta)$
pH in field <sup>(e)</sup>	13	0.01	17	0.04	14	0.02
Hydrogen	13	3	17	10	14	4
Sodium	9 <sup>x</sup>	10	16	10	12 <sup>x</sup>	8
Potassium	7 <sup>x</sup>	13	12	16	11 <sup>x</sup>	17
Ammonium	12	10	16	12	14	7
Calcium	12	26	16	14	13	11
Magnesium	11 <sup>+</sup>	8	15	10	13	7
Chloride	6	13	10	9	13 <sup>+</sup>	9
Nitrate	11 <sup>+</sup>	6	14 <sup>+</sup>	9	14	5
Sulfate	11 <sup>+</sup>	4	14 <sup>+</sup>	8	14	5
Collection	13	12	17 (14 <sup>+++</sup> )	27 (13)	14	8

a. Based on Caltech laboratory results; RAC's located 3 and 30 m apart, respectively.

b. Based on RI laboratory results; time-averaged samples per H&B.

c. Number of sample pairs; + indicates exclusion of 1 outlier pair; x indicates exclusion of 1-2 pairs near detection limits.

d. Standard deviation,  $\sigma(\Delta)$ , of relative difference between pairs (expressed in percent) where:

$$\Delta_i = 2|y_i - x_i|/(x_i + y_i)$$

e. For the pH difference ( $\Delta$ pH), with  $\sigma(\Delta)$  expressed in pH units.

There was a greater difference observed in the collection rates for the separated collectors, although most of the scatter was associated with a few outliers. Part of this may be due to temporal and spatial variability of fog density at the site, although these fluctuations were generally dampened by taking longer sampling intervals. For example, the third column in Table IV shows the improvement in the comparison for a data set with averaging times of 2 to 3 h intervals (see next section). Nonetheless, the occasional differences in collection rates did not result in greater compositional disparities for those samples.

#### Comparison of the RAC with Other Collectors

Five different collectors were operated simultaneously on five dates in June 1983 at the Henninger Flats nursery. These were (a) the Caltech RAC; (b) the Desert Research Institute jet impactor (DRI); (c) the Global Geochemistry Corp. mesh sampler (GGC); (d) the Atmospheric Science Research Center rotating string collector (ASRC); and (e) the AeroVironment rotating rod collector (AV). The RAC has been described in an earlier section. Descriptions of the others are given below.

**DRI.** The DRI linear-jet impactor was designed for use inside an experimental cloud chamber; a lower size cut between 2 and 5  $\mu\text{m}$  has been reported.<sup>64</sup> Air was drawn through three rectangular jets at a total rate of 1.2  $\text{m}^3 \text{min}^{-1}$ . The instrument contained internal impaction surfaces that rotated and moved the impacted droplets away from the air jet to minimize evaporative losses. At Henninger Flats, the DRI collector was located inside a 55 gallon drum, elevated 2 m above ground level and open at the bottom. This design feature was intended to eliminate collection of raindrops and to reduce a sampling bias that could be caused by variable wind conditions at the inlet. A fan was used to supplement the upward airflow inside the drum.

**GGC.** The GGC collector was a V-shaped, Teflon-lined tube (10-cm diameter) with its inlet approximately 0.8 m above ground level. At the inlet of the tube, a 4-cm thick polypropylene mesh of filaments (0.41 mm diameter with 96% void volume) was used to collect fog droplets with an air sampling rate of 1.7  $\text{m}^3 \text{min}^{-1}$ . The droplet size cut was below 3  $\mu\text{m}$  diameter with nearly 100% efficiency for  $D_0 > 5 \mu\text{m}$ , based on the mesh manufacturer's specifications.<sup>40</sup> The collected liquid drained into a bottle at the bottom of the V-tube.

**ASRC.** Nylon strings (0.41 mm diameter) were mounted at a slight angle from vertical between two plates which were rotated at 100 rpm. The instrument was located on a mast about 3 m above ground level. Water collected on the lower plate and was manually transferred into collection bottles at the end of each sampling period.

Table V. Comparison Between Fogwater Samples from Different Collector Designs<sup>(a)</sup>

Parameter	DRI vs RAC		GGC vs RAC		DRI vs GGC		POOLED	
	n	$\sigma(\Delta)^{(b)}$	n	$\sigma(\Delta)$	n	$\sigma(\Delta)$	n	pad <sup>(c)</sup>
pH in field <sup>(d)</sup>	16	0.08	15	0.07	15	0.11	16	0.07
Hydrogen	16	19	15	16	15	25	16	15
Ammonium	16	21*(+13) <sup>(e)</sup>	16	14*(+20)	15	19	17	24
Nitrate	16	21	16	12*(+12)	15	10*(-10)	17	17
Sulfate	16	20	16	14*(+15)	15	21	17	21
	n	Ratio <sup>(f)</sup>	n	Ratio	n	Ratio		
Sodium	14	0.4 ± 0.2	13	1.5 ± 1.5	13	0.4 ± 0.2	14	50
Potassium	11	0.8 ± 0.5	13	3.2 ± 3.9	10	0.4 ± 0.2	14	76
Calcium	14	0.4 ± 0.2	13	2.8 ± 0.7	13	0.2 ± 0.1	14	81
Magnesium	14	0.6 ± 0.3	13	1.3 ± 0.7	13	0.6 ± 0.2	14	37
Chloride	16	0.9 ± 0.2	16	1.6 ± 0.7	15	0.7 ± 0.3	17	25
LWC <sup>(g)</sup>	10	1.2 ± 0.3	10	1.2 ± 0.2	9	1.0 ± 0.3	17	41

a. Data for combined samples as given in Hering and Blumenthal (40).

RAC = Caltech rotating arm collector (CRC code "C");

DRI = Desert Research Inst. jet impactor;

GGC = Global Geochemistry Corp. mesh collector (CRC code "G").

b. Standard deviation,  $\sigma(\Delta)$ , of relative difference between pairs (for collector y vs x), expressed in percent. See Table IV note c. Pooled standard deviation (i.e., averaged for n sets) expressed as percent of pooled mean value.

d. For the pH difference ( $\Delta$ pH), with  $\sigma(\Delta)$  expressed in pH units.

e. Non-zero  $\Delta$  has statistically significant (>95%) based on t-test;  $\Delta$  (as percent) given in parentheses.

f. Mean and standard deviation for concentration ratio: [y]/[x].

g. Liquid water contents from collection rates; ratios for dense fog samples only; pad for all samples.

AV. Two fractions of droplets were collected by impaction to a Teflon-coated rod rotated at 3450 rpm. The outer part of the rod was 1.6 mm and the inner part 19 mm in diameter; the nominal size-cuts for each have been given as 2.5 and 10  $\mu$ m, respectively. The impacted droplets were transferred to stationary polyethylene troughs by centrifugal force and drained by gravity to separate collection bottles.

A detailed report on the collector intercomparison was prepared by Hering and Blumenthal,<sup>40</sup> along with a comprehensive data volume.<sup>39</sup> In the Hering and Blumenthal study, samples from all collectors were submitted to Rockwell International Corp. (RI) for analysis. Excellent agreement was found between the Caltech and RI laboratory results for most individual samples.<sup>62</sup>

Because most of the other instruments collected liquid at lower rates than the RAC, they generally required longer sampling intervals. For most of the compared data sets, volume-weighted averages were calculated for two or three sequential RAC samples in order to match the intervals required by the other collectors. For example, comparison of these combined values for simultaneous RAC samples has been presented in Table IV.

A comparison of data sets for the RAC and the DRI and GGC collectors was conducted to ascertain differences in chemical composition due to differences in the reported droplet size cuts. The combined sample results given in Hering and Blumenthal<sup>40</sup> were used in our analysis. Because the ASRC collector was an external impaction design that had not been calibrated, it was excluded from this discussion. Also, the AV sample concentrations were higher by a factor of 2 or more than any of the other collectors for all analytes except pH. Along with the low liquid water collection rates, this indicated that significant evaporative losses were occurring. The AV design relied upon gravity for removal of the impacted droplets from the exposed circular trough. This was not rapid enough and demonstrated the importance of sample preservation immediately following impaction.

The agreement among the RAC, GGC and DRI collectors was reasonably good for the dominant species (Table V), although it was less than for paired RAC collectors.<sup>62</sup> Comparison of relative differences ( $\Delta$ ) identified somewhat lower concentrations for RAC samples than for the other two collectors in several cases. The differences in collector size cuts may have caused the observed bias, if a greater fraction of smaller droplets collected by DRI and GGC designs was substantially more concentrated. However, the observed differences were primarily from the two or three samples with higher concentrations that were collected during lower LWC. The remainder of data pairing showed 1:1 correspondence in dense fog. These results suggested that compositional differences were caused by evaporation of samples within the two internal surface collectors

during light and patchy fogs. This effect was most pronounced in periods when the RAC collected measurable liquid water while GGC and DRI collectors could not. In those cases, impacted droplets had completely evaporated before sufficient volumes were able to drain to the collection bottles.

Concentrations of cation species such as sodium and calcium were routinely greater in RAC and GGC samples than in DRI samples. In Table V, the ratios for cations rather than their relative differences are given. These species are associated with soil dust and expected in the coarse particle fraction. Thus, the observed differences for cation concentrations may be caused by the collector inlets. At low wind speeds, the collection efficiency for droplets of increasing size would decrease because their inertia prevents them from following streamlines entering the inlet.<sup>21,58</sup> For example,  $St_{inlet} \leq 0.25$  assures that the inlet sampling bias remains below 30%,<sup>21</sup> for the Stokes number is based on droplet diameter, inlet velocities and the inlet radius.

For the RAC, the upper size-cut ( $D_u$ ) was estimated to be 200  $\mu\text{m}$ , for the RAC arm taken as an "inlet" and the fan-induced wind ( $1.5 \text{ m s}^{-1}$ ) as an "inlet velocity." For the GGC collector inlet geometry,  $D_u = 45 \text{ }\mu\text{m}$  was calculated for the same criterion of  $St_{inlet}$ . In the case of the DRI collector, the inlet to the drum was large (60 cm diameter), therefore collection of droplets up to 200  $\mu\text{m}$  should not be biased due to inertial considerations. However, since the inlet faced downward, this would result in an exclusion of larger droplets caused by gravity. The threshold droplet size was calculated to be 70  $\mu\text{m}$ , based on the velocity at the drum inlet ( $15 \text{ cm}^3 \text{ s}^{-1}$ ). Dry particles with greater than unit density would be excluded at even smaller sizes (e.g.,  $\rho_p = 2 \text{ g cm}^{-3}$  gives  $D_u = 35$  and 22  $\mu\text{m}$  for DRI and GGC, respectively).

In addition, it appeared that the intense research activity at the field site caused the higher levels of soil dust cations, notably calcium, in RAC and GGC samples. For example, the volume-weighted Ca/Mg equivalent ratio was 1.1 for 31 RAC samples collected at Henninger Flats earlier in 1983, before intercomparison activities had commenced. During the intercomparison, this ratio was raised to 1.9 for RAC samples and  $> 3$  for GGC samples. For DRI samples, this ratio was 1.0. The RAC and GGC collectors apparently captured dust particles along with the fog droplets while these were generally segregated at the DRI inlet. As opposed to the RAC, the GGC inlet was not more efficient for collection of larger particles. However, the positioning of their inlet too close to ground level allowed soil dust to contaminate the GGC samples, as demonstrated by the frequent disparities in cation concentrations observed for adjacent GGC collectors.<sup>62</sup>

In summary, the essential chemical characterizations of fog water were the same for each collector. Relatively good agreement among the three designs was found for concentrations of major chemical constituents such as  $\text{H}^+$ ,  $\text{NH}_4^+$ ,  $\text{NO}_3^-$  and  $\text{SO}_4^{2-}$  during most sampling periods. Collection of soil dust by RAC and GGC collectors was noted. In spite of sample evaporation or inherent differences in droplet size cuts (large and small), the collective uncertainties for major ions were between 15% and 25%. In fact, for the majority of samples, far closer agreement was achieved. For major ions, the substantial differences in collector design did not result in systematic bias in chemical composition under conditions of dense fog.

#### Liquid Water Content Measurements

The methods used to determine LWC at Henninger Flats in June 1983 included: (a) rates of collection for the various fog water collectors; (b) droplet sizing by an optical particle counter (OPC); (c) infrared (IR) extinction measurements; and (d) sampling of fog-laden air with filter papers. Measurements obtained by these methods were averaged for the RAC sampling intervals or, for comparison with other fog water collectors, the longer sampling interval.

A considerable scatter existed among measurements (Figure 8). Several methods indicated entirely different ranges of LWC. It is important to recognize that these techniques did not necessarily measure the absolute quantity of liquid water in the air; rather, they provided an operational parameter based on instrument response. A significant problem in assessing different techniques has been that there is not an accepted standard method for the determination of LWC.

#### Fog Water Collection Rates

The fog water collectors inherently provided a gravimetric assay of LWC. In fog water chemistry studies, this has the advantage that it is uniquely paired with compositional data for each sample. Estimations of LWC were based on the rate of liquid water collection normalized to the specific air sampling rate for each collector. The RAC sampled air at a flow rate of  $5 \text{ m}^3 \text{ min}^{-1}$ , given its rotation velocity and dimension. Incomplete renewal of air in the wake of the rotating arm or the omission of droplets smaller than the lower size cut would reduce the efficiency of liquid

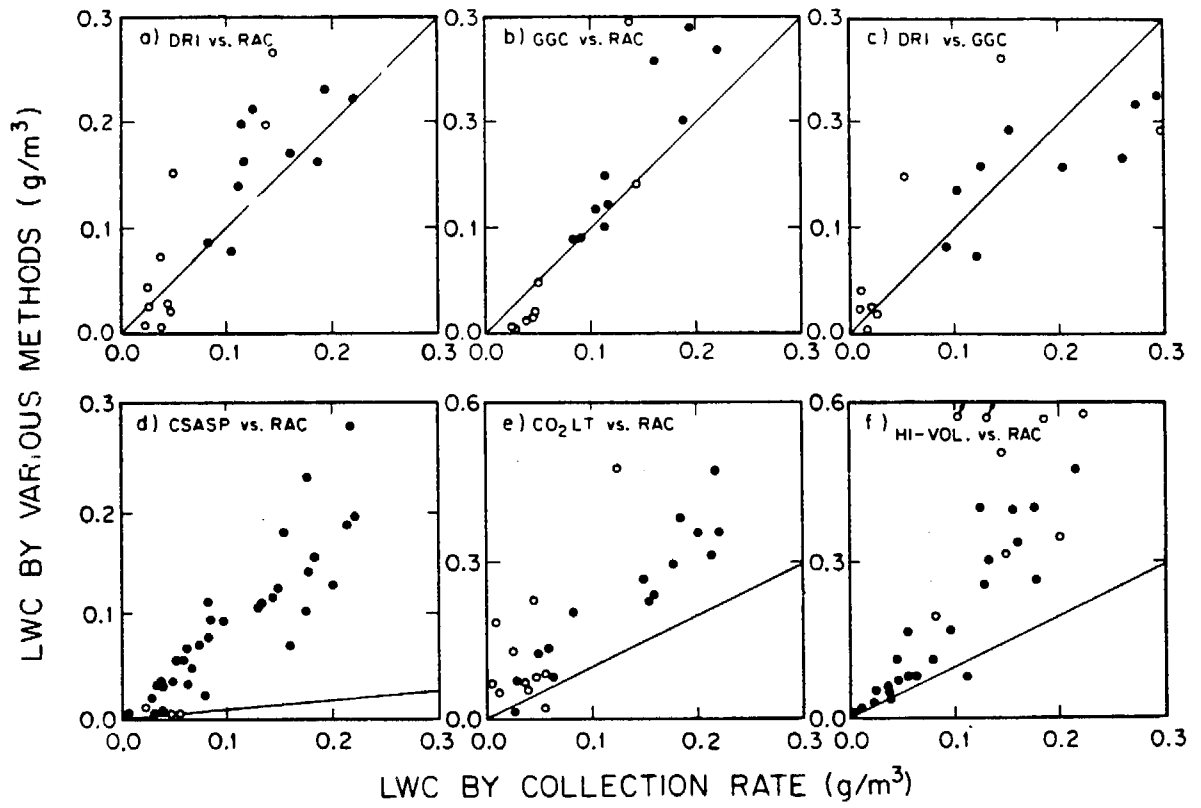


Figure 8. LWC comparisons at Henninger Flats during June 1983.

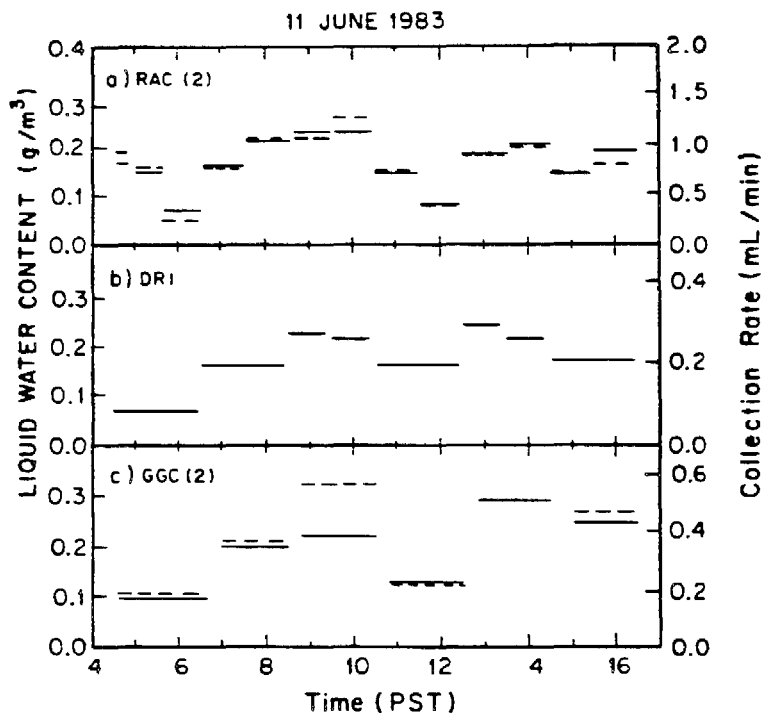


Figure 9. Fog collection rates and calculated LWC for 11 June 1983.

water collection. The RAC collection rate has been compared to the DRI and GGC collectors for which the air sampling rates could readily be measured: 1.2 and 1.7  $\text{m}^3 \text{min}^{-1}$ , respectively.

As compared to the compositional correlations, greater deviations from 1:1 agreement existed in the LWC values (Figure 8a-c). The density of fog was found to alter the relationship between collector rates. As mentioned previously, the RAC was efficient in collecting samples during periods of light fog while the other collectors were not able to operate. The RAC motion supplied ample centrifugal force for immediate removal of impacted liquid. For DRI and GGC collectors, a sufficient wetting of the internal surfaces was required before water flowed by gravity to the collection vials, and this was sometimes limited by evaporation during light or patchy fog conditions. The data that was obtained during periods of relatively stable and dense fog is indicated by the shaded circles of Figure 8a-c.

The scale and sharpness of lower size-cuts are important aspects of quantitative liquid water collection. Droplet size distributions during fog showed that > 95% of liquid water was in the range of 5 to 35  $\mu\text{m}$  diameter. Given the lower size cuts for DRI and GGC samplers, these collectors should be close to 100% efficient, except when sample evaporation becomes a problem. In contrast, between 30% and 70% of liquid water was measured in droplets larger than 20  $\mu\text{m}$ , which is the lower size cut indicated for the RAC.<sup>20</sup> Based on these estimates, the collection efficiencies of DRI and GGC designs should be 0.5 to 3 times higher than the RAC. However, the actual collection efficiencies showed a fairly close agreement (Figure 9). On the average, the DRI and GGC values were essentially the same, although each was only about 20% higher than those determined for the RAC during dense fog (see Table V).

#### *Droplet Size Spectra (CSASP Method)*

The optical particle counter used at Henninger Flats was the Classical Scattering Aerosol Spectrometer Probe (CSASP-100 HV) manufactured by Particle Measuring Systems, Inc. (Boulder, Colorado). Several droplet size distributions measured in 60-s intervals with the CSASP are

shown in Figure 10. The measured spectra agreed well with typical droplet size parameters, such as mass median diameter and spectrum shape, that have been reported in the literature for fogs<sup>35,36,60,61</sup> and specifically for intercepted stratus.<sup>31</sup> However, the LWC values resulting from integration of the size data were high by a factor of 4 to 10 compared to value determined by the other methods. These high values were unrealistic relative to previously reported LWC and to the basic principles of cloud microphysics. For example, updraft velocities typical of strongly convective clouds are generally the only conditions for which LWC values higher than  $1 \text{ g m}^{-3}$  are found.<sup>18</sup> Yet, sizing data from the CSASP at Henninger Flats indicated LWC values sometimes higher than  $2 \text{ g m}^{-3}$ !

Preliminary attempts in our laboratory to calibrate the instrument in the size range of interest, 10–30  $\mu\text{m}$ , were inconclusive except to demonstrate that significant oversizing was not occurring in this range. Based on the reported calibrations of PMS instruments,<sup>65</sup> sizing errors are generally limited to  $\pm 3\text{--}4 \mu\text{m}$ . While such errors can cause appreciable errors in LWC, they are not sufficient to cause an upward shift of the magnitude we found. Other investigators have reported somewhat similar experiences in LWC determinations with particle spectrometers in ambient fogs and haze, although not to the same extreme. Biases of two or more in calculated LWC or extinction coefficients, relative to other methods (or for side-by-side OPC's), were not uncommon.<sup>61,66-68</sup>

Nonetheless, the time series of CSASP-derived LWC were consistent with the trends measured by the other methods (compare Figure 11a and Figure 9). The scaling between values was also fairly consistent (Figure 8d) which indicated that errors in sizing, if occurring, did not appreciably change with LWC. The CSASP-measured size distributions showed that variations of LWC were primarily dependent on the droplet number concentrations. For more than tenfold changes in LWC, the measured median size did not appreciably change (Figure 11a-c).

Droplet number concentrations at Henninger Flats were compared to fog condensation nuclei (FCN) monitored during the same period by Hudson and Rogers.<sup>69</sup> They alternately measured the total condensation nuclei in fog-laden air and in air with droplets removed ( $D_0 > 2\text{--}5 \mu\text{m}$ ). By difference (total minus nonactive FCN), this indirectly provided values of droplet number concentrations between 100 and 400 per  $\text{cm}^{-3}$ . Direct comparison of simultaneous CSASP and FCN data indicated that the CSASP number concentrations were higher by a factor of  $3.8 \pm 2.1$  for 42 cases in dense fog (J. Hudson, unpublished data).

Since the CSASP data were so strongly correlated with fog water collector rates and the measured infrared extinction (see next section), we feel that this instrument provided a qualitative measurement of temporal variability in LWC and associated size spectra. These data were useful in understanding the nature of stratus cloud interactions at the mountain slope and the variability found among other methods. The existence of the fine structure of LWC during fog was hidden by the long sampling intervals required by most of the other techniques. The cause of instrument bias has not been identified with certainty, however.

#### *Filter Results (Hi-Vol Method)*

Three standard high volume (hi-vol) samplers with paper filters were operated at Henninger Flats, generally two at a time. The average for these are shown in Figure 8. There were operational difficulties associated with measurements at the site. The accumulated moisture on filters was subject to evaporation in the fogs of low density and short duration. In addition, the hi-vol samplers were oriented with the axis of the inlet facing upward. A positive bias was suspected from the direct collection of drizzle during periods of fog sampling on June 11. On dates thereafter, rain shields were deployed over the inlets.

In spite of problems associated with patchy fogs or drizzle, the hi-vol method appears to be the most direct method available for ground-based measurements of LWC. All droplets are collected on the filter, and there is no dependence on impaction efficiency or droplet size cut, as for fog water collector designs. The  $St_{inlet}$  criterion given previously indicates no inlet bias for  $D_0 < 100 \mu\text{m}$ . In stable fogs, this technique has been reported to have good precision,<sup>35</sup> although reproducibility between samplers at Henninger Flats was only fair ( $\sigma_{\Delta} = 30\%$ ).

From the limited number of intervals with reliable hi-vol samples, measurements indicated that LWC was in the range of 0.1 to  $0.4 \text{ g m}^{-3}$ . This was consistent with the range of LWC determined with the  $\text{CO}_2\text{LT}$ . Together, these two methods demonstrated that the efficiencies of the fog water collectors were below 100% in dense fog at the mountain site (Figure 8f; nondrizzle data have been indicated with shaded circles).

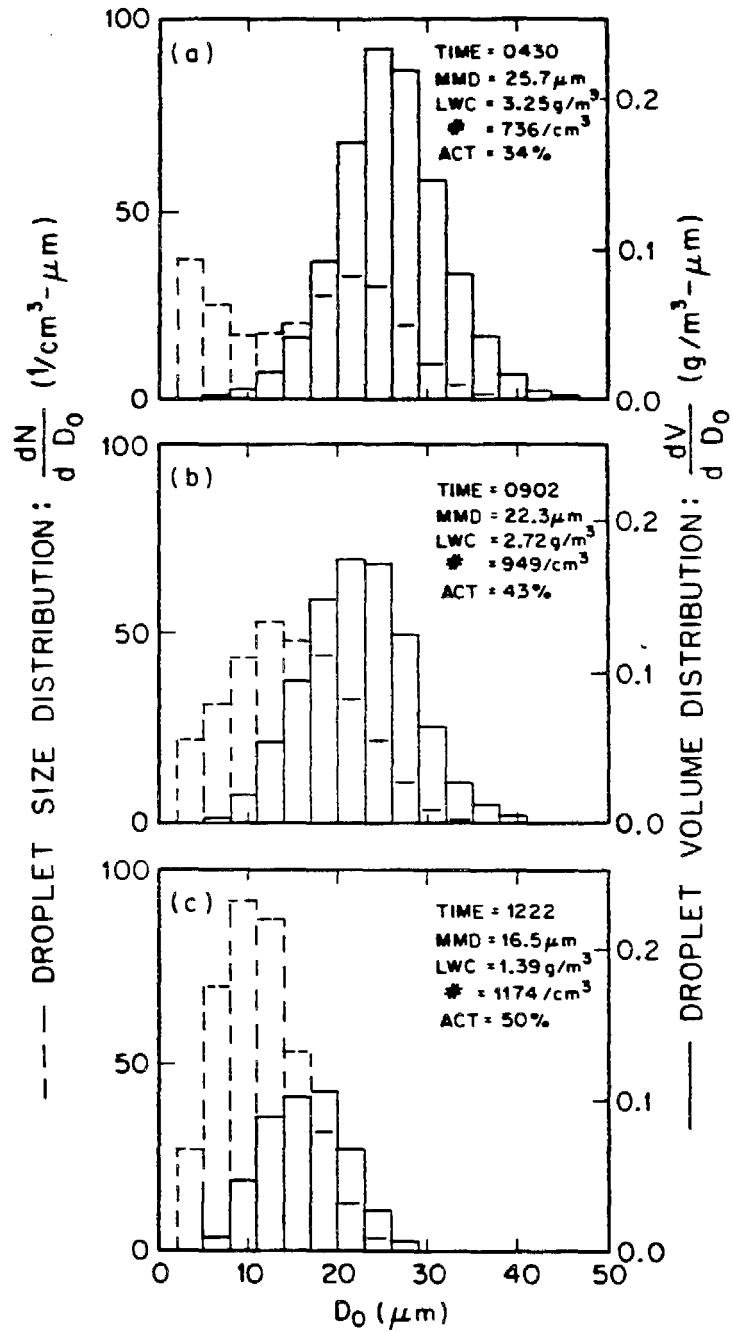


Figure 10. Droplet size and volume distributions from CSASP.

### Conclusions

Large uncertainties in measurements of LWC during fog water sampling were underscored by the wide range and considerable scatter between the methods compared. In some cases, fair correlations between methods were found. A bias at low LWC was noted for several fog water collectors and for the hi-vol filter method. Correlations improved for dense fog conditions. The best precision was found for adjacent operation of identical fog collectors.

Collection efficiencies in dense fog were somewhat lower for the RAC compared to DRI and GGC collectors. However, the factors that distinguished the collectors were not commensurate with the differences that were predicted on the basis of their nominal size cuts and droplet size distributions in fog. The magnitude of LWC indicated by IR extinction and filtration methods were roughly 50% higher than indicated from fog water collection rates. Furthermore, the higher range of LWC determined by the CO<sub>2</sub>LT and hi-vol was more consistent with the densities previously reported for intercepted clouds and fogs.

It appeared that each of the fog water collectors was less than 100% efficient. Thus, the presumption of total droplet collection by GGC or DRI collectors was not substantiated. The disparity between expected and actual collection was apparently not caused by segregation of larger droplets at the collector inlets. No substantial differences in solute concentrations were found for the dominant species. These results suggest that the actual collection characteristics of the three distinctly different designs are more closely aligned than indicated by their design specifications and respective calibrations.

A factor that contributed to the scatter observed among alternative methods was the systematic variations in instrument responses with rapidly changing fog conditions, displayed by CSASP. The uncertainty among LWC measurements was  $\pm 30\%$  to  $50\%$ . At this time, the techniques available to us precluded greater accuracy in the absolute determination of LWC.

We have estimated an average efficiency for the RAC collector to be approximately 60%. Because the chief interest of our research has been in the fog water chemistry, the RAC collection rates with this factor applied have been used to determine LWC in the field. We feel that the RAC-derived values were the most appropriate because: (a) they were highly reproducible; (b) they correlated reasonably well with the other fog collector values and other LWC measurement methods; (c) the comparison of fog collectors provided no conclusive information about the composition of the fog water fraction omitted by the collectors; (d) the validity of droplet size distributions measured by the CSASP was vitiated by an unresolved bias in LWC; and, (e) RAC-derived values were available at all field sites and for all sampling intervals.

## MODELING THE CHEMISTRY OF FOGS AND CLOUDS

### Overview

Calvert<sup>70</sup> has pointed out that gas-phase reactions of SO<sub>2</sub> with ozone (O<sub>3</sub>), hydroxyl radical (OH•) and hydroperoxyl radical (HO<sub>2</sub>•) are too slow to account for observed rates of sulfate production in humid urban atmospheres<sup>71</sup> and in wave clouds.<sup>72</sup> Consequently, the catalytic autooxidation of SO<sub>2</sub> in deliquescent haze aerosol and hydrometeors has been proposed as a viable non-photolytic pathway for the rapid formation of sulfuric acid in humid atmospheres.<sup>73-78</sup> In addition, hydrogen peroxide and ozone have been given serious consideration as important aqueous-phase oxidants of dissolved SO<sub>2</sub> as discussed by Martin.<sup>86</sup> Oxidation by H<sub>2</sub>O<sub>2</sub> seems to be most favorable under low pH conditions (pH  $\leq$  4) because of a rapid rate of reaction and a negative pH dependence that favors the facile conversion of HSO<sub>3</sub><sup>-</sup> to sulfate. In comparison, metal-catalyzed autooxidation and oxidation of S(IV) with O<sub>3</sub> tend to proceed more slowly with decreasing pH.<sup>79</sup>

Limiting factors in the autooxidation pathways are the total concentration of the active metal catalyst and its equilibrium speciation as a function of pH. Los Angeles fog water contains high concentrations of iron, manganese, copper, nickel and lead.<sup>3,4</sup> Of these metals, Fe, Mn and Cu are expected to be the most effective catalysts for the reaction of S(IV) with molecular oxygen.<sup>77-81</sup> Observed concentrations of Fe and Mn in fog of 400  $\mu$ M and 15  $\mu$ M, respectively, were not unusual.<sup>3,4,62,82</sup> Model calculations indicate that metal-catalyzed autooxidations may contribute significantly to the overall sulfate formation rate in atmospheric droplets, particularly in the range of Fe and Mn concentrations observed in urban fog.<sup>4,62,80-83</sup>

Previous efforts in this laboratory established a basic framework for the development of a model for the detailed chemistry of urban clouds and fogs.<sup>80</sup> Additional work by Chameides and

Davis,<sup>84</sup> Chameides,<sup>85</sup> Seigneur and Saxena,<sup>86</sup> and Graedel and Goldberg<sup>85</sup> has been used as a basis for improvement of our initial modeling efforts.

The original model developed by Jacob and Hoffmann<sup>80</sup> was a hybrid kinetic and equilibrium model. A basic set of 32 equilibria involving important species found in fog and cloud water were considered.<sup>3,4</sup> Superimposed on this basis set of equilibria were an additional set of seven empirical rate equations for the time-dependent, aqueous-phase oxidation of S(IV) and N(III) to produce H<sup>+</sup>, S(VI) and N(V). At each time step in the numerical computation, the complete equilibrium problem was solved for reactions that had characteristic times much shorter than the size of the time step. In addition to the purely chemical pathways, the physical processes of nucleation scavenging, droplet growth on condensation nuclei, and gas-liquid mass transfer were considered. Jacob and Hoffmann<sup>80</sup> found that the important oxidants of S(IV) and O<sub>2</sub> as catalyzed by Fe(III) and Mn(II), H<sub>2</sub>O<sub>2</sub> and O<sub>3</sub>. Nitrate production was found to be dominated by HNO<sub>3</sub> gas-phase scavenging. Gas-phase ammonia and hydrogen peroxide were also scavenged efficiently. Formation of hydroxyalkylsulfonates, due to the in situ reaction of aldehydes and S(IV), was found to significantly increase the droplet capacity for S(IV) but did not slow down the net S(IV) oxidation rate leading to cloud acidification. The concentrations of major aqueous-phase species were found to be controlled primarily by condensation, evaporation and pH. The composition of the precursor haze aerosol or cloud condensation nuclei will determine to a large extent the observed chemical speciation of the droplet phase. Hoffmann and Jacob<sup>81</sup> have considered a variation of the above model that incorporates dynamic gas-phase chemistry in addition to the aqueous-phase module. Chameides and Davis<sup>84</sup> and Chameides<sup>83</sup> have incorporated coupled gas and aqueous phase photochemistry into the development of a model for the acidification of remote marine stratiform clouds. They have shown that, in addition to the above pathways, aqueous-phase free radical pathways can contribute substantially to the generation of acidity via the in situ oxidation of S(IV) and HCHO to S(VI) and formic acid, respectively. The principal oxidants of S(IV) as identified by Chameides were H<sub>2</sub>O<sub>2</sub>, O<sub>3</sub>, OH and HO<sub>2</sub>. Parameters found to affect the S(IV) to S(VI) conversion rate were the accommodation coefficient for the reactive species of interest, the liquid water content, and the ambient levels of SO<sub>2</sub> and HNO<sub>3</sub>. Similar considerations in model development were made by Graedel and Goldberg.<sup>87</sup> Seigneur and Saxena<sup>86</sup> have adapted the Jacob and Hoffmann<sup>80</sup> approach in a coupled gas-phase and aqueous-phase kinetic model. Their results were in general agreement with Jacob and Hoffmann for the special cases of urban fogs and clouds. The main effect of the addition of the gas-phase module was to provide dynamic nonaqueous sources of HNO<sub>3</sub> and to illustrate that the gas-phase hydrocarbon chemistry will dominate OH chemistry (i.e., aqueous-phase OH chemistry due to radical scavenging appears to be inconsequential).

#### SUMMARY OF MAJOR OBSERVATIONS AND CONCLUSIONS

- Fog water collected at sites in the South Coast Air Basin of Los Angeles was consistently acidic with pH values typically ranging from 1.7 to 4. The highest acidities were observed during smog episodes. The main contributors to the acidity were nitric and sulfuric acids, with a typical equivalent ratio of 3:1. Secondary sulfate and nitrate aerosol accounted for over 80% of the fog water loading.
- Fog water collected at nonurban coastal sites was usually acidic (pH range 3 to 7). Impact of emission centers on distant coastal locations was documented. The low alkalinity of marine atmospheres make them particularly susceptible to acidification. Oxidation of oceanic dimethylsulfide could be a natural source of sulfuric acid.
- Stratus clouds collected at 2500' MSL over the Los Angeles Basin were consistently acidic, pH range 2 to 4. Cloud water concentrations were in the same range as those observed in the basin itself.
- Fog water collected in the Southern San Joaquin Valley was not consistently acidic; pH values ranged from 2.5 to 7.5. Millimolar concentrations of sulfate were typically observed, but high ammonia emissions from livestock and cropland neutralized the acid input. Visalia, which is some distance from the major emission sources, had alkaline fog water (pH 6-7.5). McKittrick, located in an oil field with little surrounding agricultural activity, had acidic fog water (pH 2.5-4.5).
- Liquid water content (LWC) was the major factor affecting ionic concentrations in fogs. As the fog formed, droplet growth diluted the droplets; as the fog dissipated, the droplets became more concentrated.
- Evidence was found for the major processes responsible for the acidification of fog water: (i) the

scavenging of acidic precursor aerosol, (ii) the scavenging of gaseous nitric acid, and (iii) oxidation of reduced sulfur components to sulfate. Conversion of  $\text{SO}_2(\text{g})$  to sulfate in fog water does not appear to proceed faster than  $10\% \text{ h}^{-1}$  and therefore cannot account for the high acidities observed at the beginning of fog events; however, sulfate production in the precursor air parcel can lead to sulfuric acid fog condensation nuclei.

- Modeling of fog water chemistry indicated that the high acidities observed can be explained by either of the three processes listed above. The main aqueous-phase S(IV) oxidants were found to be hydrogen peroxide, ozone and oxygen (catalyzed by trace metals). Aqueous-phase production of nitrate was found to be unimportant.
- The Caltech Rotation Arm Collector (RAC), which has been used to sample fog water, has been fully characterized and compared in a controlled field experiment to the performance of collectors of other design. Evaporation of droplets during all stages of collection was shown to be negligible. Experimental calibration indicated a lower size cut of 15–20  $\mu\text{m}$ . Field data show an overall liquid water collection rate of about 60%. The field intercomparison of fog water collectors used by various investigators confirmed that our sampler collects representative samples.
- A screen collector (lower size cut 2  $\mu\text{m}$ , sampling rate  $20 \text{ m}^3 \text{ min}^{-1}$ ) was designed and has been used in the field. Side-by-side comparison indicates that samples collected with this collector and with the rotating arm have similar concentrations.
- Concentrations of S(IV) in fog water were far in excess of those expected to be in equilibrium with ambient  $\text{SO}_2(\text{g})$ . Elevated formaldehyde concentrations suggest the formation of a formaldehyde-S(IV) complex; kinetic and model studies have shown that this complex is very stable and that its formation leads to high aqueous-phase S(IV) concentrations.
- Extensive Bakersfield fog water data indicated an important removal to the ground of pollutants scavenged by the fog droplets. This was ascribed to the slow residence time of the supermicron fog droplets in the atmosphere. In a stagnant atmosphere, this deposition was suspected to alleviate build-up of suspended particles. On the mountain slopes surrounding the Los Angeles Basin, such nonrecipitating wet deposition was shown to be a significant source of overall pollutant deposition.
- Concentrations of  $\text{NH}_4^+$ ,  $\text{NO}_3^-$  and  $\text{SO}_4^{2-}$  in urban fog water samples are routinely on the order of  $10^{-3} \text{ M}$ .
- The relative importance of  $\text{NO}_3^-$  and  $\text{SO}_4^{2-}$  reflects their emission pattern in the vicinity. Nitrate exceeds  $\text{SO}_4^{2-}$  by a factor of 2–3 in Los Angeles where vehicle emissions of  $\text{NO}_x$  are significant. Sulfate equals or exceeds nitrate in the Southern San Joaquin Valley where emissions from oil-production facilities are important.
- Ammonia emissions in the Southern San Joaquin Valley are sufficient to neutralize most of the acidity present. Acid anion concentrations in Bakersfield are comparable to those in Los Angeles, but very few fog water samples had  $\text{pH} < 4$ ; ammonium was about equal to the sum of  $\text{NO}_3^-$  and  $\text{SO}_4^{2-}$ .
- Droplet growth and evaporation is a major factor determining fog water concentrations—the highest concentrations are observed as fog dissipates.
- Deposition of fog droplets appears to be significant. The mass of solute per volume of air decreases over the course of a fog event. Repeated fogs may diminish the build-up of pollutants during stagnation episodes.
- No statistical evidence for aqueous-phase sulfur oxidation can be found for events. However, over the course of stagnation episodes in the Southern San Joaquin Valley, the sulfate fraction in the aerosol increases. However, mass balance analyses indicate that S(VI) is produced at the rate of 7–10%  $\text{h}^{-1}$  during fog episodes.
- Concentrations of S(IV) and  $\text{CH}_2\text{O}$  in fog and cloud water on the order of  $10^{-4} \text{ M}$  are routinely found in urban areas. Peak values are about  $10^{-3} \text{ M}$ .
- The partial pressure of  $\text{SO}_2$  during fog is much too low to support all of the S(IV) as free S(IV) ( $\text{SO}_2 \cdot \text{H}_2\text{O} + \text{HSO}_3^- + \text{SO}_3^{2-}$ ). The difference is due to the presence of hydroxymethanesulfonate, a S(IV)-HCHO adduct that has been identified and quantified using mobile phase ion chromatography.
- The solute loading (mass/ $\text{m}^3$  air) in fog is comparable to that in the aerosol.
- The  $\text{NO}_3^-/\text{SO}_4^{2-}$  ratio in fog is high than in the dry aerosol preceding the fog, which suggests that gaseous  $\text{HNO}_3$  is incorporated into the fog.
- Deposition from fog by sedimentation or impaction may be comparable to rainfall deposition at some mountain sites. Trees are very efficient collectors and are often bathed with impacted fog.

Fogwater impacting on vegetation routinely has a pH 3, which may be injurious to sensitive species.

- In addition to formaldehyde, fog- and cloudwater contain a variety of higher aldehydes. Acetaldehyde and propanal (or acrolein) often have concentrations comparable to formaldehyde.
- Low molecular weight carboxylic acids are present in fog and cloudwater at about  $10^{-4}$  M. Formic and acetic acid dominate.

#### ACKNOWLEDGMENTS

We are grateful to the California Air Resources Board, the National Center for Atmospheric Research, and the U.S. Environmental Protection Agency for their support of the research described above. In particular we would like to thank Dr. J. Calvert, Dr. M. Dodge, Dr. J. Holmes, Dr. D. Lawson, Dr. R. Papetti and Mr. E. Fujita for their assistance in making this research possible.

#### REFERENCES

1. Jacob, D. J., J. M. Waldman, J. W. Munger, and M. R. Hoffmann. "A Field Investigation of Physical and Chemical Mechanisms Affecting Pollutant Concentrations in Fog Droplets," *Tellus* 36B:272-285 (1984).
2. Waldman, J. M., J. W. Munger, D. J. Jacob, R. C. Flagan, J. J. Morgan, and M. R. Hoffmann. "Chemical Composition of Acid Fog," *Science* 218:677-680 (1982).
3. Munger, J. W., D. J. Jacob, J. M. Waldman, and M. R. Hoffmann. "Fogwater Chemistry in an Urban Atmosphere," *J. Geophys. Res.* 88C:5109-5121 (1983).
4. Jacob, D. J., J. M. Waldman, J. W. Munger, and M. R. Hoffmann. "Chemical Composition of Fogwater Collected Along the California Coast," *Environ. Sci. Tech.* 19:730-735 (1985).
5. Waldman, J. M., J. W. Munger, D. J. Jacob, and M. R. Hoffmann. "Chemical Characterization of Stratus Cloudwater and Its Role as a Vector for pollutant Deposition in a Los Angeles Pine Forest," *Tellus* 37B:91-108 (1985).
6. Houghton, H. G. "On the Chemical Composition of Fog and Cloud Water," *J. Meteorol.* 12:355-357 (1955).
7. Mrose, H. "Measurements of pH, and Chemical Analyses of Rain-, Snow-, and Fog-Water," *Tellus* 18:266-270 (1966).
8. Mack, E. J., U. Katz, C. W. Rogers, et al. "An Investigation of the Meteorology, Physics, and Chemistry of Marine Boundary Layer Processes," Report CJ-6017-M-1, Calspan Corp., Buffalo, NY (1977).
9. Okita, T. "Concentrations of Sulfate and Other Inorganic Materials in Fog and Cloud Water and in Aerosol," *J. Meteor. Soc. Japan* 46:120-126 (1968).
10. Lazrus, A. L., H. W. Baynton, and J. P. Lodge. "Trace Constituents in Oceanic Cloud Water and Their Origin," *Tellus* 22:106-114 (1970).
11. Hoffmann, M. R. "Comment on Acid Fog," *Environ. Sci. Technol.* 18:61-64 (1984).
12. Commins, B. T., and R. E. Waller. "Observations from a Ten-Year Study of Pollution at a Site in the City of London," *Atmos. Environ.* 1:49-68 (1967).
13. Firket, J. "Fog Along the Meuse Valley," *Trans. Faraday Soc.* 32:1192-1197 (1936).
14. Schrenk, H. H., H. Heiman, G. D. Clayton, W. M. Gafefer, and H. Wexler. "Air Pollution in Donora, PA: Epidemiology of the Unusual Smog Episode of October 1948, Preliminary Report." *Public Health Bull.* 306:1-73 (1949).
15. Thomas, M. D., R. H. Hendricks, and G. R. Hill. "Some Impurities in the Air and Their Effects on Plants," in *Air Pollution: Proc. of U.S. Tech. Conf.*, L. McCabe, Ed. (New York: McGraw-Hill), pp. 41-47 (1952).
16. Granett, A. L., and R. C. Musselman. "Simulated Acid Fog Injures Lettuce." *Atmos. Environ.* 18:887-891 (1984).
17. Schebatskoy, T., and R. M. Klein. "Response of Spruce and Birch Foliage to Leaching by Acidic Mists," *J. Environ. Qual.* 12:189-195 (1983).
18. Pruppacher, H. R., and J. D. Klett. *Microphysics of Clouds and Precipitation* (Amsterdam: Reidel), pp. 9-27, 136-148 and 412-421 (1978).
19. Mack, E. J., and R. J. Pilie. "Fog Water Collector," U.S. Patent No. 3889532 (1975).
20. Jacob, D. J., R-F. T. Wang, and R. C. Flagan. "Fogwater Collector Design and Characterization," *Environ. Sci. Technol.* 18:827-833 (1984).
21. Davies, C. N., and M. Subari. "Aspiration Above Wind Velocity of Aerosols with Thin-

- Walled Nozzles Facing and at Right Angles to the Wind Direction," *J. Aerosol Sci.* 13:59-71 (1982).
22. Appel, B. R., S. M. Wall, Y. Tokiwa, and M. Haik. "Simultaneous Nitric Acid, Particulate Nitrate, and Acidity Measurements in Ambient Air," *Atmos. Environ.* 14:549-554 (1980).
  23. Cadle, S. H., R. J. Countess, and N. A. Kelly. "Nitric Acid and Ammonia Concentrations in Urban and Rural Locations," *Atmos. Environ.* 16:2501-2506 (1980).
  24. Russell, A. G., and G. R. Cass. "Acquisition of Regional Air Quality Data Model Validation for Nitrate, Sulfate, Ammonium Ion and their Precursors," *Atmos. Environ.* 18:1815-1827 (1984).
  25. John, W., and G. Reischl. "A Cyclone for Size-Selective Sampling of Ambient Air," *J. Air Pollut. Control Assoc.* 30:872-876 (1980).
  26. Derrick, M., and J. Moyers. "Precise and Sensitive Water Soluble Ion Extraction Method for Aerosol Samples Collected on Polytetrafluoroethylene Filters," *Anal. Lett.* 14A:1637-1642 (1981).
  27. Dionex Corporation, "Determination of Anions in Acid Rain," Application note 31, Dionex Corp., Sunnyvale, CA (1981).
  28. Solorzano, L. "Determination of Ammonia in Natural Waters by the Phenol Hypochlorite Method," *Limnol. Oceanogr.* 14:799-801 (1967).
  29. Russell, A. G. "Analysis of Oxalic Acid Impregnated Filters for Ammonia Determination," Open File Report 83-1, Environmental Quality Laboratory, California Institute of Technology, Pasadena, CA (1983).
  30. Dasgupta, P. K., K. De Cesare, and J. C. Ullrey. "Determination of Atmospheric Sulfur Dioxide Without Tetrachloromercurate(II) and the Mechanism of the Schiff Reaction," *Anal. Chem.* 52:1912-1922 (1980).
  31. Humphrey, R. E., M. H. Ward, and W. Hinze. "Spectrophotometric Determination of Sulfite with 4,4-Dithiopyridine and 5,5-Dithiobis(2-Nitrobenzoic Acid)," *Anal. Chem.* 42:698-702 (1970).
  32. Munger, J. W., D. J. Jacob, and M. R. Hoffmann. "The Occurrence of Bisulfite-Aldehyde Addition Products in Fog- and Cloudwater," *J. Atmos. Chem.* 1:335-350 (1984).
  33. Nash, T. "The Colorimetric Estimation of Formaldehyde by Means of the Hantzsch Reaction," *Biochem. J.* 55:426-421 (1953).
  34. Smith, R. V., and P. W. Erhardt. "Nash Determination for Formaldehyde in the presence of Bisulfite," *Anal. Chem.* 47:2454-2462 (1975).
  35. Piliie, R. J., E. J. Mack, W. C. Kolmund, W. J. Eadie, and C. W. Rogers. "The Life Cycle of Valley Fog. Part II: Fog Microphysics," *J. Appl. Meteor.* 14:364-374 (1975).
  36. Roach, W. T., R. Brown, S. J. Caughey, J. A. Garland, and C. J. Readiness. "The Physics of Radiation Fog: I—A Field Study," *Quart. J. R. Meteor. Soc.* 102:313-333 (1976).
  37. Goodman, J. "The Microstructure of California Coastal Fog and Stratus," *J. Appl. Meteorol.* 16:1056-1067 (1977).
  38. Knollenberg, R. G. "Techniques for Probing Cloud Microstructure," in *Clouds, Their Formation, Optical Properties, and Effects*, P. V. Hobbs and A. Deepak, Eds. (New York: Academic Press).
  39. Hering, S. V., and D. L. Blumenthal. "Fog Sampler Intercomparison Study: Data Volume," Prepared for Coordinating Research Council, Atlanta, GA (1983).
  40. Hering, S. V., and D. L. Blumenthal. "Fog Sampler Intercomparison Study: Final Report," Prepared for Coordinating Research Council, Atlanta, GA (1985).
  41. Jacob, D. J., J. M. Waldman, Munger, J. W. and M. R. Hoffmann. "A Field Investigation of Physical and Chemical Mechanisms Affecting Pollutant Concentrations in Fog Droplets," *Tellus* 36B:272-285 (1984).
  42. Jacob, D. J., J. W. Munger, J. M. Waldman, and M. R. Hoffmann. "The H<sub>2</sub>SO<sub>4</sub>-HNO<sub>3</sub>-NH<sub>3</sub> System at High Humidities and in Fogs: I. Spatial and Temporal Patterns in the San Joaquin Valley of California," *J. Geophys. Res.* 91D:1073-1088 (1986).
  43. Jacob, D. J., J. M. Waldman, J. W. Munger, and M. R. Hoffmann. "The H<sub>2</sub>SO<sub>4</sub>-HNO<sub>3</sub>-NH<sub>3</sub> System at high Humidities and in Fogs: II. Comparison of Field Data with Thermodynamic Calculations," *J. Geophys. Res.* 91D:1089-1096 (1986).
  44. Bassett, M. E., and J. H. Seinfeld. "Atmospheric Equilibrium Model of Sulfate and Nitrate Aerosols," *Atmos. Environ.* 17:2237-2252 (1983).
  45. Grosjean, D. "Formaldehyde and Other Carbonyls in Los Angeles Ambient Air," *Environ. Sci. Technol.* 16:254-262 (1982).

46. National Research Council, *Formaldehyde and Other Aldehydes*, National Academy Press, Washington, D.C. (1981).
47. Grosjean, D., and B. Wright. "Carbonyls in Urban Fog, Ice Fog, Cloudwater, and Rainwater," *Atmos. Environ.* 17:2093-2096 (1983).
48. Richards, L. W., J. A. Anderson, D. L. Blumenthal, J. A. McDonald, G. L. Kok, and A. L. Lazrus. "Hydrogen Peroxide and Sulfur(IV) in Los Angeles Cloudwater," *Atmos. Environ.* 17:911-914 (1983).
49. Munger, J. W., C. Tiller, and M. R. Hoffmann. "Identification of Hydroxymethanesulfonate in Fog Water," *Science* 231:247-249 (1986).
50. Boyce, S. D., and M. R. Hoffmann. "Kinetics and Mechanism of the Formation of Hydroxymethanesulfonic Acid at Low pH," *J. Phys. Chem.* 88:4740-4746 (1984).
51. Deister, U., R. Neeb, G. Helas, and P. Warneck. "The Equilibrium  $\text{CH}_2(\text{OH})\text{SO}_3^- + \text{H}_2\text{O}$  in Aqueous Solution: Temperature Dependence and Importance in Cloud Chemistry," *J. Phys. Chem.* (in press).
52. Kok, G. L., S. N. Gitlin, and A. L. Lazrus. "Kinetics of the Formation and Decomposition of Hydroxymethanesulfonate," *J. Geophys. Res.* (in press).
53. Kerp, W. *Arbb. Kaisel. Gesundh.* 421:180 (1904); *Chem. Zentralblatt* 7511:56-59 (1904).
54. Donally, L. H. *Ind. Eng. Chem. Anal. Ed.* 5:91-92 (1933).
55. Olson, T. M., and M. R. Hoffmann. "On the Kinetics of Formaldehyde-S(IV) Adduct Formation in Slightly Acidic Solution," *Atmos. Environ.* (in press).
56. Olson, T. M., S. D. Boyce, and M. R. Hoffmann. "Kinetics, Thermodynamics and Mechanism of the Formation of Benzaldehyde-S(IV) Adducts," *J. Phys. Chem.* (in press).
57. Tukey, H. B., Jr. "The Leaching of Substances from Plants," *Ann. Rev. Plant Physiol.* 71:305-324 (1970).
58. May, K. R. "Physical Aspects of Sampling Airborne Microbes," in *Airborne Microbes*, P. H. Gregory and J. L. Monteith, Eds., 60-80 (1967).
59. Israel, R., and D. E. Rosner. "Use of a Generalized Stokes Number to Determine the Aerodynamic Capture Efficiency of Non-Stokesian Particles from a Compressible Gas Flow," *Aerosol Sci. Technol.* 2:45-51 (1983).
60. Garland, J. A. "Some Fog Droplet Size Distributions Obtained by an Impactor Method," *Quart. J. R. Meteor. Soc.* 97:483-494 (1971).
61. Justo, J. E., and G. G. Lala. "Radiation Fog Field Programs - Recent Studies," Publ. No. 869, Atmospheric Sciences Research Center, State University of New York, Albany (1983).
62. Waldman, J. M. "Depositional Aspects of Fogs and Clouds," PhD Thesis, California Institute of Technology, Pasadena, CA (1986).
63. Kennedy, J. B., and A. M. Neville. *Basic Statistical Methods for Engineers and Scientists*, 2nd ed., (New York: Harper and Row, Publ., 1976) 198-220.
64. Katz, U. "A Droplet Impactor to Collect Liquid Water from Laboratory Clouds for Chemical Analysis," in *Communications a la VII Conference Internationale sur la Physique des Nuages*, Laboratoire Associe de Meteorologie Physique, Aubiere, France, 697-700 (1980).
65. Pinnick, R. G., D. M. Garvey, and L. D. Duncan. "Calibration of Kröllenberg FSSP Light-Scattering Counters for Measurements of Cloud Droplets," *J. Appl. Meteor.* 20:1049-1057 (1981).
66. Baumgardner, D. "An Analysis and Comparison of Five Water Droplet Measuring Instruments," *J. Clim. Appl. Meteor.* 22:891-910 (1983).
67. Richards, L. W., J. A. Anderson, D. L. Blumenthal, S. C. Duckhorn, and J. A. McDonald. "Characteristics of Reactants, Reaction Mechanisms, and Reaction Products Leading to Extreme Acid Rain and Acid Aerosol Conditions in Southern California," Report RR-83-6, California Air Resources Board, Sacramento, CA (1983).
68. Jensen, D. R., R. Jeck, G. Trusty, and G. Schacher. "Intercomparison of Particle Measuring Systems, Inc.'s Particle-Size Spectrometers," *Opt. Engin.* 22:746-752 (1983).
69. Hudson, J. G., and C. F. Rogers. "Interstitial CCN Measurements Related to Mixing in Clouds." Presented at 9th Intern. Cloud Physics Conference, August 21-28, Tallinn, USSR (1984).
70. Calvert, J. G. in *Acid Precipitation*,  $\text{SO}_2$ ,  $\text{NO}$ , and  $\text{NO}_2$  Oxidation Mechanisms: Atmospheric Considerations (Stoneham, MA: Butterworth Publishers, 1984).
71. Cass, G. R. "Methods for Sulfate Air Quality Management with Applications to Los Angeles, Methods for Sulfate Air Quality Management with Applications to Los Angeles," PhD Thesis, California Institute of Technology, Pasadena, CA (1977).

72. Hegg, D. A., and P. V. Hobbs. "Measurements of Sulfate Production in Natural Clouds," *Atmos. Environ.* 16:2663-2668 (1982).
73. Hegg, D. A., and P. V. Hobbs. "Oxidation of Sulfur Dioxide in Aqueous Systems with particular Reference to the Atmosphere," *Atmos. Environ.* 12:241-253 (1978).
74. Kaplan, D. J., D. M. Himmelblau, and C. Kanaoka. "Oxidation of Sulfur dioxide in Aqueous Ammonium Sulfate Aerosols Containing Manganese as a Catalyst," *Atmos. Environ.* 15:763-773 (1981).
75. Penkett, S. A., B. M. R. Jones, and A. E. J. Eggleton. "A Study of SO<sub>2</sub> Oxidation in Stored Rainwater Samples," *Atmos. Environ.* 13:139-147 (1979).
76. Penkett, S. A., B. M. R. Jones, K. A. Brice, and A. E. J. Eggleton. "The Importance of Atmospheric Ozone and Hydrogen Peroxide in Oxidizing Sulfur Dioxide in Cloud and Rainwater," *Atmos. Environ.* 13:123-137 (1979).
77. Beilke, S., and G. Gravenhorst. "Heterogeneous SO<sub>2</sub>-Oxidation in the Droplet Phase," *Atmos. Environ.* 12:231-239 (1978).
78. Martin, L. R. "Kinetic Studies of Sulfite Oxidation in Aqueous Solution," in *Acid Precipitation*, J. G. Calvert, Ed. (Stoneham, MA: 1984), pp. 63-100.
79. Hoffmann, M. R., and S. D. Boyce. "Catalytic Autoxidation of Aqueous Sulfur Dioxide in Relationship to Atmospheric Systems," in *Trace Atmospheric Constituents: Properties, Transformations and Fates*, S. E. Schwartz, Ed. *Adv. Environ. Sci. Technol.* 12:147-189 (1983).
80. Jacob, D. J., and M. R. Hoffmann. "A Dynamic Model for the Production of H<sup>+</sup>, NO<sub>3</sub><sup>-</sup>, and SO<sub>4</sub><sup>2-</sup> in Urban Fog," *J. Geophys. Res.* 88C:6611-6621 (1983).
81. Hoffmann, M. R., and D. J. Jacob. "Kinetics and Mechanisms of the Catalytic Oxidation of Dissolved Sulfur Dioxide in Aqueous Solution: An Application to Nighttime Fog-Water Chemistry," in *Acid Precipitation*, J. G. Calvert, Ed. (Boston, MA: Butterworth Publ., 1984).
82. Jacob, D. J. "The Origins of Inorganic Acidity in Fogs," PhD Thesis, California Institute of Technology, Pasadena, CA (1985).
83. Hoffmann, M. R., and J. G. Calvert. "Chemical Transformation Modules for Eulerian Acid Deposition Models Vol.II: The Aqueous-Phase Chemistry," EPA/NCAR Report DW 930237, March (1985).
84. Chameides, W. L., and D. D. Davis. "The Free Radical Chemistry of Cloud Droplets and its Impact upon the Composition of Rain," *J. Geophys. Res.* 87C:4863-4877 (1982).
85. Chameides, W. L. "The Photochemistry of a Remote Marine Stratiform Cloud," *J. Geophys. Res.* 89D:4739-4755 (1984).
86. Seigneur, C., and P. Saxena. "A Study of Atmospheric Acid Formation in Different Environments," *Atmos. Environ.* 18:2109-2124 (1984).
87. Gradedel, T. E. and K. I. Goldberg. "Kinetics Studies of Raindrop Chemistry 1. Inorganic and Organic Processes," *J. Geophys. Res.* 88C:10865-10882 (1983).



## CHAPTER 9

# KINETICS AND MECHANISMS OF CHEMICAL REACTIONS IN CLOUDS AND FOGS

by

Michael R. Hoffmann

Environmental Engineering Science  
W. M. Keck Laboratories  
California Institute of Technology  
Pasadena, California 91125

A paper presented at the

European Science Foundation Symposium on  
Cloud Chemistry

July, 1987  
Cambridge, England



## Introduction

Clouds, fogs, and haze aerosols are subjected to the same chemical processes because of their physical similarities. For example, cloud- and fogwater droplets are found in the size range of 2 to 50  $\mu\text{m}$ , while deliquescent haze aerosol will be in the range of 0.01 to 1  $\mu\text{m}$ . On the other hand, raindrops are approximately 100 times larger than cloud and fog water droplets (0.1 to 3 mm). However, a more important determinant of aqueous-phase chemistry within the droplets is the liquid water content (LWC); values of LWC range from 0.1 to 1.0  $\text{g m}^{-3}$  in clouds, from 0.01 to 0.5  $\text{g m}^{-3}$  in fogs, and from 10 to 100  $\mu\text{g m}^{-3}$  in haze aerosols. The presence of condensation nuclei, which are composed of both soluble and insoluble materials, is essential for the formation of atmospheric water droplets. Accretion or evaporation of water to or from the condensation nuclei or droplet is forced by the difference between the ambient and local humidities, and is affected by the droplet surface tension and the chemical potential of the solutes in the liquid phase. During droplet growth, the temperature within the droplet differs from the ambient temperature due to the release of latent heat, which in turn depends upon the instantaneous growth rate.

Fog and cloud droplets are highly effective at scavenging certain gases and particles present in the atmosphere. The overall fraction of material incorporated into fog droplets depends upon nucleation scavenging and gas transfer. The initial chemical speciation may be altered by *in situ* chemical transformations and subsequent droplet-phase scavenging. The total concentration of species  $i$  in a parcel of air is given by

$$[C_i]_T = [C_i]L + P_{C_i}(RT)^{-1} + [C_i]_a \quad (1)$$

where  $[C_i]_T$  is the total concentration of  $C_i$  ( $\text{mol m}^{-3}$ ) in the atmosphere,  $[C_i]_f$  is the concentration of  $C_i$  in the droplet phase in units of  $\text{mol m}^{-3}$  ( $[C_i]_f = L[C_i]$ ),  $[C_i]_g$  is the concentration ( $\text{mol m}^{-3}$ ) of  $C_i$  in the gas phase ( $[C_i]_g = P_{C_i}(RT)^{-1}$ ), and  $[C_i]_a$  is the

concentration of  $C_i$  in the non-activated aerosol.  $R$  is the universal gas constant ( $\text{atm m}^3 \text{mol}^{-1} \text{K}^{-1}$ ) and  $T$  is temperature in degrees K.

Fog- and cloudwater often have extremely low pH values (e.g.  $1.7 < \text{pH} < 4$ ) and extremely high concentrations of sulfate (1 to 20 mM), nitrate (1 to 20 mM), ammonium ion (0.1 to 20 mM) and trace metals (1 to 1000  $\mu\text{M}$ ). Waldman et al. (1) and Munger et al. (2) have summarized concentrations reported for fogs and clouds sampled in California and elsewhere around the world. Of special interest are the high values observed for  $\text{SO}_4^{2-}$ ,  $\text{NO}_3^-$ , S(IV),  $\text{CH}_2\text{O}$ , Fe, Mn, Pb and Cu in fogwater. These values and their time-dependent changes indicate that fogs and clouds provide a very reactive environment for the accumulation of  $\text{HNO}_3$  and  $\text{H}_2\text{SO}_4$ . Concomitant incorporation of  $\text{NH}_3$  gas and calcareous dust into the droplet phase neutralizes some of the acidity. In the pH domain typically encountered in fogs and clouds (pH 2-7), absorption of  $\text{SO}_2(\text{g})$ ,  $\text{HNO}_3(\text{g})$ ,  $\text{H}_2\text{O}_2(\text{g})$ , and  $\text{NH}_3(\text{g})$  is thermodynamically favorable because of their relatively high Henry's Law coefficients.

Of the metals commonly found in atmospheric water droplets, Fe, Mn and Cu are expected to be potential catalysts for the *in situ* oxidation of S(IV) with molecular oxygen. Iron and Mn have been found in concentrations as high as 400  $\mu\text{M}$  and 15  $\mu\text{M}$  in fog (1-7). Model calculations indicate that metal-catalyzed autoxidations along with oxidation by  $\text{H}_2\text{O}_2$ ,  $\text{O}_3$ , and OH may contribute significantly to the overall sulfate formation rate in atmospheric droplets, particularly in the range of Fe and Mn concentrations observed in urban fog (8-10).

In addition to transition metal ions a wide variety of other chemical constituents have been found in clouds. For example, carbonyl compounds, such as aldehydes and ketones, have been found to influence liquid-phase sulfur dioxide chemistry through their reactions with  $\text{SO}_2$  to form stable  $\alpha$ -hydroxyalkanesulfonates. Field measurements have detected formaldehyde at concentrations of greater than 100  $\mu\text{M}$  in fog- and cloudwater samples collected in Southern California (11-13). The concentrations of acetaldehyde.

glyoxal, methylglyoxal, and hydroxyacetaldehyde occasionally approach or exceed that of  $\text{CH}_2\text{O}$ . In addition to each one of the aldehydes present the corresponding carboxylic acid has been observed, although formic and acetic acid dominate the low molecular weight carboxylic acids. They are found in concentrations as high as  $100 \mu\text{M}$ .

The presence of  $\text{CH}_2\text{O}$  and  $\text{H}_2\text{O}_2$  ( $2 - 50 \mu\text{M}$ ) in conjunction with  $\text{S(IV)}$  at levels higher than those predicted by gas/liquid solubility equilibria suggests that  $\alpha$ -hydroxymethanesulfonate ( $\text{HMS}$ ,  $\text{HOCH}_2\text{SO}_3^-$ ) production stabilizes a fraction of  $\text{S(IV)}$  with respect to oxidation. Equilibrium calculations using available thermodynamic and kinetic data for the reaction of  $\text{SO}_2$  and  $\text{CH}_2\text{O}$  demonstrate that elevated concentrations of  $\text{S(IV)}$  in fog water cannot be achieved without consideration of sulfonic acid production,  $\text{HORHSO}_3^-$  (11). Munger et al. (13) have identified and quantified HMSA using ion-pairing chromatography. Other  $\text{S(IV)}$  adducts which have been observed in cloudwater droplets include those formed with glyoxal, methylglyoxal, acetaldehyde, and hydroxyacetaldehyde.

Jacob et al. (14-17) have systematically characterized the interaction of  $\text{H}_2\text{SO}_4$ ,  $\text{HNO}_3$ ,  $\text{NH}_3$  and in fog, aerosol, and the gas phase. The observed spatial patterns of concentrations were shown to closely reflect the distribution of  $\text{SO}_2$ ,  $\text{NO}_x$ , and  $\text{NH}_3$  emissions within well-defined regions. Furthermore, they (16) have compared field data for the  $\text{H}_2\text{SO}_4$ - $\text{HNO}_3$ - $\text{NH}_3$  system with thermodynamic calculations of the aerosol composition. Close agreement has been found between field measurements and theoretical predictions. Their field studies have shown that typical wintertime conversion rates for  $\text{S(IV)}$  in fogs were about  $5 \%$   $\text{hr}^{-2}$  and about  $1 \%$   $\text{hr}^{-2}$  in haze aerosol.

## Kinetic Considerations of Droplet-Phase Reactions

Gas-phase reactions of  $\text{SO}_2$  with ozone ( $\text{O}_3$ ), hydroxyl radical ( $\text{OH}\cdot$ ), and hydroperoxyl radical ( $\text{HO}_2\cdot$ ) are too slow to account for observed rates of sulfate production

in humid urban atmospheres (18–19) and in wave clouds (20). Consequently, the catalytic autoxidation of  $\text{SO}_2$  in deliquescent haze aerosol and hydrometeors appears to be a viable non-photolytic pathway for the rapid formation of sulfuric acid in humid atmospheres (21–26). In addition, hydrogen peroxide and ozone have been established as important aqueous-phase oxidants of dissolved  $\text{SO}_2$  (26). Oxidation by  $\text{H}_2\text{O}_2$  seems to be most favorable under low pH conditions ( $\text{pH} < 4$ ) because of a rapid rate of reaction and a negative pH-dependence that favors the facile conversion of  $\text{HSO}_3^-$  to sulfate. In comparison, metal-catalyzed autoxidation and oxidation of S(IV) with  $\text{O}_3$  tend to proceed more slowly with decreasing pH (27).

Limiting factors in the autoxidation pathways are the total concentration of the active metal catalyst and its equilibrium speciation as a function of pH. Los Angeles fog water contains high concentrations of iron, manganese, copper, nickel and lead (3,4,6,7). Of these metals, Fe, Mn and Cu are expected to be the most effective catalysts for the reaction of S(IV) with molecular oxygen (25–27). Model calculations indicate that metal-catalyzed autoxidations may contribute significantly to the overall sulfate formation rate in atmospheric droplets, particularly in the range of Fe and Mn concentrations observed in urban fog. However, the composition of the precursor haze aerosol or cloud condensation nuclei will determine to a large extent the observed chemical speciation of the droplet phase.

Chameides (28) has predicted based on model calculations that aqueous-phase free radical pathways can contribute substantially to the generation of acidity via the *in situ* oxidation of S(IV) and HCHO to S(VI) and formic acid, respectively. The principal oxidants of S(IV) as identified by Chameides were  $\text{H}_2\text{O}_2$ ,  $\text{O}_3$ ,  $\cdot\text{OH}$ , and  $\text{HO}_2\cdot$ . Parameters found to affect the S(IV) to S(VI) conversion rate were the accommodation coefficient for the reactive species of interest, the liquid water content, and the ambient levels of  $\text{SO}_2$  and  $\text{HNO}_3$ . Seigneur and Saxena (29) have predicted that gas-phase hydrocarbon chemistry will dominate  $\cdot\text{OH}$  chemistry (i.e., aqueous-phase  $\cdot\text{OH}$  chemistry due to radical scavenging

appears to be inconsequential). While Mozurkewich (30) argues that nitrate radical,  $\text{NO}_3$ , is unlikely to play an important role in the nighttime chemistry of a cloud because of its low Henry's Law constant ( $\sim 0.03 \text{ M atm}^{-2}$ ). Jacob (31) has shown that radical pathways are very important for the chemistry of remote clouds in terms of formate production and in terms of the buildup of peroxymonosulfuric acid, a S(VI)-peroxide intermediate of high oxidation potential.

Aqueous-phase pathways for the production of nitric acid are relatively minor contributors to nitrate accumulation in the droplet phase because of the low Henry's Law constants for  $\text{NO}_2$  and  $\text{NO}$  and because of second-order reaction kinetics with respect to  $[\text{NO}_2]$  (32-33). The predominant pathways for S(IV) transformation involve reactions with  $\text{H}_2\text{O}_2$ ,  $\text{O}_3$ ,  $\text{O}_2$  ( $\text{Fe}^{3+}$  and  $\text{Mn}^{2+}$  catalyzed),  $\cdot\text{OH}$ ,  $\text{HONO}$ ,  $\text{CH}_3\text{OOH}$ ,  $\text{CH}_3\text{CO}_3\text{H}$ ,  $\text{PAN}$ ,  $\text{HO}_2\cdot$ ,  $\text{HCHO}$ , and soot.

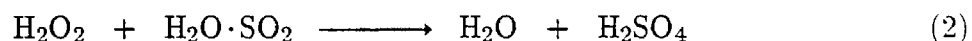
A summary of rate expressions and kinetic data for these reactions is given in Table 1. In order to understand the potential importance of each reaction over a broad range of pH, a comparison of calculated reaction rates for an idealized cloud with a liquid water content (LWC) of  $0.2 \text{ g m}^{-3}$  at  $25^\circ\text{C}$  and gas-phase concentrations of reactive components typical of the Los Angeles atmosphere can be made. We clearly see in these calculations that pH is the master variable for this comparative system of reactions. The simple calculations show that  $\text{H}_2\text{O}_2$  is the most effective oxidant of S(IV) in an open-phase system over the entire pH range. Below pH 4.0, hydrogen peroxide appears to be the sole reactant capable of producing environmentally significant S(IV) oxidation rates. Above pH 4, a number of kinetic pathways in addition to the S(IV)- $\text{H}_2\text{O}_2$  reaction become viable potential contributors to net S(IV) oxidation. Ozone,  $\cdot\text{OH}$ ,  $\text{HO}_2\cdot$ ,  $\text{HONO}$  and Fe(III)- and Mn(II)-catalyzed autoxidation are major contributors to S(IV) oxidation above pH 4. With an idealized "sticking coefficient" of 1.0 for  $\cdot\text{OH}$ , the  $\cdot\text{OH}$  pathway may proceed as rapidly as  $500 \text{ \% hr}^{-1}$  at pH 5.0. Likewise, the predicted conversion rate for the above reactants at pH 5.0 are as follows:  $\text{H}_2\text{O}_2$  ( $331 \text{ \% hr}^{-1}$ ),  $\text{O}_3$  ( $131 \text{ \% hr}^{-1}$ ),  $\text{HO}_2\cdot$  ( $2.0 \text{ \% hr}^{-1}$ ),  $\text{HONO}$  ( $36.3$

% hr<sup>-1</sup>), Fe(III)/O<sub>2</sub> (200.0 % hr<sup>-1</sup>), and Mn(II)/O<sub>2</sub> (95.5 % hr<sup>-1</sup>). At slightly higher pH. PAN and peroxyacetic acid will contribute somewhat to the net S(VI) production rate.

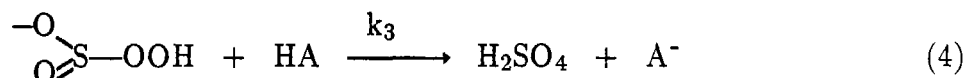
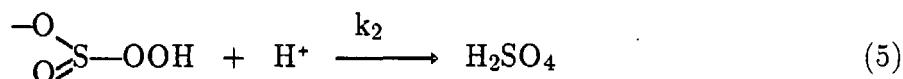
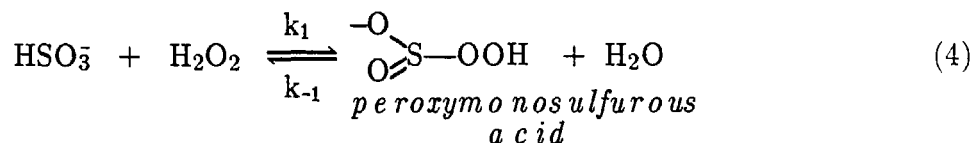
In addition to the oxidation pathways for S(IV) mentioned above, one additional pathway for S(IV) transformation involves the reversible formation of  $\alpha$ -hydroxymethanesulfonate or other hydroxyalkylsulfonates or disulfonates from the *in situ* reactions between RCHO and S(IV). The details of the thermodynamics of this system have been presented by Munger et al. (11) and Munger et al. (13). Using the kinetic data and rate law of Boyce and Hoffmann (34) as shown in Table 1 the calculated formation rate of HOCH<sub>2</sub>SO<sub>3</sub><sup>-</sup> at pH 5.0 is 43.6 % hr<sup>-1</sup> and at pH 7.0 it is 1.95 x 10<sup>5</sup> % hr<sup>-1</sup>. These results suggest that RCHO/S(IV) adducts form preferentially near sources of SO<sub>2</sub> and RCHO in near-neutral, aquated haze aerosol. Because of the extremely slow dissociation kinetics for these adducts, the sulfonate complexes are metastable in more acidic environments with lower P<sub>SO<sub>2</sub></sub> and P<sub>RCHO</sub>. Unfavorable reaction kinetics at pH 3 does not necessarily mean that these adducts should not be found. It does indicate that proximity to sources and transport considerations are very important.

## Reaction Mechanisms

### *Hydrogen Peroxide and Sulfur Dioxide*



The oxidation of aquated sulfur dioxide proceeds via a nucleophilic displacement of HSO<sub>3</sub><sup>-</sup> by H<sub>2</sub>O<sub>2</sub> to form peroxymonosulfurous acid as an intermediate which in turn undergoes an acid-catalyzed (both specific acid and general acid) rearrangement to give the products as described by the stoichiometry of equation 2 (36). The mechanism can be written as follows:



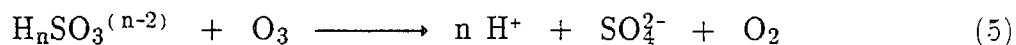
This mechanism was originally proposed by Hoffmann and Edwards (37) and reaffirmed by many other investigators (38). Similar mechanisms have been proposed by Lind et al. (39) for the oxidation of S(IV) by methyl hydroperoxide, and peroxyacetic acid. The theoretical rate expression that results from this mechanism is as follows:

$$\nu = \frac{d[\text{S(VI)}]}{dt} = \frac{k_1 K_{a1} [\text{H}_2\text{O}_2] [\text{S(IV)}]}{(k_{-1} + k_2 [\text{H}^+] + k_3 [\text{HA}]) (K_{a1} + [\text{H}^+])} (k_2 [\text{H}^+] + k_3 [\text{HA}]) \quad (5)$$

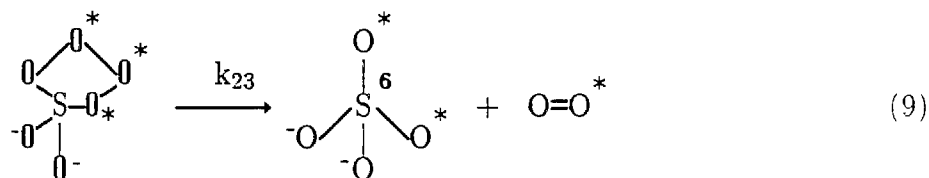
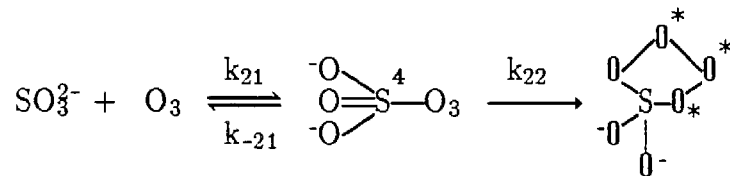
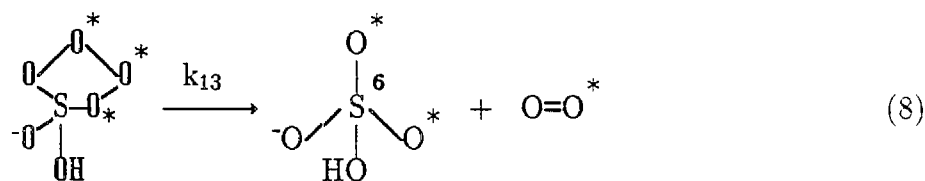
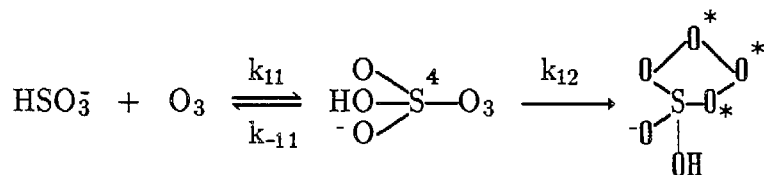
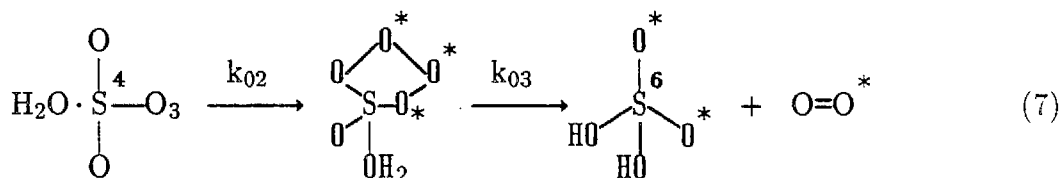
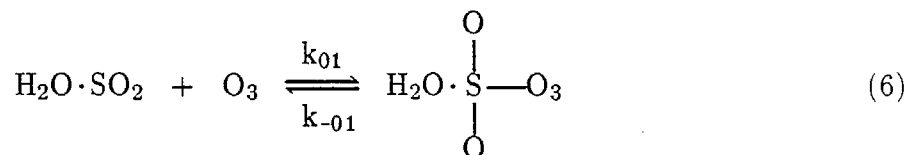
where HA represents any general acid (i.e. weak acid or proton donor). This rate law reduces to the form given in Table 2 when the general acid-catalyzed pathway of eqn. 4 is ignored.

### *Ozone and Sulfur Dioxide*

The oxidation of aquated sulfur dioxide by ozone (40)



proceeds via three independent pathways that involve a nucleophilic attack on ozone by  $\text{SO}_3^{2-}$ ,  $\text{HSO}_3^-$ , and  $\text{H}_2\text{O}\cdot\text{SO}_2$ . The starred oxygens indicate labeled oxygen ( $^{18}\text{O}$ ).



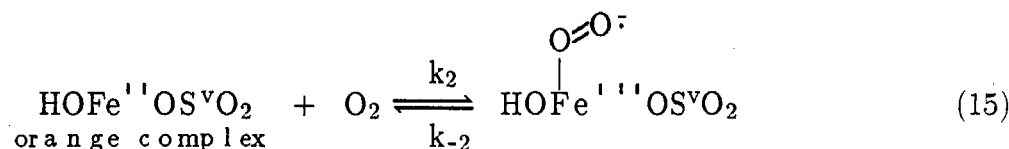
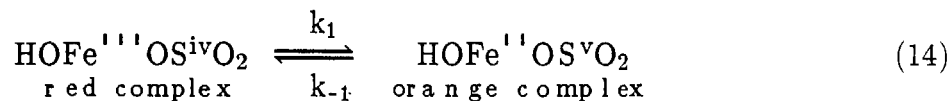
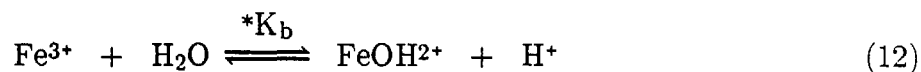
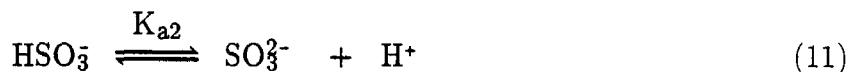
The theoretical rate expression that results from the mechanisms of eqns. 6–9 is as follows:

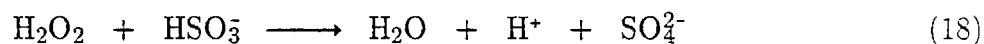
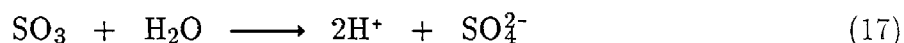
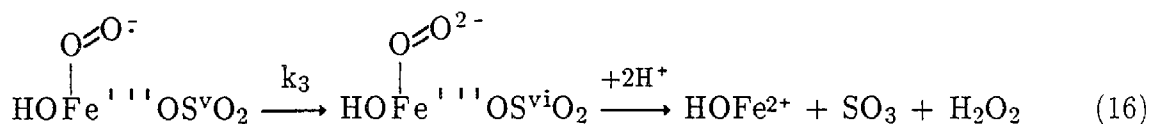
$$\nu = \left[ \frac{k_{02}k_{01}}{(k_{-01} + k_{02})} [\text{H}_2\text{O} \cdot \text{SO}_2] + \frac{k_{12}k_{11}}{(k_{-11} + k_{12})} [\text{HSO}_3^-] + \frac{k_{22}k_{21}}{(k_{-21} + k_{22})} [\text{SO}_3^{2-}] \right] [\text{O}_3] \quad (10)$$

Equation 10 is readily reduced to the form given in Table 1.

### *Oxygen and Sulfur Dioxide as Catalyzed by Fe(III)*

In light of our present work and the work of others (41–46) the following mechanism is proposed for the autoxidation of S(IV):





A rate expression can be derived from the above mechanism by applying the steady-state

approximation around the intermediate,  $\text{HOFe}^{\text{III}}\text{OS}^{\text{V}}\text{O}_2$ , such that the rate of production of sulfate is given by

$$\frac{d[\text{SO}_4^{2-}]}{dt} = k_3 \left[ \text{HOFe}^{\text{III}}\text{OS}^{\text{V}}\text{O}_2 \right] \quad (19)$$

or

$$\frac{d[\text{SO}_4^{2-}]}{dt} = \left[ \frac{k_2}{k_3 + k_{-2}} \right] \left[ \frac{k_1}{k_2[\text{O}_2] + k_{-1}} \right] K_4 \alpha_1 \beta_1 [\text{Fe(III)}][\text{S(IV)}][\text{O}_2] \quad (20)$$

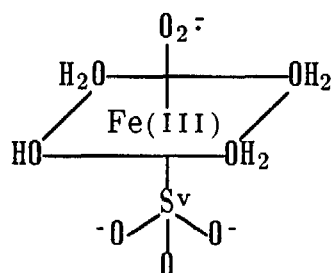
We can reduce Eq. 20 to the following form by assuming that  $k_3 \gg k_{-2}$  and  $k_2[\text{O}_2] \gg k_{-1}$  (these approximations are valid given the magnitude of stability constants (i.e.  $K_4' = k_2/k_{-2}$ ) and rate constants for ligand substitution):

$$\frac{d[\text{SO}_4^{2-}]}{dt} = k_1 K_4 \alpha_2 \beta_1 [\text{Fe(III)}][\text{S(IV)}] \quad (21)$$

At pH 4,  $\beta_1 \sim 1$ ,  $k_1 \sim 0.04 \text{ s}^{-1}$  and  $k_1 K_4 = 1.0 \times 10^6 \text{ M}^{-1} \text{ s}^{-1}$ . If we compare the predicted rate expression of Eq. 21 to the composite rate law (Eq. 22) obtained by analysis of the empirical data given the investigators listed in Table 3,

$$-\frac{d[\text{S(IV)}]}{dt} = k[\text{Fe(III)}][\text{S(IV)}] \alpha_2 \quad (22)$$

we see that  $k \approx k_1 K_4$ . The value obtained for  $k$  given in Table 4 is  $1.2 \times 10^6 \text{ M}^{-1} \text{ s}^{-1}$  while the calculated value of  $k_1 K_4$  is  $1.0 \times 10^6 \text{ M}^{-1} \text{ s}^{-1}$  (41). The active catalytic intermediate of Eq. 19 can be drawn as follows:



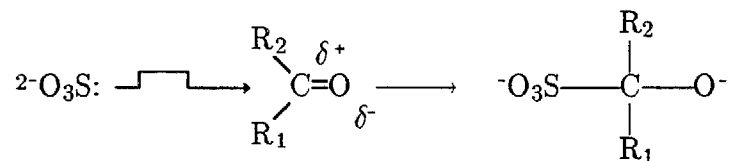
in order to reflect the known geometry for octahedrally-coordinated Fe(III) and to reflect the Fe-O-S mode of bonding as determined by Raman measurements (41).

Although Fe has been found in high ( $\approx 100 \mu\text{M}$ ) concentrations in atmospheric droplets, much of this iron would be in form of solid particles or colloids. Ferric oxides, such as  $\text{Fe}_2\text{O}_3$ , have been identified as components of airborne particles. Other sulfite complexes, such as  $\alpha$ -hydroxyalkylsulfonates, have larger stability constants than the Fe(III)-S(IV) complexes ( $K$  for the  $\text{HSO}_3^-/\text{HCHO}$  adduct =  $[\text{HOCH}_2\text{SO}_3^-]/[\text{HCHO}]_T[\text{HSO}_3^-]$ , =  $10^7$ ). Thus, given the stability constant  $K_1 = 10^{6.6}$  for  $\text{FeSO}_3^\ddagger$ , the ratio of  $[\text{Fe(III)}]_T : [\text{HCHO}]_T$  would have to be approximately 30 at pH 2 or  $3 \times 10^2$  at pH 5 for comparable concentrations of  $\text{FeSO}_3^\ddagger$  to coexist with  $\text{HOCHSO}_3^-$ . Aldehydes have been found in much higher concentrations than Fe(III) in cloud-, fog- and rainwater systems.

therefore S(IV) speciation is likely to be dominated by  $\text{RC(OH)SO}_3^-$  chemistry rather than  $\text{Fe(SO}_3)_n^{3-2n}$ .

### *Formation of Carbonyl-S(IV) Adducts*

The reversible formation of S(IV)-carbonyl adducts occurs via nucleophilic addition. This involves the attack of a nucleophile, with its lone-pair electrons, on the carbon atom of the carbonyl group. Using sulfite as an example, the addition step and associated displacement of electrons can be illustrated as follows:

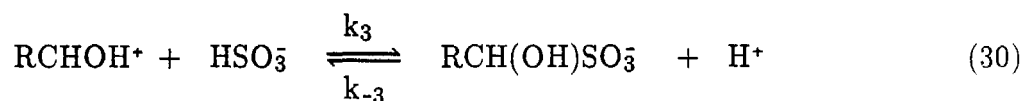
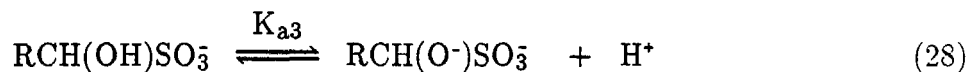
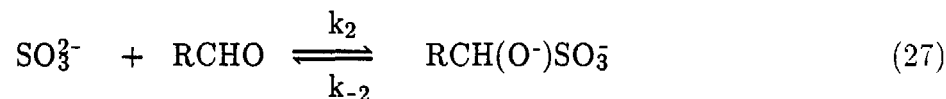
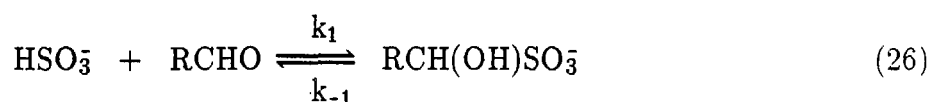
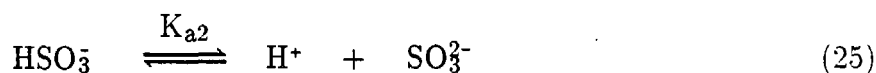
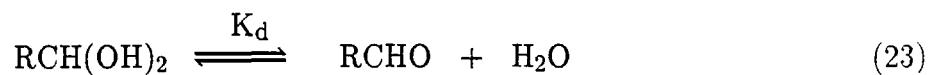


Polarization induced by the electronegative carbonyl oxygen and by the substituents  $\text{R}_1$  and  $\text{R}_2$  results in a partial positive charge at the carbon atom and hence a favorable site for nucleophilic attack. As sulfite approaches the carbon atom, oriented perpendicular to the plane of the carbonyl group, it displaces a pair of  $\pi$ -bond electrons and forms a stable  $\sigma$ -bond.

The order of increasing reactivity among aqueous S(IV) species has been experimentally demonstrated to be in the direction of increasing nucleophilic character (47-53):  $\text{H}_2\text{O}\cdot\text{SO}_2 < \text{HSO}_3^- < \text{SO}_3^{2-}$ . The second-order rate constants for the reaction of bisulfite and sulfite with isobutyraldehyde, formaldehyde, benzaldehyde, and methylglyoxal are compared in Table 4. The transition state for reaction with  $\text{HSO}_3^-$  may involve a cyclic, high entropy intermediate whereas that for  $\text{SO}_3^{2-}$  does not; and that the difference in entropy of activation is a major reason for the faster addition reactions of  $\text{SO}_3^{2-}$ .

The following elementary steps adequately describe the reaction of most aldehydes

with S(IV).

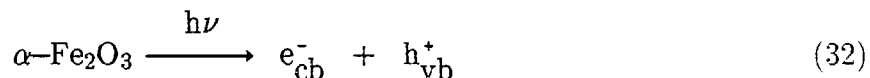


The theoretical rate expression that results from this mechanism has the following form far from equilibrium:

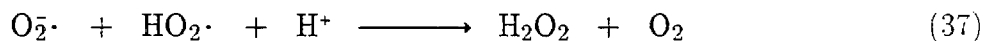
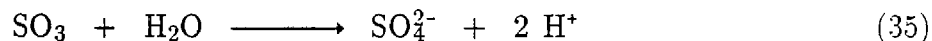
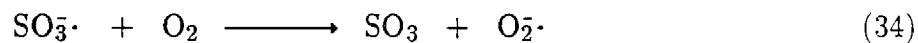
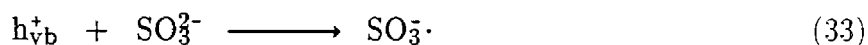
$$\frac{d[\text{RCH(OH)SO}_3^-]}{dt} = (k_1[\text{SO}_3^{2-}] + k_2[\text{HSO}_3^-] + k_3K_H[\text{H}^+][\text{HSO}_3^-])[\text{RCHO}] \quad (31)$$

### *Heterogeneous Photocatalytic Oxidation of Sulfur Dioxide*

Metal oxide semiconductors such as  $\alpha\text{-Fe}_2\text{O}_3$  can function either as photosensitizers or as photocatalysts (54). Absorption of a photon with an energy equal to or greater than the bandgap energy,  $E_g$ , of a semiconductor results in the transient formation of an electron/hole pair (i.e. exciton).



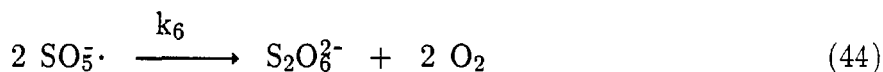
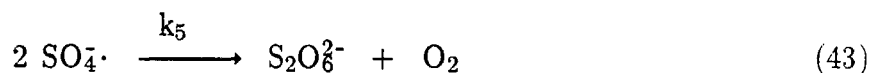
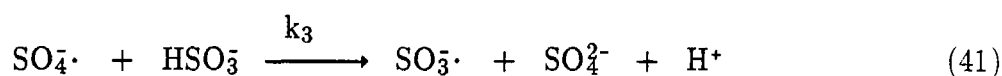
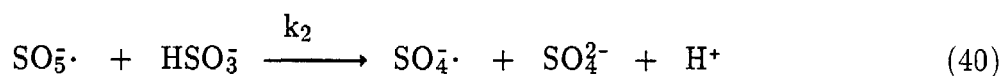
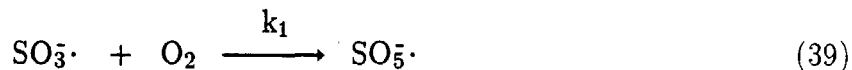
In the absence of suitable electron and hole scavengers adsorbed to the surface of a semiconductor particle, recombination occurs within 100 ns. However, when appropriate scavengers are present the valance band holes,  $h_{\text{vb}}^+$ , function as powerful oxidants while the conduction band electrons,  $e_{\text{cb}}^-$ , function as moderately powerful reductants. Aqueated sulfur dioxide can be readily oxidized on the particle surface as follows:



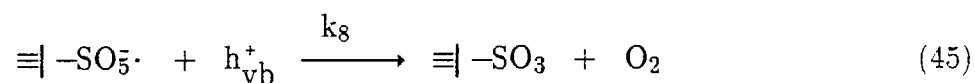
The rate law that arises from this surface-limited mechanism is

$$\nu = \Phi\beta(1 - e^{-\gamma\{\text{Fe}_2\text{O}_3\}}) \left[ \frac{K [\text{HSO}_3^-]}{1 + K [\text{HSO}_3^-]} \right] \quad (38)$$

where  $\Phi$  is the intrinsic quantum yield { i.e.  $\text{S(IV)} + h\nu_{\text{cb}} \rightarrow \text{SO}_3^- \cdot$ },  $K$  is the adsorption equilibrium constant,  $\beta$  is the incident photon flux ( $\text{M min}^{-1}$ ),  $\{\text{Fe}_2\text{O}_3\}$  is the mass concentration of catalyst ( $\text{g L}^{-1}$ ), and  $\gamma$  is a function of the apparent absorptivity of the solid ( $\text{L g}^{-1}$ ). When the number of reactive surface sites is limiting desorption of  $\text{SO}_3^- \cdot$  radical from the surface can occur. This will lead to the following free radical chain reaction in aqueous solution:



An additional free-radical termination step involves the surficial reaction of  $\text{SO}_5^- \cdot$

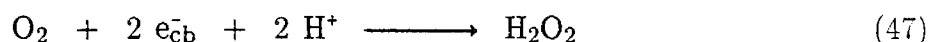


Given this mechanism the following rate expression is obtained (55):

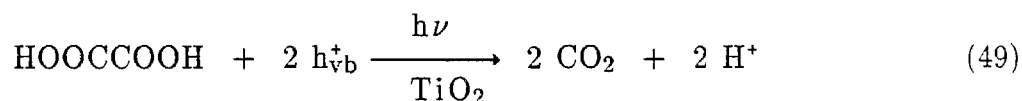
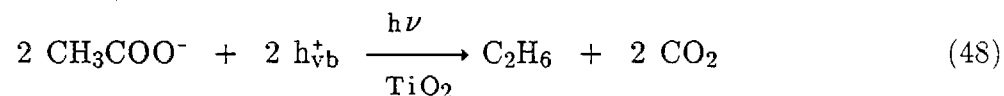
$$-\frac{d[\text{S(IV)}]}{dt} = -\frac{k_3 k_8}{4k_7} \{M_x O_y\} [\text{HSO}_3^-] +$$

$$[\text{HSO}_3^-] \sqrt{\left[ \frac{k_3 k_8}{4k_7} \right]^2 \{M_x O_y\}^2 + \frac{k_3^2}{2k_7} \Phi \beta (1 - e^{-\gamma \{M_x O_y\}}) \left[ \frac{K [\text{HSO}_3^-]}{1 + K [\text{HSO}_3^-]} \right]} \quad (46)$$

The photocatalytic production of hydrogen peroxide on particle surfaces has been clearly established (56).



In addition to the photocatalytic production of peroxide, the photocatalytic oxidation of weak organic acids such as acetate/acetic acid can proceed simultaneously as follows:



## References

1. Liljestrand, H. M. Ph.D. Thesis, California Institute of Technology, Pasadena, 1980.
2. Liljestrand, H. M.; Morgan, J. J. *Environ. Sci. Technol.* 1981, **15**, 333-338.
3. Waldman, J. M.; Munger, J. W.; Jacob, D. J.; Hoffmann, M. R. *Tellus* 1985, **37B**, 91-108.
4. Munger, J. W.; Jacob, D. J.; Waldman, J. W.; Hoffmann, M. R. *J. Geophys. Res.* 1983, **88C**, 5109-5121.
5. Jacob, D. J.; Wang, R. T.; Flagan, R. C. *Environ. Sci. Tech.* 1984, **18**, 827-833.
6. Jacob, D. J.; Waldman, J. M.; Munger, J. W.; Hoffmann, M. R. *Environ. Sci. Technol.* 1985, **19**, 730-735.
7. Waldman, J. M.; Munger, J. W.; Jacob, D. J.; Flagan, R. C.; Morgan, J. J.; Hoffmann, M. R. *Science*, **218**, 677-680.
8. Jacob, D. J.; Hoffmann, M. R. *J. Geophys. Res.* 1983, **88**, 6611-6621.
9. Jacob, D. J. Ph.D. Thesis, California Institute of Technology, Pasadena, 1985.
10. Hoffmann, M. R.; Jacob, D. J.; in "SO<sub>2</sub>, NO and NO<sub>2</sub> Oxidation Mechanisms: Atmospheric Consideration"; Calvert, J. G., Ed.; ACID PRECIPITATION SERIES Vol. 3, Butterworth Publishers: Boston, 1984; 101-172.
11. Munger, J. W., Jacob, D. J., and Hoffmann, M. R., *J. Atmos. Chem.* 1984, **1**, 335-350.
12. Waldman, J. M. Ph.D. Thesis, California Institute of Technology, Pasadena, CA, 1986.
13. Munger, J. W.; Tiller, C.; Hoffmann, M. R. *Science* 1986, **231**, 247-249.
14. Jacob, D. J.; Waldman, J. M.; Munger, J. W.; Hoffmann, M. R. *Tellus* 1984, **36B**, 272-285.
15. Jacob, D. J.; Waldman, J. M.; Munger, J. W.; Hoffmann, M. R. *J. Geophys Res.* 1986, **91D**, 1089-1096.
16. Jacob, D. J.; Munger, J. W.; Waldman, J. M.; Hoffmann, M. R. *J. Geophys Res.* 1986, **91D**, 1073-1088.
17. Jacob, D. J.; Shair, F. H.; Waldman, J. M.; Munger, J. W.; Hoffmann, M. R. *Atmos. Environ.* 1987, **21**, 1305-1313.
18. Calvert, J. G. in Acid Precipitation, SO<sub>2</sub>, NO, and NO<sub>2</sub> Oxidation Mechanisms: Atmospheric Considerations, Butterworth Publishers, Stoneham, MA (1984).

19. Cass, G. R., Ph.D. Thesis, California Institute of Technology, Pasadena, CA (1977).
20. Hegg, D. A.; Hobbs, P. V. *Atmos. Environ.* 1982, **16**, 2663–2668.
21. Hegg, D. A. and Hobbs, P. V. *Atmos. Environ.* 1978, **12**, 241–253.
22. Kaplan, D. J., Himmelblau, D. M. and Kanaoka, C. *Atmos. Environ.* 1981, **15**, 763–773.
23. Penkett, S. A., Jones, B. M. R. and Eggleton, A. E. J. *Atmos. Environ.* 1979, **13**, 139–147.
24. Penkett, S. A., Jones, B. M. R., Brice, K. A. and Eggleton, A. E. J. *Atmos. Environ.* 1979, **13**, 123–137
25. Beilke, S. and Gravenhorst, G. *Atmos. Environ.* 1978, **12**, 231–239.
26. Martin, L. R. "Kinetic Studies of Sulfite Oxidation in Aqueous Solution," in *Acid Precipitation*, edited by J. G. Calvert, Butterworth Publishers, Stoneham, MA, 63–100 (1984).
27. Hoffmann, M. R. and Boyce, S. D. "Catalytic Autoxidation of Aqueous Sulfur Dioxide in Relationship to Atmospheric Systems," in *Trace Atmospheric Constituents: Properties, Transformations and Fates*, S. E. Schwartz, ed. *Adv. Environ. Sci. Technol.* 1983, **12**, 147–189.
28. a. Chameides, W. L. and D. D. Davis, *J. Geophys. Res.*, 1982, **87C**, 4863–4877.  
b. Chameides, W. L., *J. Geophys. Res.*, 1984, **89D**, 4739–4755.  
c. Chameides, W. L., *J. Geophys. Res.* 1986, **91D**, 5331–5337.
29. Seigneur, C. and P. Saxena, *Atmos. Environ.* 1984, **18**, 2109–2124.
30. Mozurkewich, M., *J. Geophys. Res.* 1986, **91D**, 14569–14570.
31. Jacob, D. J., *J. Geophys. Res.* 1986, **91D**, 9807–.
32. Lee, Y. N. and Schwartz, S. E., *J. Geophys. Res.*, 1981, **86**, 11971–11983.
33. Schwartz, S. E., "Gas–Aqueous Reactions of Sulfur and Nitrogen Oxides in Liquid–Water Clouds," in *SO<sub>2</sub>, NO and NO<sub>2</sub> Oxidation Mechanisms: Atmospheric Considerations*, Calvert, J. G., Ed.; Butterworth: Boston, 1984; Vol. 3, pp. 173–208.
34. Boyce, S. D.; Hoffmann, M. R. *J. Phys. Chem.* 1984, **88**, 4740–4746.
35. Hoffmann, M. R. and Calvert, J. G. "Chemical Transformation Modules for Eulerian Acid Deposition Models Vol.II: The Aqueous–Phase Chemistry," EPA/NCAR Report DW 930237, March (1985).
36. J. V. McArdle and M. R. Hoffmann, 1983, *J. Phys. Chem.*, **87**, 5425–5429.
37. M. R. Hoffmann and J. O. Edwards, 1975, *J. Phys. Chem.*, **79**, 2096–2098.

38. a. Kunen, S. M., A. L. Lazrus, G. L. Kok, and G. G. Heikes, *J. Geophys. Res.* 1983, **88**, 3671—
- b. Y. -N. Lee, J. Shen, P. J. Klotz, S. E. Schwartz, and L. Newman, *J. Geophys. Res.* 1986, **91D**, 13264—13274.
- c. Martin, L. R. and D. E. Damschen, *Atmos. Environ.* 1981, **15**, 1615—
- d. Overton, J. H., Jr., *Atmos. Environ.* 1985, **19**, 687—
39. J. A. Lind, A. L. Lazrus, and G. L. Kok, *J. Geophys. Res.* 1986, **92D**, 4171—4178.
40. Hoffmann, M. R. *Atmos. Environ.* 1986, **20**, 1145—1154.
41. a. Hoffmann, M. R. and A. P. K. Hong, *Sci. Total Environ.* 1987, **64**, 99—115.
- b. Conklin, M. H. and M. R. Hoffmann, "Metal Ion-S(IV) Chemistry I, II., & III., in press, *Environ. Sci. Technol.* 1988, **22**, 000—000.
42. Fuzzi, S., 1978, *Atmos. Env.*, **12**, 1439—1442.
43. Brimblecombe, P. and D.J. Spedding, 1974, *Atmos. Env.*, **8**, 937—945.
44. Neytzell-de Wilde, F.G. and L. Traverner in *2nd U.N. Intl. Conf. Peaceful Uses for Atomic Energy Proc. Vol. 3* (1958), pp. 303—317.
45. Aubuchon, C., *The Rate of Iron Catalyzed Oxidation of Sulfur Dioxide by Oxygen in Water* (Ph.D. Thesis, John Hopkins U., Baltimore, MD, 1976).
46. Olson, T.M., S.D. Boyce and M.R. Hoffmann, 1986, *J. Phys. Chem.*, **90**, 2482—2488.
47. Olson, T.M. and M.R. Hoffmann, 1986, *Atmos. Env.*, **20**, 2277—2278.
48. Skrabal, A. and R. Skrabal, 1936, *Sitz. Akad. Wirs. Wien*, **145**, 617—647.
49. Green, L. R. and J. Hine, 1974, *J. Org. Chem.*, **39**, 3896—3901.
50. Gubareva, M.A. *J. Gen. Chem. (USSR)* 1947, **17**, 2259—64.
51. Betterton, E.A., and M.R. Hoffmann, 1987, *J. Phys. Chem.* **91**, 3011—3020.
52. Betterton, E. A., Y. Erel and M. R. Hoffmann, 1988, *Environ. Sci. Technol.* **22**, 92—99, 1987.
53. Olson, T. M. and M. R. Hoffmann, 1988, *J. Phys. Chem.* **92**, 533—540.
54. Bahnemann, D. W. and M. R. Hoffmann, 1987, *Proc. Electrochem. Soc.*, "Stabilization of Free Radical Intermediates on Metal Oxide Surfaces."
55. Hong, A., D. W. Bahnemann, and M. R. Hoffmann, 1987, *J. Phys. Chem.* **91**, 6245—6251.
54. Kormann, C., D. Bahnemann, and M. R. Hoffmann, 1988, *Environ. Sci. Technol.*, **22**, 000—000.

Table 1. Recommended Rate Laws and Rate Constants According to Hoffmann and Calvert (35) for 25.0 °C for the Oxidation of S(IV) in Aqueous Solution.

OXIDANT	RATE LAW & RATE CONSTANTS
$O_3$	$\nu = (k_0\alpha_0 + k_1\alpha_1 + k_2\alpha_2)[O_3][S(IV)]$ $k_0 = 2.40 \times 10^4 \text{ (M}^{-1}\text{s}^{-1}\text{)}$ $k_1 = 3.70 \times 10^5 \text{ (M}^{-1}\text{s}^{-1}\text{)}$ $k_2 = 1.50 \times 10^9 \text{ (M}^{-1}\text{s}^{-1}\text{)}$
$H_2O_2$	$\nu = k[H^+][H_2O_2][S(IV)]\alpha_1(1 + K[H^+])^{-1}$ $k = 7.50 \times 10^7 \text{ (M}^{-2}\text{s}^{-1}\text{)}$ $K = 13 \text{ M}^{-1}$
$\cdot OH$	$\nu = (k_1\alpha_1 + k_2\alpha_2)[OH][S(IV)]$ $k_1 = 9.50 \times 10^9 \text{ (M}^{-1}\text{s}^{-1}\text{)}$ $k_2 = 5.50 \times 10^9 \text{ (M}^{-1}\text{s}^{-1}\text{)}$
HONO	$\nu = k[H^+][HSO_3^-][NO_2^-]$ $k = 1.75 \times 10^7 \text{ (M}^{-1}\text{s}^{-1}\text{)}$
$CH_3OOH$	$\nu = k[H^+][CH_3OOH][S(IV)]\alpha_1$ $k = 1.75 \times 10^7 \text{ (M}^{-1}\text{s}^{-1}\text{)}$
$CH_3CO_3H$	$\nu = (k_3[H^+] + k_2)[HSO_3^-][CH_3CO_3H]$ $k_3 = 3.64 \times 10^7 \text{ (M}^{-1}\text{s}^{-1}\text{)}$ $k_2 = 6.01 \times 10^2 \text{ (M}^{-1}\text{s}^{-1}\text{)}$
PAN	$\nu = k[PAN][S(IV)]\alpha_2$ $k = 1.0 \times 10^5 \text{ (M}^{-1}\text{s}^{-1}\text{)}$
Fe(III)/ $O_2$	$\nu = k[Fe(III)][S(IV)]\alpha_2$ $k = 1.20 \times 10^6 \text{ (M}^{-1}\text{s}^{-1}\text{)}$
Mn/ $O_2$	$\nu = k_2[Mn(II)][S(IV)]\alpha_1 + k_1K_1[Mn(II)]^2$ $k_2 = 3.40 \times 10^3 \text{ (M}^{-1}\text{s}^{-1}\text{)}$ $k_1 = 2.0 \times 10^9 \text{ (M}^{-1}\text{s}^{-1}\text{)}$ $K_1 = 1.26 \times 10^{-10}$

Soot  $\nu = k_1 K_1 [C_x] [S(IV)]^2 A^{-1}$

$A = 1 + K_2 [S(IV)] + K_1 [S(IV)]^2$   
 $k_1 = 1.04 \times 10^7 \text{ (mol g}^{-1}\text{s}^{-1}\text{)}$   
 $K_1 = 4.92 \times 10^8 \text{ (M}^{-2}\text{)}$   
 $K_2 = 2.96 \times 10^5 \text{ (M}^{-1}\text{)}$

HCHO  $\nu = (k_1 \alpha_1 + k_2 \alpha_2) K_d [S(IV)] [HCHO]_T (K_d + 1)^{-1}$

$k_1 = 79 \text{ (M}^{-1}\text{s}^{-1}\text{)}$   
 $k_2 = 2.48 \times 10^7 \text{ (M}^{-1}\text{s}^{-1}\text{)}$   
 $K_d = 5.5 \times 10^{-4}$

HO<sub>2</sub>·  $\nu = (k_1 \alpha_1 \beta_0 + k_2 \alpha_2 \beta_1) [S(IV)] [HO_2]_T$

$k_1 = 1.0 \times 10^6 \text{ (M}^{-1}\text{s}^{-1}\text{)}$   
 $k_2 = 1.0 \times 10^5 \text{ (M}^{-1}\text{s}^{-1}\text{)}$   
 $K_{a1} = 1.3 \times 10^{-5} \text{ (M}^{-1}\text{)}$   
 $\beta_0 = K_{a1} ([H^+] + K_{a1})^{-1}$   
 $\beta_1 = [H^+] ([H^+] + K_{a1})^{-1}$

Table 2. Henry's Law Constants and Acidity Constants at 25.0 °C.

Species	[C] (atm)	H (M atm <sup>-1</sup> )	[C] (M)	pK <sub>1</sub>	pK <sub>2</sub>
HONO	1.0 × 10 <sup>-9</sup>	4.9 × 10 <sup>1</sup>	4.9 × 10 <sup>-8</sup>	3.15	—
CH <sub>3</sub> OOH	2.0 × 10 <sup>-11</sup>	1.0 × 10 <sup>3</sup>	2.0 × 10 <sup>-7</sup>	11.5	—
CH <sub>3</sub> COO <sub>2</sub> H	1.0 × 10 <sup>-12</sup>	1.0 × 10 <sup>4</sup>	1.0 × 10 <sup>-7</sup>	8.20	—
PAN	3.0 × 10 <sup>-8</sup>	3.6 × 10 <sup>0</sup>	1.1 × 10 <sup>-7</sup>	—	—
HO <sub>2</sub>	4.0 × 10 <sup>-12</sup>	5.0 × 10 <sup>4</sup>	2.0 × 10 <sup>-6</sup>	4.45	—
HCHO	3.0 × 10 <sup>-8</sup>	6.3 × 10 <sup>3</sup>	1.9 × 10 <sup>-4</sup>	—	—
OH	1.0 × 10 <sup>-13</sup>	2.0 × 10 <sup>2</sup>	2.0 × 10 <sup>-22</sup>	11.9	—
H <sub>2</sub> O <sub>2</sub>	1.0 × 10 <sup>-9</sup>	1.6 × 10 <sup>5</sup>	1.6 × 10 <sup>-4</sup>	11.65	—
O <sub>3</sub>	5.0 × 10 <sup>-8</sup>	1.0 × 10 <sup>-2</sup>	5.0 × 10 <sup>-11</sup>	—	—
SO <sub>2</sub>	2.0 × 10 <sup>-8</sup>	1.2 × 10 <sup>0</sup>	3.2 × 10 <sup>-5</sup>	1.89	7.22

$[S(IV)] = H_{SO_2} P_{SO_2} \alpha_0^{-1}$ ,  $\alpha_0 \equiv [SO_2 \cdot H_2O] / [S(IV)]$ ,  $\alpha_1 \equiv [HSO_3^-] / [S(IV)]$ ,  $\alpha_2 \equiv [SO_3^{2-}] / [S(IV)]$ ,  
pH = 5.0

$$\alpha_0 = \frac{[H^+]^2}{([H^+]^2 + K_{a1} [H^+] + K_{a1} K_{a2})}$$

$$\alpha_1 = \frac{K_{a1} [H^+]}{([H^+]^2 + K_{a1} [H^+] + K_{a1} K_{a2})}, \alpha_2 = \frac{K_{a1} K_{a2}}{([H^+]^2 + K_{a1} [H^+] + K_{a1} K_{a2})}$$

Table 3. Formation Constants for Selected Bisulfite-Aldehyde Adducts

Aldehyde	${}^eK_1^*$	$K_1^\dagger$	T(°C)	$\mu$ (M)	Ref.
HCHO	$8.33 \times 10^6$	$6.60 \times 10^9$	25	0.01	(48)
CH <sub>3</sub> CHO	—	$6.90 \times 10^5$	25	0.02	(52)
CH <sub>3</sub> CH <sub>2</sub> CHO	$1.30 \times 10^4$	—	20	0.01	(49)
C <sub>6</sub> H <sub>5</sub> CHO	$4.80 \times 10^3$	$9.55 \times 10^3$	25	1.00	(47)
CHOCHO	$2.81 \times 10^4$	—	25	0.02	(53)
CH <sub>3</sub> COCHO	$8.21 \times 10^8$	$8.13 \times 10^8$	25	0.20	(51)
HOCH <sub>2</sub> CHO	—	$2.00 \times 10^6$	25	0.20	(52)

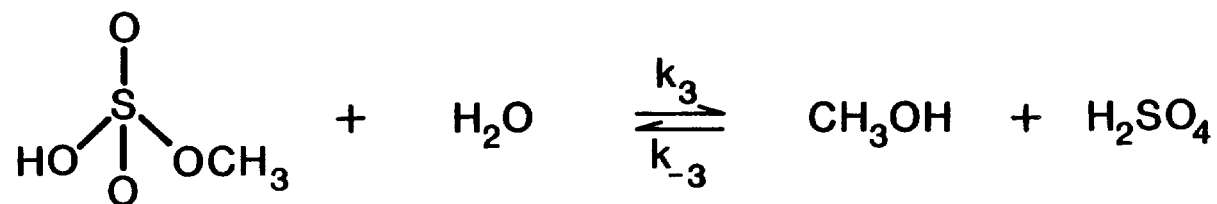
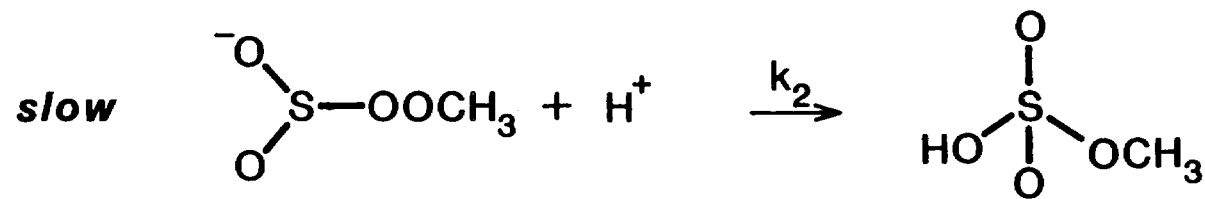
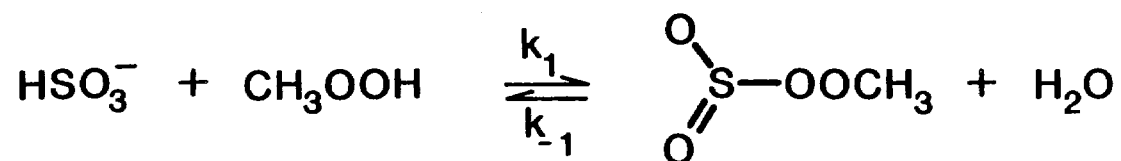
$$* {}^eK_1 = [\text{RCH(OH)SO}_3^-] / ([\text{RCHO}] + [\text{RCH(OH)}_2]) [\text{HSO}_3^-] \quad (\text{M}).$$

$$\dagger K_1 = [\text{RCH(OH)SO}_3^-] / [\text{RCHO}] [\text{HSO}_3^-] \quad (\text{M}).$$

Table 4. Rate Constants for the Rate Expression of Eqn. 31 (25 °C).

RCHO	$k_2$ (M <sup>-1</sup> s <sup>-1</sup> )	$k_1$ (M <sup>-1</sup> s <sup>-1</sup> )	$\mu$ (M)	Ref.
HCHO	$2.48 \times 10^7$	$7.90 \times 10^2$	1.0	(34)
C <sub>6</sub> H <sub>5</sub> CHO	$2.10 \times 10^4$	0.71	1.0	(47)
(CH <sub>3</sub> ) <sub>2</sub> CHCHO	$1.40 \times 10^4$	—	0.1	(48)
CH <sub>3</sub> COCHO	$3.66 \times 10^8$	$3.45 \times 10^3$	0.2	(51)
CHOCHO	$1.04 \times 10^7$	$6.50 \times 10^2$	0.2	(53)

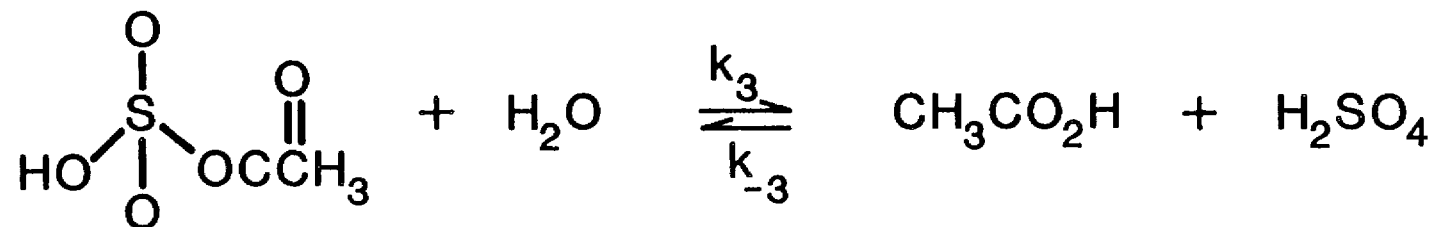
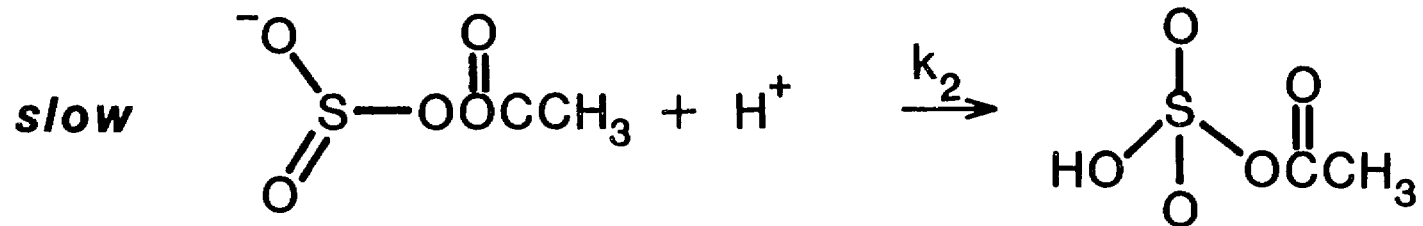
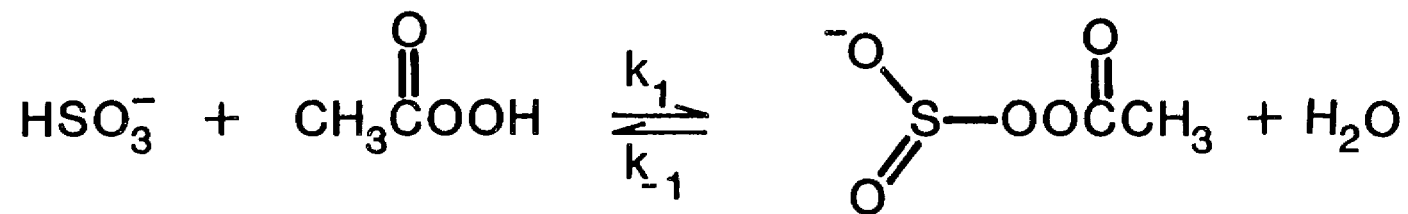
## METHYL HYDROPEROXIDE



$$K_3 = 0.11$$

$$k_3 = 7 \times 10^{-3} \text{ M}^{-1} \text{ s}^{-1}$$

# PEROXYACETIC ACID



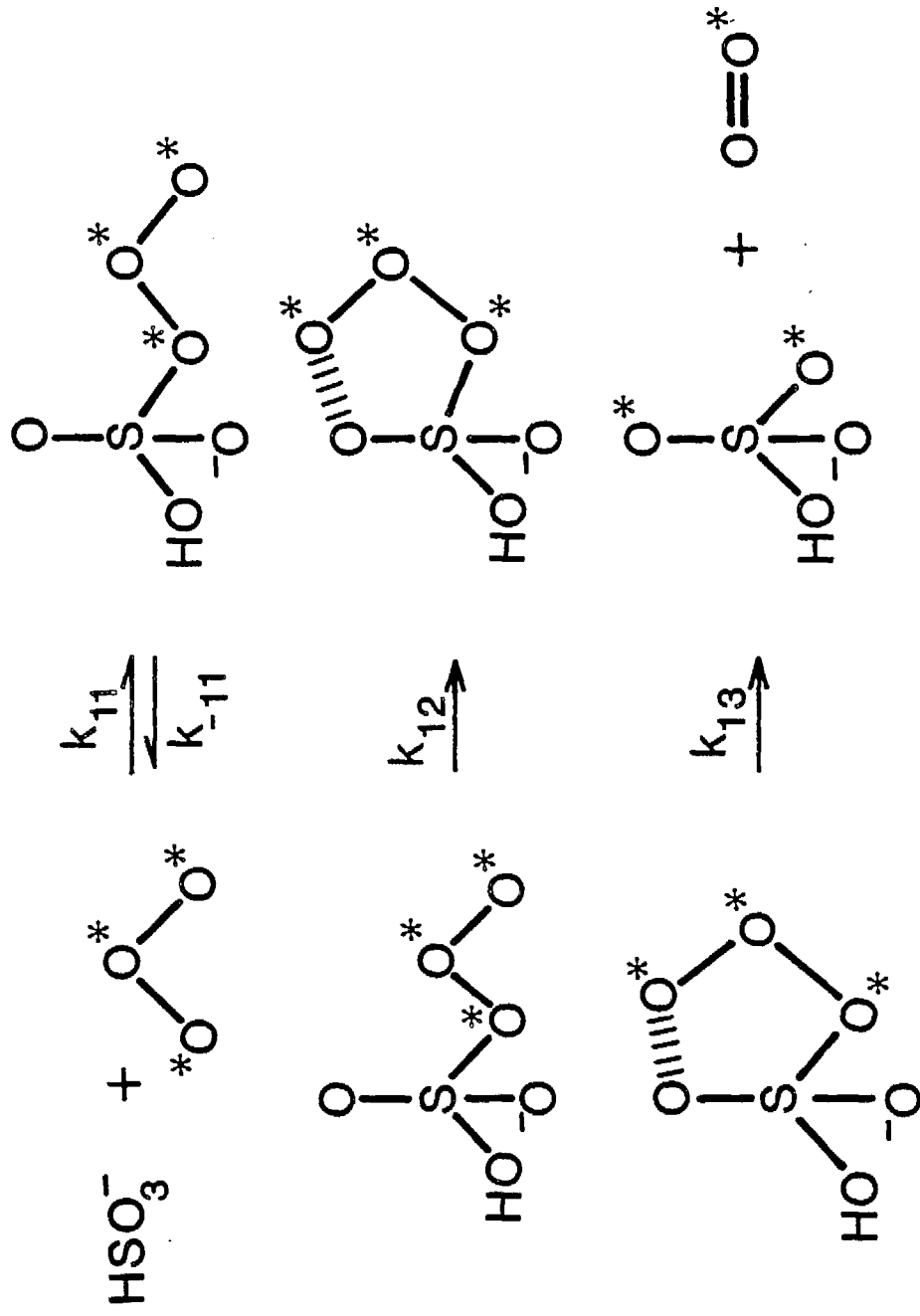
$$v = k [H^+] [ROOH] [HSO_3^-]$$

R	$k = k_2 k_1 / k_{-1} \text{ (M}^{-2} \text{s}^{-1})^*$	$K_{1†} \text{ (M atm}^{-1})^†$
H-	$7.2 \times 10^7$	$7.4 \times 10^4$
CH <sub>3</sub> -	$1.7 \times 10^7$	$2.2 \times 10^2$
$\begin{array}{c} \text{O} \\ \parallel \\ \text{CH}_3\text{C}- \end{array}$	$3.5 \times 10^7$	$4.7 \times 10^2$

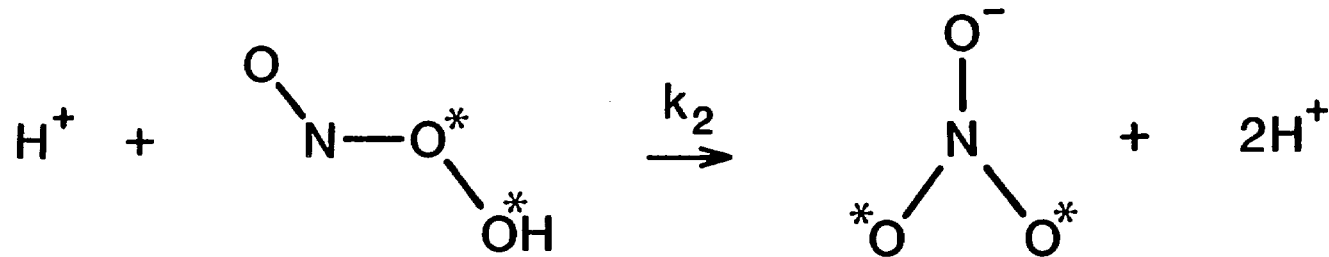
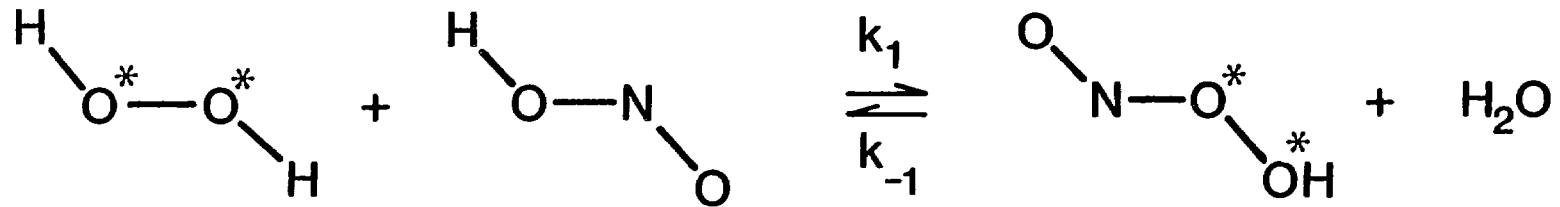
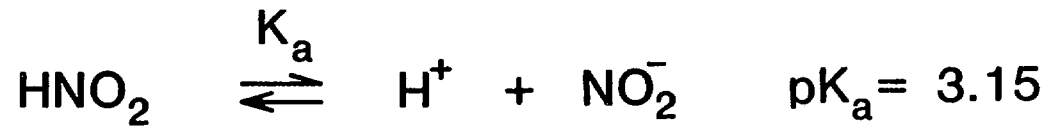
\* Lind et al. (1987)  
18 °C

† Lind & Kok (1986)  
25 °C

# S(IV) AND O<sub>3</sub>



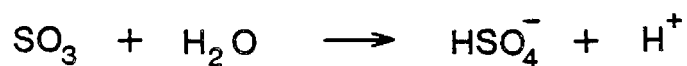
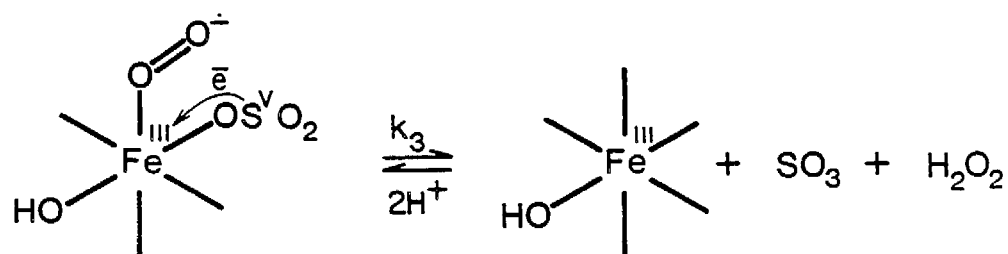
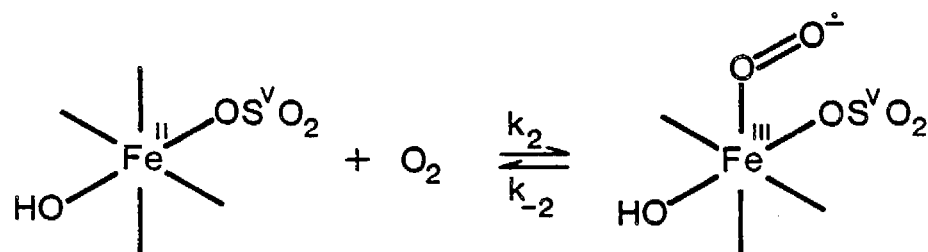
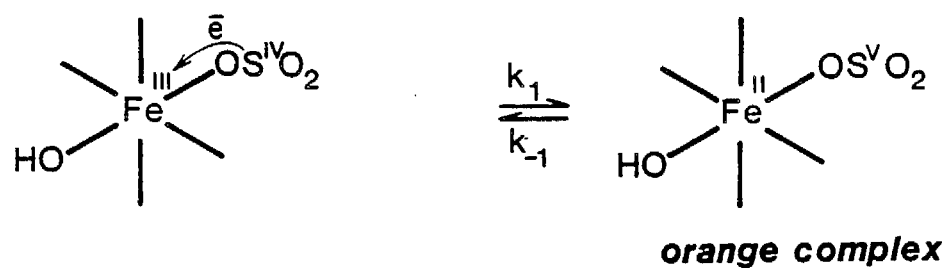
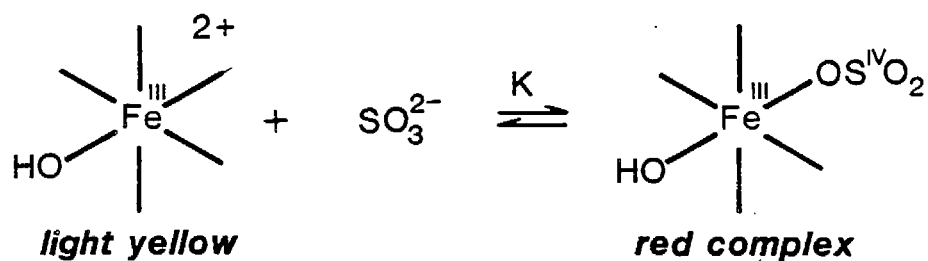
# OXIDATION OF HONO BY H<sub>2</sub>O<sub>2</sub>



$$v = \frac{k_2 k_1}{k_{-1}} [\text{H}^+] [\text{HNO}_2] [\text{H}_2\text{O}_2]$$

$$\frac{k_2 k_1}{k_{-1}} = 6.3 \times 10^3 \text{ M}^{-2} \text{ s}^{-1} \quad (\text{Lee \& Lind, 1986})$$

## Fe(III)-CATALYZED AUTOXIDATION OF S(IV)



## CHAPTER 10

# Cloudwater Chemistry in Sequoia National Park

by

Jeff Collett, Jr., Bruce Daube, Jr., J. William Munger, and Michael R. Hoffmann\*

Environmental Engineering Science  
W. M. Keck Laboratories  
California Institute of Technology  
Pasadena, California 91125

Submitted to

*Atmospheric Environment*

April 1988

## Abstract

Cloudwater was sampled during the fall of 1985 and the spring of 1986 in Sequoia National Park in the southern Sierra Nevada Mountains of California. Concentrations of major species in the cloudwater vary widely both within one cloudwater impaction event and from one event to another. The pH values of the samples range from 4.4 to 5.7. Organic acids are seen to be important contributors to the chemical composition of the cloudwater at this site.

The advance of cold fronts seems to lead to higher aerosol and gas phase concentrations in the Park than would be seen under normal mountain-valley circulations, particularly during the night and morning hours. The arrival of these increased concentrations prior to and during cloud impaction on the mountain slopes leads to higher cloudwater concentrations than would otherwise be expected. Estimates of annual deposition rates of  $\text{NO}_3^-$ ,  $\text{SO}_4^{2-}$ ,  $\text{NH}_4^+$ , and  $\text{H}^+$  due to cloudwater impaction are comparable to those measured from rainfall.

## Introduction

Interception of acidic cloudwater has been implicated as a possible contributor to the decline of forest stands both in North America and Europe (McLaughlin, 1985). Plant injury in forests has been observed to increase at higher elevations where immersion in cloudwater is more frequent and other stress factors become important (Johnson and Siccama, 1983). In order to estimate the potential impact of acidic cloudwater deposition on forest communities several issues must be addressed. Aside from the difficult questions concerning dose-response relationships between ambient cloudwater and members of the plant community, these include the frequency of cloud impaction in the area of interest, the rate of cloudwater deposition to the plant surfaces, and the chemical composition of the deposited cloudwater. Contributions by cloudwater to acidic deposition should also be compared to contributions by rainfall and dry deposition.

Sequoia National Park (SNP), located in the southern Sierra Nevada Mountains of California has extensive stands of conifers which may be sensitive to acidic cloudwater deposition. Emissions from the San Joaquin Valley and clouds associated with incoming frontal systems frequently pass through the Park (Smith et al., 1981). In order to assess the severity of the problem we began a preliminary study of cloudwater chemistry in SNP. The results of that study, the first of its kind in the Sierra Nevada Mountains, are discussed below.

## Site Description and Measurement Techniques

### • Sampling Sites

Cloudwater samples were collected at two sites in SNP during the fall of 1985 and the spring of 1986. The main collection site is situated on a granite outcrop (elev. 1856 m) at the Lower Kaweah Research Site below Giant Forest (see Fig. 1). The surrounding forest community is mixed conifer. The same site is used for NADP rainfall collection (Stohlgren and Parsons, 1987). The second site is located 3 km to the southwest at the

Deer Ridge turnout on the General's Highway. The elevation here is approximately 1490 m.

#### • Measurement Techniques

Cloudwater samples were collected with the Caltech Active Strand Collector (CASC) depicted in Figure 2. The CASC (Daube et al., 1987a) is an improved version of the collectors described in detail elsewhere (Jacob et al., 1985a, Daube et al., 1987b). The CASC employs a fan to draw air across six angled banks of 510  $\mu\text{m}$  teflon strands at a velocity of 9  $\text{m s}^{-1}$ . Cloudwater droplets in the air parcel are collected on the strands by inertial impaction. The collected droplets run down the strands, aided by gravity and aerodynamic drag forces, through a teflon sample trough into a collection bottle.

The major ions,  $\text{Cl}^-$ ,  $\text{SO}_4^{2-}$ , and  $\text{NO}_3^-$ , were measured in our laboratory using a Dionex 2020i ion chromatograph with a Dionex AS-4 column and a bicarbonate-carbonate eluent.  $\text{Na}^+$ ,  $\text{Ca}^{2+}$ , and  $\text{Mg}^{2+}$  concentrations were determined using a Varian Techtron AA6 atomic absorption spectrophotometer.  $\text{NH}_4^+$  was measured by the phenol-hypochlorite method (Solorzano, 1967) using an Alpkem flow injection analyzer. Organic acids were preserved by adding chloroform (Keene et al., 1983) to an aliquot of the cloudwater sample immediately after collection and later analyzed by ion exclusion and normal ion chromatography run in parallel.

Aerosol and gas measurements were also made at the Lower Kaweah site using filter packs. Flow rates were controlled by critical orifices and verified with a calibrated flowmeter. Teflon filters (Gelman Zefluor, 1  $\mu\text{m}$  pore size) were used to collect the aerosol for determination of major ions. An oxalic acid impregnated glass fiber backup filter was used to collect  $\text{NH}_3(\text{g})$ . A nylon backup filter was used to collect  $\text{HNO}_3(\text{g})$ . The nylon filters were extracted in the bicarbonate-carbonate eluent and the rest of the filters in distilled, deionized water on a reciprocating shaker. The extracts were then analyzed by the same methods that were used on the cloudwater samples.

## Results and Discussion

A total of twelve cloudwater samples were collected during five cloud impaction events. All of the sampled events were associated with cold fronts approaching from the north or northwest. The first eleven samples were collected at the Lower Kaweah site. The last sample was collected on May 6, 1986, at the Deer Ridge site because temperatures at Lower Kaweah were near 0 °C and the collected droplets froze on the CASC.

### · Cloudwater Composition

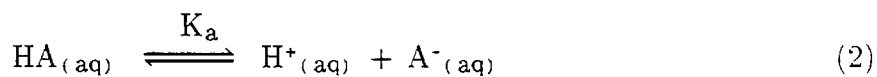
Table 1 summarizes the chemical composition of the samples. In Figure 3 the cloudwater loadings of  $\text{NH}_4^+$ ,  $\text{NO}_3^-$ , and  $\text{SO}_4^{2-}$  are presented. (The cloudwater loading of a species is defined as the amount of that species present in cloudwater per unit volume of air. It is equivalent to the cloudwater concentration multiplied by the liquid water content of the cloud). Also listed here are the estimated values of cloud liquid water content (LWC), derived from the sample collection rate and the theoretical collection efficiency of the CASC.

Wide variations are seen in both the cloudwater concentrations and loadings of all the major species. The nitrate loading, for example, ranges from less than 1 neq  $\text{m}^{-3}$  up to about 60 neq  $\text{m}^{-3}$ . The ratio of  $\text{NO}_3^-$  to  $\text{SO}_4^{2-}$  varies from below 0.5 in the fall samples to more than 1.5 in some of the spring samples. The pH of the samples ranges from 4.4 to 5.7. The last sample, which is the most acidic, is not the sample with the highest ionic loading, indicating the importance of the ionic composition of the sample in determining its acidity.

The next to the last column of Table 1 presents the calculated inorganic ion balance for each sample (sum of measured inorganic anions/sum of measured cations). For those samples with low ionic loadings it is not surprising to see this ratio differ significantly from

1.0 since relative analytical error increases near the detection limits. With the exception of the May 6 sample, however, there seems to be a consistent anion deficit, even for those samples with higher loadings. Upon collection of samples 4/24c, 5/03b, 5/03c, and 5/03d, a 2 ml aliquot of each sample was set aside and preserved with 50  $\mu$ l of chloroform. Each aliquot was analyzed for the presence of formic acid, acetic acid, lactic acid, pyruvic acid, and propanoic acid. Table 2 lists the concentrations of the organic anions expected to be in each sample based on the measured concentrations of each acid and the pH of the samples as measured in the field. In sample 5/03b the total of the concentrations of formate, acetate, lactate, and propionate is comparable to the sulfate concentration and is nearly twice the nitrate concentration. The concentrations in the other two samples are smaller, but still significant. Including these organic anions in the ion balances for the three samples changes them from 0.88, 0.62, 0.70, and 0.85 to 0.95, 0.97, 0.97, and 1.10, respectively. These ratios are within the error of the analytical procedures.

Low molecular weight organic acids are seen to be important contributors to the overall chemical composition of SNP cloudwater. This is not surprising since lower molecular weight organic acids have been shown to be important components of fog and cloudwater in the San Joaquin Valley below (Jacob et al., 1986b) and in rainwater collected at remote as well as urban sites (Galloway et al., 1984; Kawamura and Kaplan, 1984). The solubility of low molecular weight carboxylic acids is enhanced by their dissociation (see eqn. 2). Because the cloudwater samples had pH values above the  $pK_a$  values of these acids they effectively scavenged the organic acids from the gas phase. When the pH of the cloudwater falls below the  $pK_a$  values of the organic acids the solubility of these acids is diminished.



### • Aerosol and Gas Phase Measurements

During the period May 1 to May 6, 1986, aerosol was continuously sampled at the Lower Kaweah site. The aerosol, collected generally in six hour samples, was analyzed for  $\text{NO}_3^-$ ,  $\text{SO}_4^{2-}$ ,  $\text{Cl}^-$ ,  $\text{NH}_4^+$ ,  $\text{Na}^+$ ,  $\text{Ca}^{2+}$ , and  $\text{Mg}^{2+}$ . Simultaneous measurements were made of the gas phase concentrations of nitric acid and ammonia. Figure 4 presents the results obtained for the aerosol loadings of  $\text{NO}_3^-$ ,  $\text{SO}_4^{2-}$ ,  $\text{NH}_4^+$ , and  $\text{Cl}^-$ . Normally, upslope winds, caused by the heating of the air along the mountain slopes, should transport pollutants from the San Joaquin Valley to Lower Kaweah. Drainage flows that begin as the sun sets and the air in contact with the slopes cools bring cleaner air to the site and transport the aerosol back down into the valley. This pattern seems to be reflected in the data for May 4.

The data for the periods May 2 – May 3 and May 5 – May 6 show a distinctly different trend. In both periods aerosol loadings rose through the first day and continued to either rise or remain at elevated levels overnight and through some portion of the second day. A similar trend was observed in the gas phase concentrations. A cold front passed through the region during both periods. The arrows on Figure 4 show the approximate times at which clouds began to impact the cloud collection site at Lower Kaweah.

Figure 5 depicts the typical behavior of air masses during the passage of a cold front. The advancing denser cold air mass wedges its way under the warmer air mass. As the warm air mass is lifted and cooled, cloud formation and precipitation often result. Such a large scale lifting of a warm air mass previously in contact with the floor of the San Joaquin Valley could increase loadings of aerosol and gas phase species in the adjacent mountains. If the disturbance is large enough, the mountain–valley circulation may be overcome, resulting in a pattern of increased pollutant loadings at elevation until the front has passed. The data from May 2 – 3 and May 5 – 6 are consistent with this scenario.

It has been shown previously (Jacob et al., 1985, 1986a,b, 1987) that cloudwater

composition is in large part determined by the composition of the precursor aerosol and soluble gases. The possible coupling of peak gas phase and aerosol concentrations with the arrival of a front, as mentioned above, suggests that cloudwater loadings in Sequoia National Park or similar locations might be expected to be higher than would be predicted based on average gas phase and aerosol concentrations at the same location.

#### • Cloudwater Deposition

The volume-weighted average concentrations of the 12 cloudwater samples collected in SNP during this study provide the best available estimate of the average cloudwater composition there. These can be used, along with estimates of the average cloudwater deposition rate and the annual average number of hours of cloudwater impaction, to estimate the cloudwater contribution to acidic deposition in the vicinity of Lower Kaweah. Lovett (1984) estimated cloudwater deposition rates to a subalpine balsam fir forest that varied linearly from 0.2 to 1.2 mm hr<sup>-1</sup> for canopy top wind speeds of 2 to 10 m s<sup>-1</sup>. The much taller forest in SNP should be expected to receive at least the same deposition rate under similar conditions. Selecting a moderate wind speed of 6 m s<sup>-1</sup> yields a deposition rate of approximately 0.7 mm hr<sup>-1</sup>. Data from a current study we are conducting indicates that 100 hours per year of cloud impaction at 2000 m in the Park is a conservative estimate. Annual deposition rates of H<sup>+</sup>, NH<sub>4</sub><sup>+</sup>, NO<sub>3</sub><sup>-</sup>, and SO<sub>4</sub><sup>2-</sup> calculated using the above information are summarized in Figure 6. Also depicted here are the annual average deposition rates for the same ions at the Lower Kaweah site contributed by rainfall (Stohlgren and Parsons, 1987). The estimated cloudwater deposition rates of all four ions are comparable to the measured rainfall inputs. While the estimates of cloudwater contributions to deposition in the region are crude, an attempt has been made to keep them on the conservative side. The potential importance of this deposition mechanism therefore seems clear. Further investigation is needed to refine the estimates made above and to lead to an increased understanding of the relative contributions of the different pathways leading

to acidic deposition in SNP.

## Conclusions

Cloudwater was sampled during the fall of 1985 and the spring of 1986 in Sequoia National Park in the southern Sierra Nevada Mountains of California. Concentrations of major species in the cloudwater vary widely both within one cloudwater impaction event and from one event to another. The pH values of the samples range from 4.4 to 5.7. The most acidic sample was not the sample with the highest concentrations of  $\text{NO}_3^-$  and  $\text{SO}_4^{2-}$ , indicating the importance of the ionic composition of the sample in determining its acidity. Organic acids are seen to be important contributors to the chemical composition of the cloudwater here.

The advance of cold fronts seems to lead to higher aerosol and gas phase loadings in the Park than would be seen under normal mountain - valley circulations, particularly during the night and morning hours. The arrival of these increased loadings prior to and during cloud impaction on the mountain slopes leads to higher cloudwater concentrations than would otherwise be expected. Estimates of annual deposition rates of  $\text{NO}_3^-$ ,  $\text{SO}_4^{2-}$ ,  $\text{NH}_4^+$ , and  $\text{H}^+$  due to cloudwater impaction are comparable to those measured from rainfall.

## Acknowledgments

We are grateful to the National Park Service, particularly the research staff at Sequoia National Park, for allowing us access to the sampling sites. This work was supported by a contract with the California Air Resources (Contract No. A4-075-32).

## References

B. C. Daube, Jr., R. C. Flagan and M. R. Hoffmann (1987a) Active Cloudwater Collector. United States Patent No. 4,697,462.

B. C. Daube, Jr., K. D. Kimball, P. A. Lamar and K. C. Weathers (1987b) Two new ground-level cloud water sampler designs which reduce rain contamination. *Atmos. Environ.* **21**, 893-900.

J. N. Galloway, G. E. Likens, W. C. Keene and J. M. Miller (1982) The composition of precipitation in remote areas of the world. *J. Geophys. Res.* **87**, 8771-8786.

D. J. Jacob, J. M. Waldman, M. Haghi, M. R. Hoffmann and R. C. Flagan (1985a) Instrument to collect fogwater for chemical analysis. *Rev. Sci. Instrum.* **56**, 1291-1293.

D. J. Jacob, J. M. Waldman, J. W. Munger and M. R. Hoffmann (1985b) Chemical composition of fogwater collected along the California coast. *Envir. Sci. Technol.* **19**, 730-736.

D. J. Jacob, J. W. Munger, J. M. Waldman and M. R. Hoffmann (1986a) The  $\text{H}_2\text{SO}_4\text{-HNO}_3\text{-NH}_3$  system at high humidities and in fogs: 1. Spatial and temporal patterns in the San Joaquin Valley of California. *J. Geophys. Res.* **91**, 1073-1088.

D. J. Jacob, J. M. Waldman, J. M. Munger and M. R. Hoffmann (1986b) The  $\text{H}_2\text{SO}_4\text{-HNO}_3\text{-NH}_3$  system at high humidities and in fogs: 2. Comparison of field data with thermodynamic calculations. *J. Geophys. Res.* **91**, 1089-1096.

D. J. Jacob, F. H. Shair, J. M. Waldman, J. W. Munger and M. R. Hoffmann (1987) Transport and oxidation of  $\text{SO}_2$  in a stagnant foggy valley. *Atmos. Environ.* **21**, 1305-1314.

A. H. Johnson and T. G. Siccama (1983) Acid deposition and forest decline. *Envir. Sci. Technol.* **17**, 294A-305A.

K. Kawamura and I. R. Kaplan (1984) Capillary gas chromatography determination of volatile organic acids in rain and fog samples. *Anal. Chem.* **56**, 1616-1620.

W. C. Keene, J. N. Galloway and J. D. Holden (1983) Measurement of weak organic acidity in precipitation from remote areas of the world. *J. Geophys. Res.* **87**, 8771-8786.

G. M. Lovett (1984) Rates and mechanisms of cloud water deposition to a subalpine balsam fir forest. *Atmos. Environ.* **18**, 361-371.

S. B. McLaughlin (1985) Effects of air pollution on forests: A critical review. *J. Air Poll. Control Assoc.* **35**, 512-534.

T. B. Smith, D. E. Lehrman, D. D. Reible and F. H. Shair (1981) The origin and fate of airborne pollutants within the San Joaquin Valley. Final Report to the California Air Resources Board, CARB-RR-81-15

L. Solorzano (1967) Determination of ammonia in natural waters by the phenol-hypochlorite method. *Limnol. Oceanogr.* **14**, 799-801.

T. J. Stohlgren and D. J. Parsons (1987) Variation of wet deposition chemistry in Sequoia National Park, California. *Atmos. Environ.* **21**, 1369-1374.

Table 1. Chemical Composition of Sequoia Cloudwater

Date	Time	pH	Na <sup>+</sup>	NH <sub>4</sub> <sup>+</sup>	Ca <sup>2+</sup>	Mg <sup>2+</sup>	Cl <sup>-</sup>	NO <sub>3</sub> <sup>-</sup>	SO <sub>4</sub> <sup>2-</sup>	-/+	L
10/21a	0927–1000	5.0	8	29	12	4	4	11	28	0.62	0.15
b	1000–1100	4.8	2	16	9	1	1	6	18	0.57	0.21
c	1100–1200	5.1	1	8	4	1	3	3	13	0.84	0.21
d	1200–1410	5.4	1	*	2	1	*	*	*	**	0.09
4/24a	1142–1305	5.0	680	1526	308	266	491	1140	665	0.82	0.03
b	1305–1405	4.8	157	594	58	47	129	354	269	0.86	0.16
c	1405–1505	4.8	231	900	72	66	192	537	396	0.88	0.04
5/03a	1200–1300	5.4	35	448	41	20	44	205	121	0.68	0.24
b	1300–1335	5.7	27	493	34	16	29	206	120	0.62	0.10
c	2015–2115	5.6	11	149	24	8	17	62	58	0.70	0.22
d	2115–2215	5.6	10	93	22	8	18	44	54	0.85	0.06
5/06a	1200–1250	4.4	44	132	18	***	55	94	83	1.00	0.22

\* below 1 μN, \*\* concentrations too low to make accurate calculation, \*\*\* not measured, ion balance calculated for measured species.

Table 2. Organic Anions in Sequoia Cloudwater

Sample	pH	Formate	Acetate	Pyruvate <sup>*</sup>	Lactate <sup>*</sup>	Propionate <sup>*</sup>	-/+
		←————— $\mu\text{N}$ —————→					
4/24c	4.8	68.5	13.8	11.5	0	5.2	0.95
5/03b	5.7	106.7	72.8	0	15.4	7.2	0.97
c	5.6	31.0	18.6	0	0	2.5	0.97
d	5.6	19.6	8.5	0	4.6	0	1.10

\* Identification of this species is tentative.

## Captions

- Figure 1. Map of Sequoia National Park showing the two sites used for cloudwater sampling. The inset shows the location of the Park relative to the San Joaquin Valley and the rest of California.
- Figure 2. The Caltech Active Strand Collector (CASC). The length of the collector is 0.91 m (36 in.). Total sampled flow is 21.1 m<sup>3</sup>/min.
- Table 1. Chemical composition of the cloudwater samples collected in Sequoia National Park during the fall of 1985 and the spring of 1986. Ion balances (-/+ ) are given for the ions listed. Liquid water content values are estimates based on the cloudwater collection rate and the theoretical collection efficiency of the Caltech Active Strand Collector (CASC).
- Figure 3. Cloudwater loadings of ammonium, nitrate, and sulfate in samples collected during the fall of 1985 and the spring of 1986 in Sequoia National Park.
- Table 2. Concentrations of carboxylate anions in cloudwater samples from Sequoia National Park collected during the spring of 1986. The ion balance (-/+ ) shown here includes these carboxylate anions as well as the inorganic ions listed for these samples in Table 1.
- Figure 4. Aerosol Loadings of sulfate, nitrate, ammonium, and chloride measured at the Lower Kaweah research site in Sequoia National Park during the period 5/1-5/6/87. The arrows on the figures denote the times at which clouds were observed to begin impacting the hillside at the site.
- Figure 5. Typical behavior of warm and cold air masses during the advance of a cold front. In the figure the cold air mass is moving toward the right, wedging itself under the less dense warm air mass.
- Figure 6. Annual deposition of major ions to the Lower Kaweah research site in Sequoia National Park by rainwater (measured, Stohlgren and Parsons, 1987) and cloudwater (estimated). Estimates of cloudwater deposition are based on a cloudwater deposition rate of 0.7 mm/hr for 100 hr/yr (see the text for details). The average chemical composition of the cloudwater was taken as the volume-weighted average composition of the cloudwater sampled in the Park during the fall of 1985 and the spring of 1986.

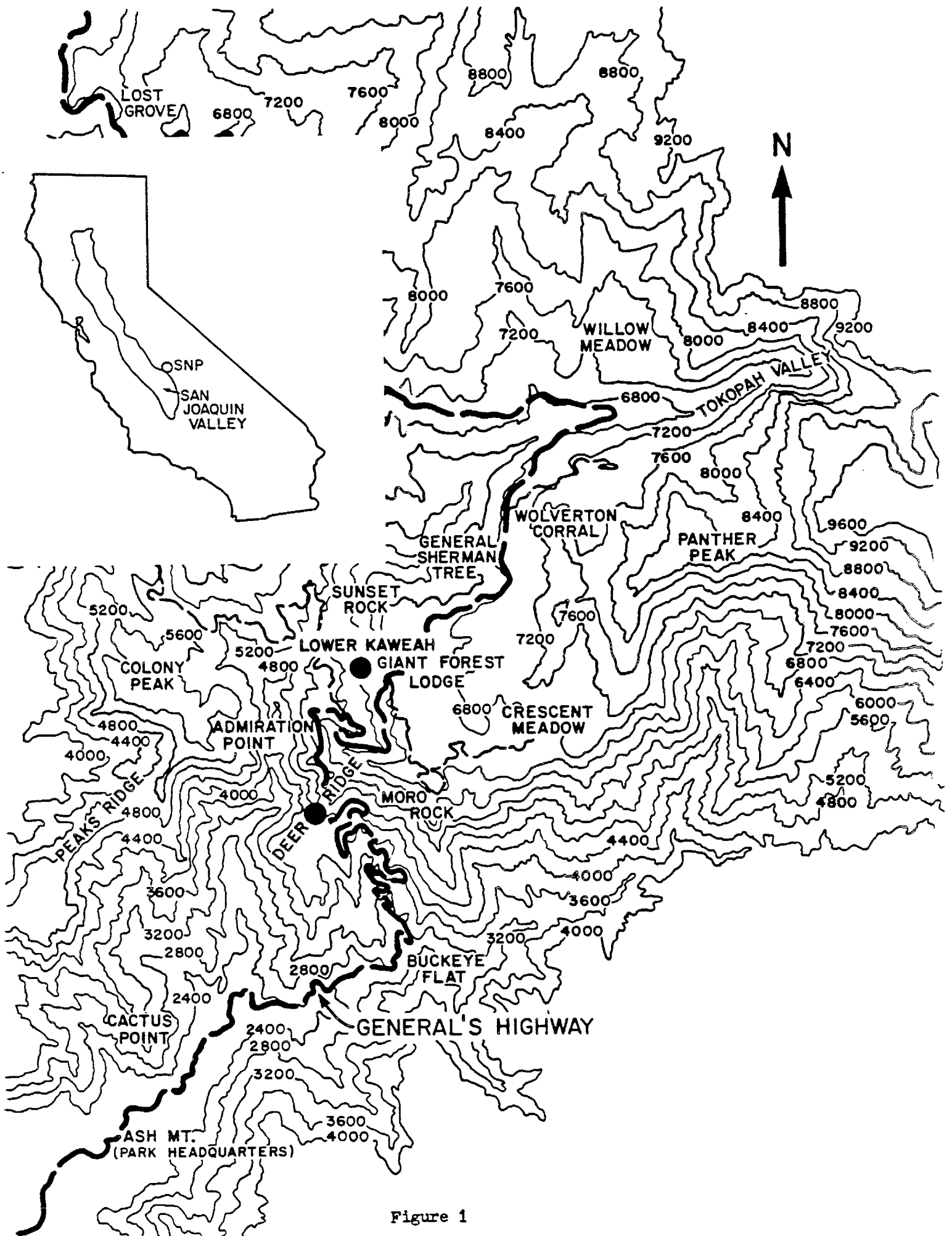


Figure 1

# Active Strand Fogwater Collector

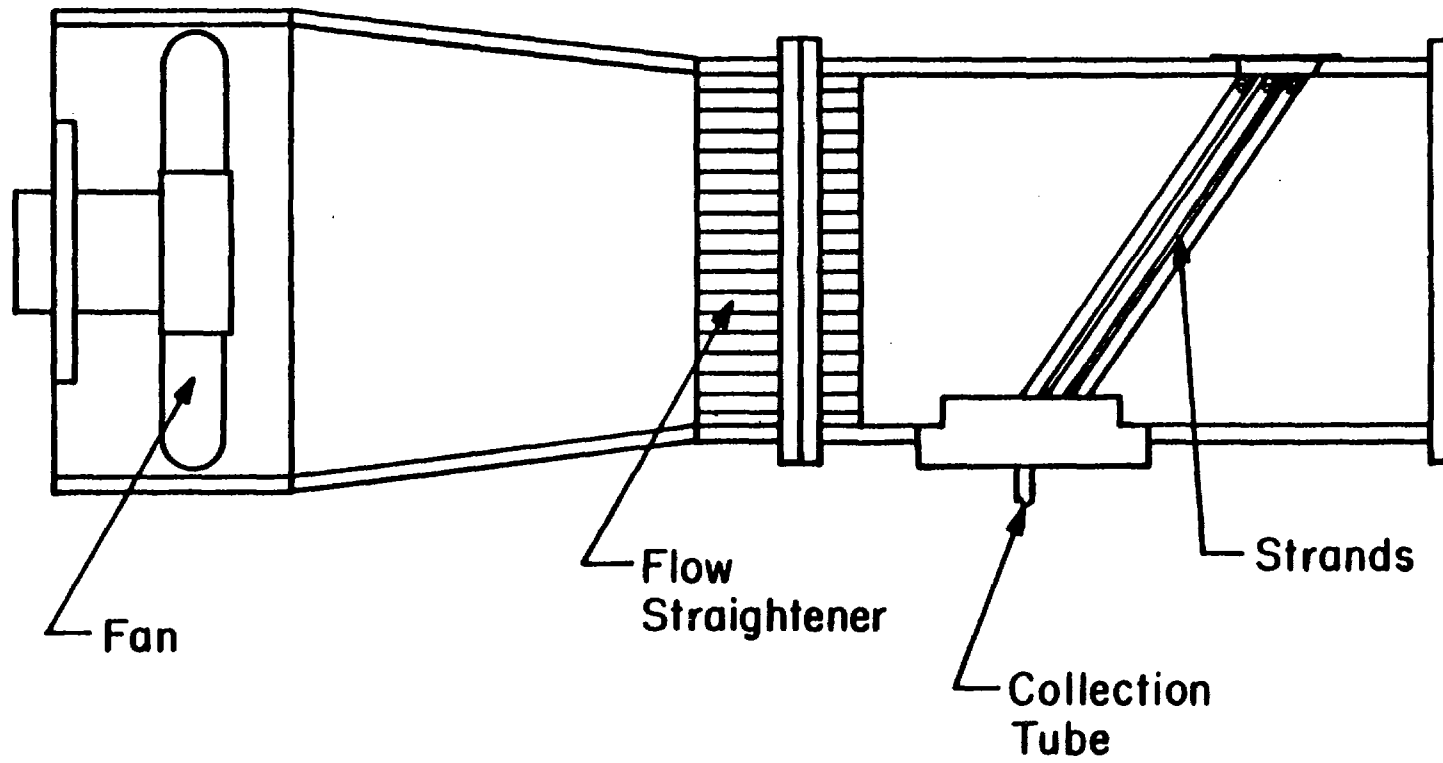


Figure 2

# SEQUOIA CLOUDWATER MAJOR IONS

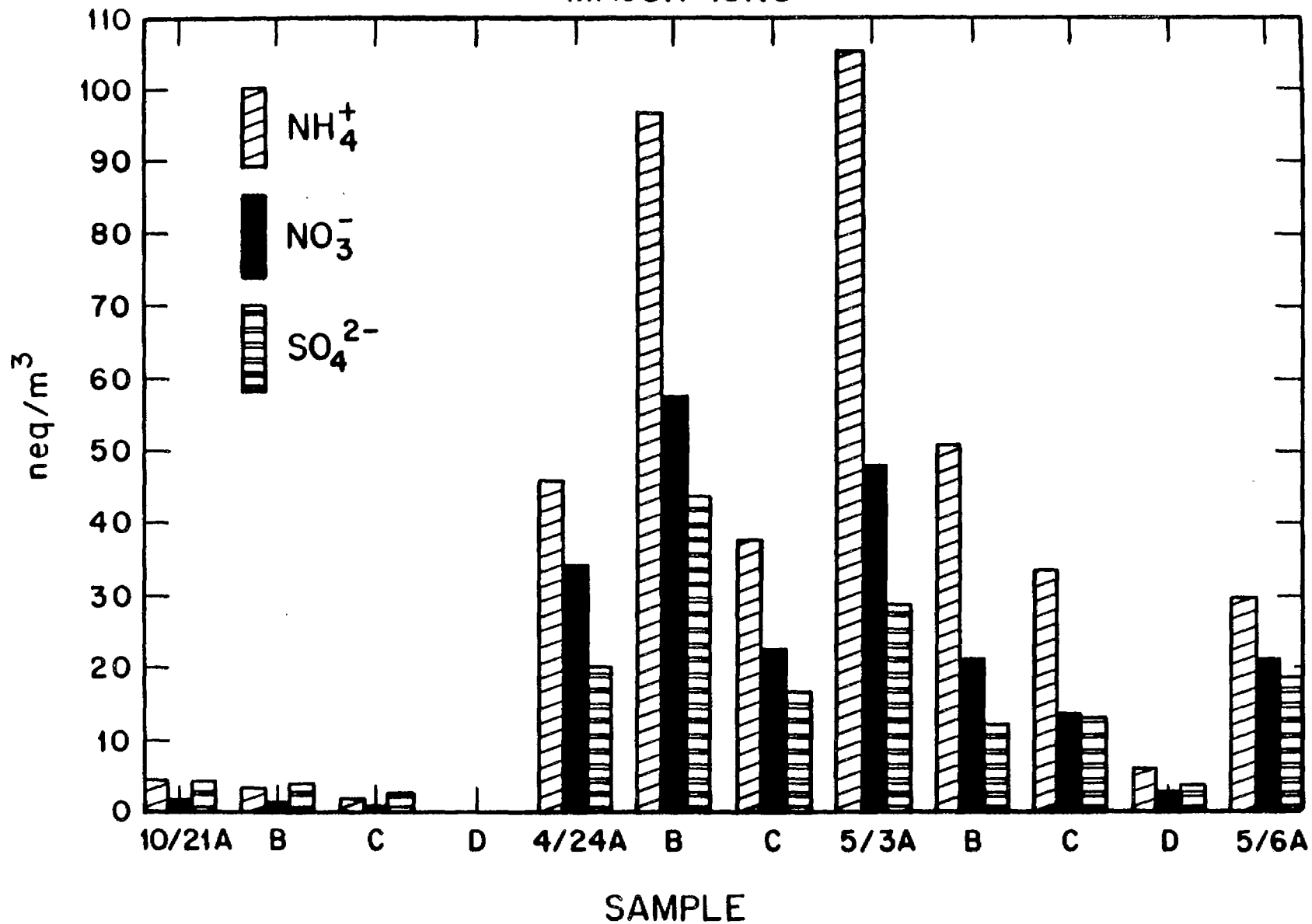


Figure 3

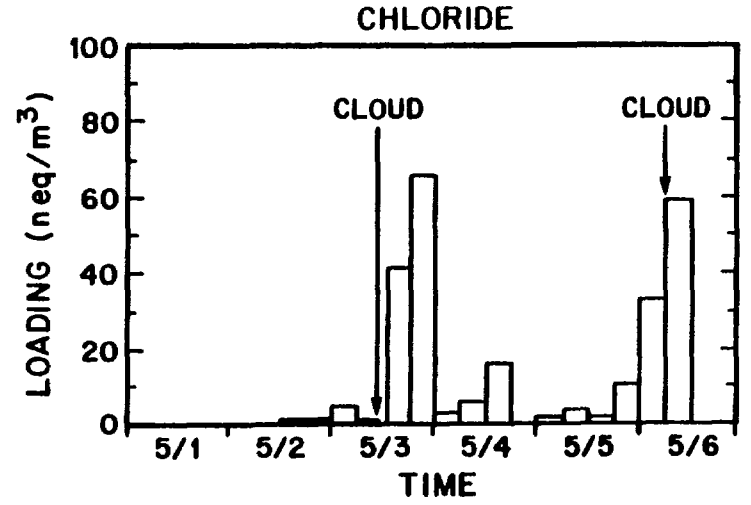
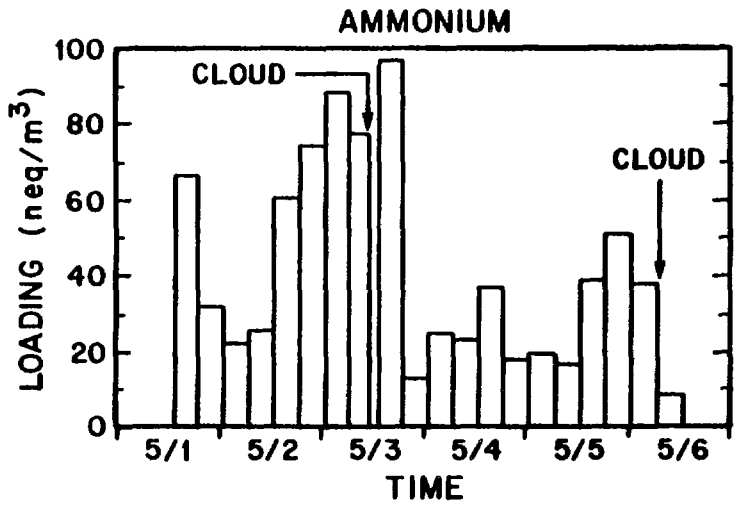
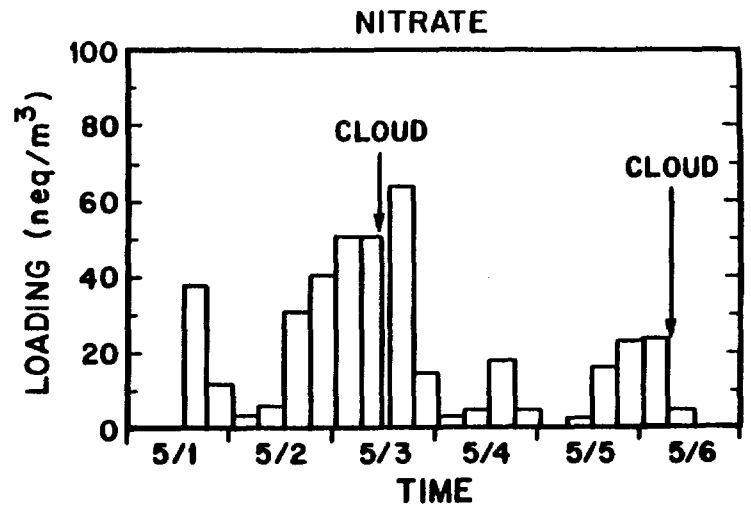
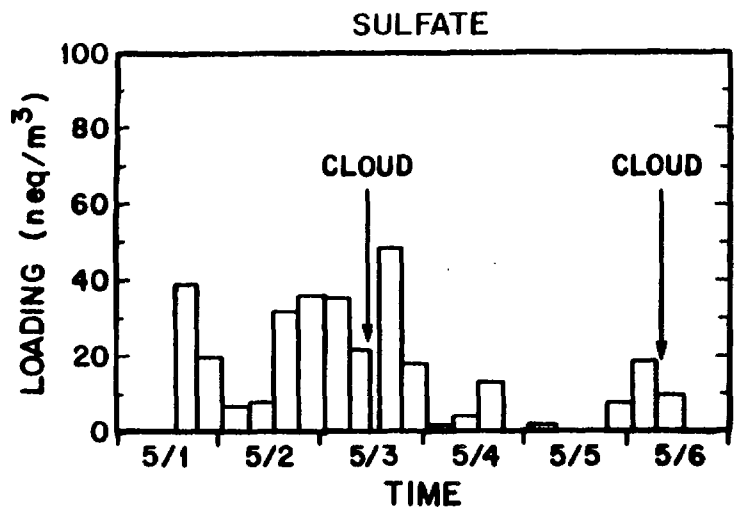


Figure 4

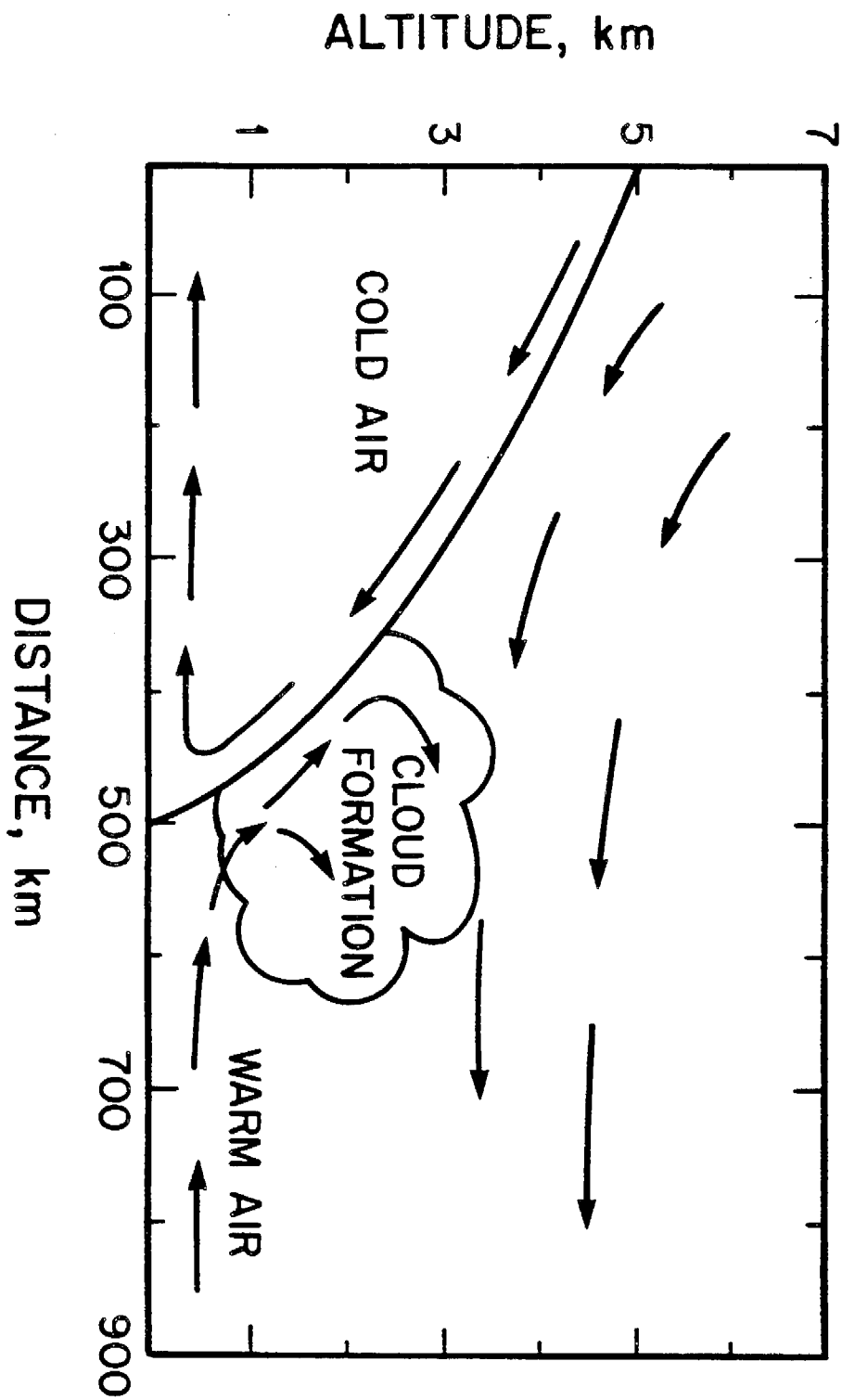


Figure 5

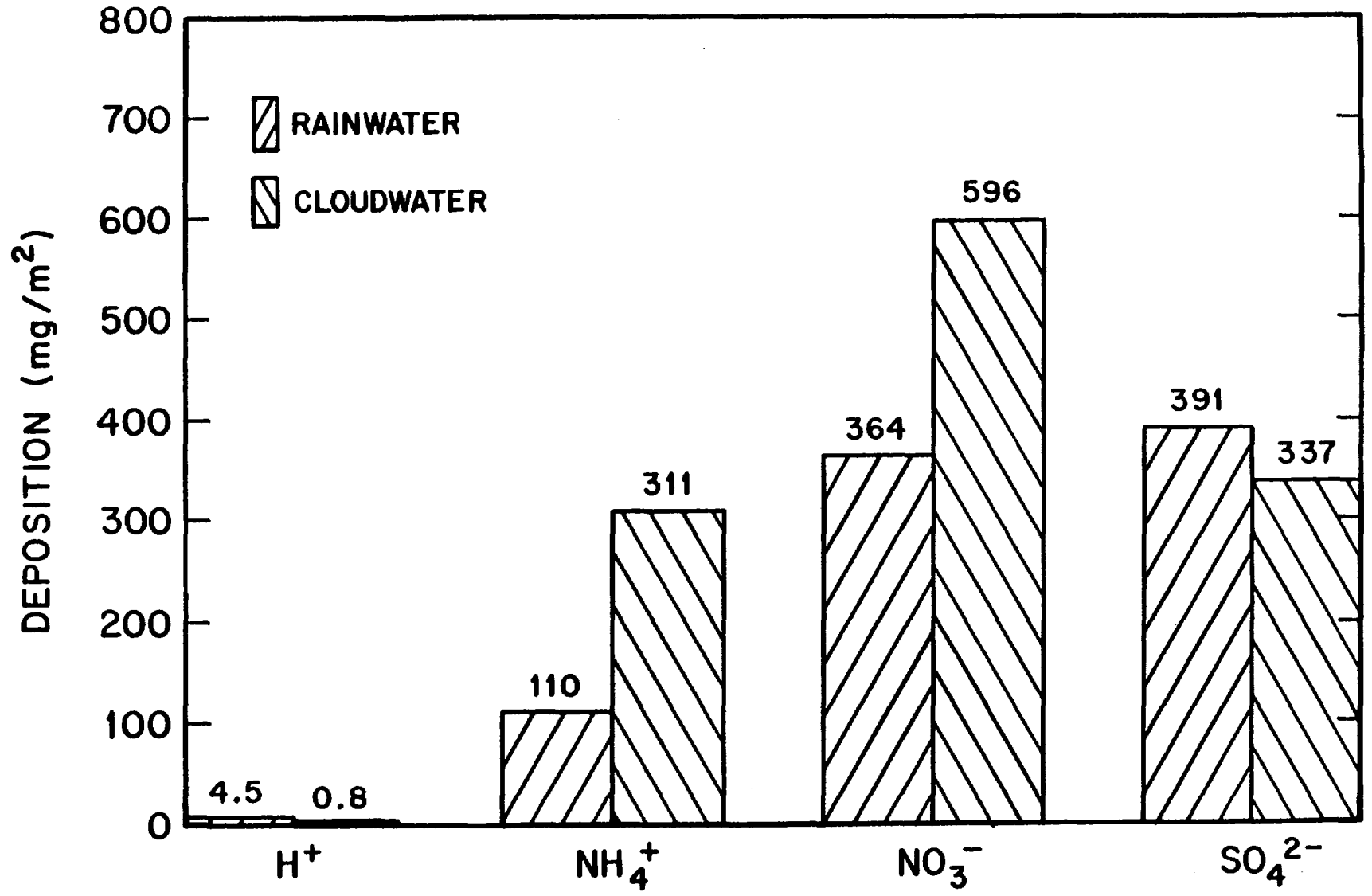


Figure 6



Reprint Series  
17 January 1986, Volume 231, pp. 247-249

**SCIENCE**

CHAPTER 11

**Identification of Hydroxymethanesulfonate in  
Fog Water**

J. WILLIAM MUNGER, CHRISTINE TILLER, MICHAEL R. HOFFMANN\*

# Identification of Hydroxymethanesulfonate in Fog Water

J. WILLIAM MUNGER, CHRISTINE TILLER, MICHAEL R. HOFFMANN\*

Previous studies have suggested that hydroxymethanesulfonate ion (HMSA) can be an important species in fog and cloud water. Formation of HMSA explains observed excesses of sulfur in the S(IV) state (+4 oxidation state) and formaldehyde (CH<sub>2</sub>O) in fogs and clouds. HMSA was determined in fog water by a novel ion-pairing chromatographic technique. Concentrations in samples collected in Bakersfield, California, within 5 kilometers of major sources of sulfur dioxide (SO<sub>2</sub>), were as high as 300 micromoles per liter. Total CH<sub>2</sub>O and S(IV) concentrations, which were measured independently, ranged from 10 to 200 and 5 to more than 300 micromoles per liter, respectively. Concentrations of CH<sub>2</sub>O, S(IV), and HMSA at Buttonwillow, California, which is 15 kilometers from the nearest source of SO<sub>2</sub>, were less than those at Bakersfield but not absent. These data confirm that HMSA forms in atmospheric water droplets and can reach appreciable concentrations. HMSA represents an important source of acidity for water droplets and may also play a role in long-distance transport and transformation of SO<sub>2</sub>.

**H**YDROXYMETHANESULFONATE, THE HSO<sub>3</sub><sup>-</sup> adduct of CH<sub>2</sub>O, has been postulated as an important S(IV) species in fog and cloud water (1). We define SO<sub>2(aq)</sub> as the sum of SO<sub>2</sub> · H<sub>2</sub>O + HSO<sub>3</sub><sup>-</sup> + SO<sub>3</sub><sup>2-</sup>; we define S(IV) as the sum of SO<sub>2(aq)</sub> plus all other species with sulfur in the +4 oxidation state (that is, aldehyde adducts, HORHSO<sub>3</sub><sup>-</sup>, and metal complexes, (Me)<sub>n</sub>(SO<sub>3</sub>)<sub>n</sub><sup>m-2m</sup>). This sum is identical to the measured concentration of S(IV), [S(IV)]. The formation of hydroxymethanesulfonate (HMSA) allows an apparent excess of S(IV) and CH<sub>2</sub>O compared to the amounts present in Henry's law equilibrium to exist in the droplet phase. Because HMSA is a strong acid, its formation will acidify droplets without S(IV) oxidation. Furthermore, the formation of HMSA allows S(IV) to coexist with oxidants such as H<sub>2</sub>O<sub>2</sub> and O<sub>3</sub> (2-4).

The thermodynamics and kinetics of reaction between CH<sub>2</sub>O and dissolved SO<sub>2</sub> to form HMSA have been determined. Kerp (5), Donally (6), Deister *et al.* (7), and Kok *et al.* (4) have all reported values near 10<sup>7</sup> M<sup>-1</sup> for the equilibrium constant (defined by  $K = [\text{HMSA}]/[\text{HSO}_3^-][\text{CH}_2\text{O}]$ ). The stability of the CH<sub>2</sub>O:HSO<sub>3</sub><sup>-</sup> adduct will be at a maximum in the pH range 3 to 5, where HSO<sub>3</sub><sup>-</sup> is the dominant form of SO<sub>2(aq)</sub>. The rate at which HMSA forms in a droplet can be calculated from the rate constants determined by Boyce and Hoffmann (8). For CH<sub>2</sub>O and SO<sub>2</sub> partial pressures of 1 × 10<sup>-9</sup> and 5 × 10<sup>-9</sup> atm at pH 3, the HMSA formation rate is 1.6 nM hour<sup>-1</sup>. It increases by about a factor of 100 for each

unit increase in pH to 0.1M hour<sup>-1</sup> at pH 7. The formation rate increases linearly with gas-phase concentration; lower temperatures also increase the formation rate somewhat because of increased gas solubility. The rate of HMSA decomposition increases with pH (4, 7); this can be expressed as  $R = k_d[\text{HMSA}][\text{OH}^-]$ . The value of  $k_d$  derived from the data of Kok *et al.* (4) and Deister *et al.* (7) between pH 4 and 5.6 is 3.6 × 10<sup>3</sup> M<sup>-1</sup> sec<sup>-1</sup>. The characteristic time for HMSA dissociation (time for a 1/e decrease in concentration) evaluated from this expression decreases from 579 to 25

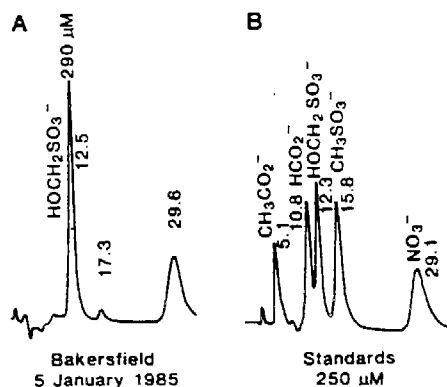


Fig. 1. Representative chromatograms for (A) a sample of fog water collected in Bakersfield, California, and (B) a solution containing formate, acetate, HMSA, methanesulfonate, and nitrate. The numbers indicate retention times in minutes. Neither methanesulfonate nor hydroxyethanesulfonate was present in the fog water samples. The peak at 17.3 minutes was present in many samples.

hours as pH varies from 4 to 5.6. Dynamic models of fog and cloud-water chemistry (9) indicate that HMSA could be the major S(IV) species in droplets when pH exceeds 5. Appreciable [S(IV)] would form in the droplet phase immediately after condensation. However, the suggestion by Richards *et al.* (2) that the presence of CH<sub>2</sub>O prevents oxidation of S(IV) by H<sub>2</sub>O<sub>2</sub> is not substantiated by model calculations (9) or experiments (3, 4). In an open system, SO<sub>2</sub> will continually dissolve in the droplet and be available as SO<sub>2(aq)</sub> to react with H<sub>2</sub>O<sub>2</sub>. High [HMSA] may be found in more acidic environments if HMSA is formed before droplet acidification. Prior formation is also indicated by the coexistence of HMSA and H<sub>2</sub>O<sub>2</sub>.

An interesting feature of HMSA chemistry is that the conditions most conducive to the production of HMSA are not suitable for its preservation. It forms most rapidly above pH 5 but will not be preserved unless the droplets are subsequently acidified. High concentrations of oxidant will compete for SO<sub>2(aq)</sub>, but, once HMSA forms, it is fairly resistant to oxidation by H<sub>2</sub>O<sub>2</sub> and O<sub>3</sub> (3, 4). We suggest that a likely environment for rapid HMSA formation is in SO<sub>2</sub> source plumes, where concentrations of the precursor species are high, pH is near neutral, and oxidant concentrations are low. As the plume is diluted, equilibrium between HMSA and its precursors may not be maintained because of the slow dissociation kinetics, especially if continued SO<sub>2(aq)</sub> oxidation generates additional acidity in the droplet. Equilibrium will be maintained only between gaseous SO<sub>2</sub> and SO<sub>2(aq)</sub>.

The presence of HMSA in a variety of environments is indicated by circumstantial evidence. Analyses of Los Angeles fog and cloud water, which had pH in the range 2 to 4, indicated that total S(IV) and CH<sub>2</sub>O were supersaturated with respect to Henry's law equilibrium with SO<sub>2(g)</sub> and CH<sub>2</sub>O<sub>(g)</sub> (1, 2). Similar observations were made in the San Joaquin Valley (1). Warneck *et al.* (10) observed that [CH<sub>2</sub>O] in aerosol over Germany was supersaturated with respect to the gas phase and postulated that HMSA was present. Snider and Dawson (11) suggested that enhanced concentrations of carbonyls in Arizona rainwater compared to the gas phase may indicate aqueous-phase production of carbonyl. Their observations may also be accounted for by the formation of sulfonic acids. No analyses were per-

Environmental Engineering Science, W. M. Keck Laboratories, California Institute of Technology, Pasadena 91125.

\*To whom correspondence should be addressed.

formed in these earlier studies to confirm the presence of HMSA.

The southern San Joaquin Valley of California offers an amenable environment for studying aqueous-phase atmospheric chemistry. Oil field operations supply a major source of SO<sub>2</sub>, hydrocarbons, and NO<sub>x</sub>, while extensive agricultural activity produces large amounts of NH<sub>3</sub>; thus pH is maintained near neutral in aerosol and fog droplets. During the winter the valley is frequently capped by a temperature inversion, leading to persistent atmospheric stagnation with widespread fogs or low clouds (12). This combination of high concentrations of precursors, humid conditions, sufficient NH<sub>3</sub> to neutralize acidity, and stagnation is conducive to the formation of HMSA.

In earlier studies of fog in the San Joaquin Valley during the winters of 1982–83 and 1983–84 (1, 12) we have observed [S(IV)] up to 3 × 10<sup>-3</sup>M and [CH<sub>2</sub>O] up to 7 × 10<sup>-4</sup>M. These values were far in excess of the Henry's law equilibrium for dissolution of SO<sub>2</sub> at the ambient levels of 0 to 50 parts per billion (1 ppb = 1 × 10<sup>-9</sup> atm).

During December 1984 and January 1985 we sampled fog in Bakersfield and Buttonwillow, California; the sampling sites (13) and fog collection procedure (14) have been described. Immediately after collection, the pH was determined with a combination electrode and individual aliquots were preserved for later determination of [S(IV)] and [CH<sub>2</sub>O] (15, 16). The analytical procedures are designed to measure total species. However, our results suggest that the efficiency of the Nash method for CH<sub>2</sub>O determination is less than 100 percent when HMSA is present. HMSA was determined by ion-pairing chromatography and identi-

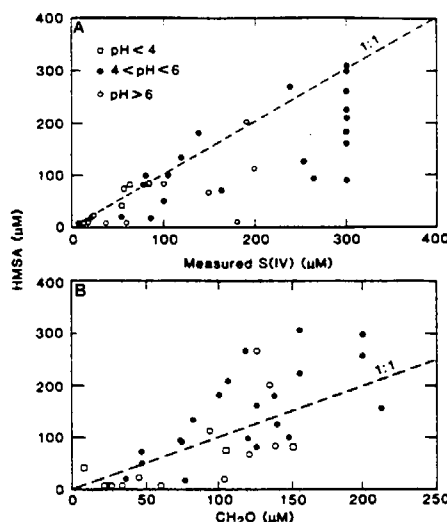


Fig. 2. (A) [HMSA] at Bakersfield plotted against measured [S(IV)]; [S(IV)] greater than 300 μM saturated the reagents used. Points plotted at 300 μM had [S(IV)] in excess of the saturation level. (B) [HMSA] at Bakersfield plotted against measured [CH<sub>2</sub>O].

fied by retention time (17). Standards containing hydroxyethanesulfonic acid and methanesulfonic acid were also analyzed to determine their retention times. A representative chromatogram is given in Fig. 1. The difference between standard and sample retention times was less than 2 percent. We recognize that identification based on retention time is not definitive; however, other species such as formate and acetate, likely to be present in fog water, elute separately. The instability of HMSA and the difficulty of obtaining large sample volumes preclude the use of mass spectrometry for confirmation. In samples with high pH, some of the HMSA could have decomposed between sampling and analysis; the results presented

here should be considered lower bounds for [HMSA].

Table 1 presents the volume-weighted mean and ranges of [S(IV)], [CH<sub>2</sub>O], and [HMSA] and pH for each fog event sampled. Figure 2A shows the apparently linear relation between HMSA and S(IV) at Bakersfield (r<sup>2</sup> = 0.65). The residual variance is due to the presence of free SO<sub>2(aq)</sub> in high pH samples and possibly some HMSA decomposition before analysis. The highest [HMSA] was found in samples with moderate pH (5.5 to 6.5). Samples with higher or lower pH had lower [HMSA]. Low pH will retard the formation of adduct, while high pH will prevent its preservation in the atmosphere and in sample bottles.

There is also an apparently linear relation between [HMSA] and [CH<sub>2</sub>O] (r<sup>2</sup> = 0.54) (Fig. 2B). The appearance of excess HMSA as compared to total CH<sub>2</sub>O in many samples indicates that I<sub>2</sub>, added in order to prevent the interference of S(IV) in CH<sub>2</sub>O analysis, is not totally effective. Appreciable concentrations of free CH<sub>2</sub>O should exist in the droplet because of the high effective Henry's law constant.

During the sampling program, [SO<sub>2</sub>] was always less than 30 ppb and usually less than 10 ppb (18). This partial pressure of SO<sub>2</sub> was sufficient to account for all the S(IV) observed during most of the sampling periods when fog water pH values varied from 5 to 7. Nevertheless, HMSA was an important fraction of the S(IV) measured. In the two fog events that were in the low pH domain, the equilibrium of SO<sub>2(aq)</sub> with ambient SO<sub>2(g)</sub> was not sufficient to account for all the measured S(IV). During an 8-hour period in the middle of the fog event on 5 January 1985, when the pH varied from 5.5 to 4.8, the measured [S(IV)] was continually above the upper detection limit (250 μM). The concentration of free SO<sub>2(aq)</sub>, as calculated from the sample pH and SO<sub>2</sub> partial pressure = 10 ppb (an upper limit for the period), was less than half the measured [S(IV)]. In terms of the Henry's law dissolution, S(IV) was supersaturated by a factor of 10 during the fog event of 19 January. The pH during this event was 3.7 to 4.9; [HMSA] and [S(IV)] were about 60 to 80 μM, with higher values at the beginning and end of the fog event when the liquid water content was lower. [CH<sub>2</sub>O] during this event was generally higher than [HMSA], suggesting the presence of free CH<sub>2</sub>O.

At Buttonwillow, [S(IV)] and [CH<sub>2</sub>O] were considerably less than at Bakersfield. This is consistent with the greater distance between major pollution sources and Buttonwillow as compared to Bakersfield; [SO<sub>4</sub><sup>2-</sup>] and [NO<sub>3</sub><sup>-</sup>] were lower at Button-

Table 1. Volume-weighted average of concentrations for various species in fog water samples.

Date*	Sample pH	Concentration of species (μM)			n†
		S(IV)	CH <sub>2</sub> O	HMSA	
<i>Bakersfield, California</i>					
12/28/84	5.9	150	98	140	6
1/3/85	5.2	130	78	76	10
1/4/85	6.9	18	32	0	5
1/5/85	4.6	≥230	110	120	13
1/8/85	7.4	16	27	0	1
1/10/85	6.1	180	‡		2
1/14/85	5.9	150	120	65	3
1/19/85	4.1	89	150	79	10
1/20/85	3.0	84	160		2
<i>Buttonwillow, California</i>					
1/3/85	5.1	36	55		6
1/4/85	6.2	9	28		7
1/5/85	6.1	22	33	0	11

\*The date given is that of the morning on which the fog event ended. †Number of consecutive samples collected over the course of each fog event. The sampling period was generally 1 hour. ‡Not analyzed because of insufficient sample volume.

willow as well (13). The pH was usually in the range 5.5 to 7, although two samples had pH < 5 with [S(IV)] less than 10  $\mu\text{M}$ . HMSA was not determined in all the samples from Buttonwillow, but little or none was observed in the samples that were analyzed. As noted above, the lifetime of HMSA at pH 5.6 is 25 hours and should decrease further as pH rises. Thus HMSA may decompose during advection from SO<sub>2</sub> source areas to Buttonwillow. More HMSA and S(IV) is observed at Bakersfield because of its proximity to the oil fields in Oildale. If the atmosphere in the valley were not buffered by NH<sub>3</sub> emissions, then HMSA would have a longer residence time.

The results of this study support the hypothesis that HMSA may be an important species in fog and cloud water. The pattern of [HMSA] in the fog samples is consistent with the formation of HMSA during favorable conditions of high SO<sub>2</sub> and intermediate pH and preservation by subsequent acidification. Over the pH range of 5.5 to 7, which is typical of the samples from the San Joaquin Valley, the chemical lifetime of HMSA is shorter than the time for atmospheric transport within the valley (19). Appreciable [HMSA] or [S(IV)] was not observed at Buttonwillow. Observations of excess [S(IV)] and [CH<sub>2</sub>O] in fog and cloud water from the more acidic Los Angeles basin indicate that other conditions may also allow the formation of HMSA.

#### REFERENCES AND NOTES

- J. W. Munger, D. J. Jacob, M. R. Hoffmann, *J. Atmos. Chem.* **1**, 335 (1984); J. W. Munger, D. J. Jacob, J. M. Waldman, M. R. Hoffmann, *J. Geophys. Res.* **88**, 5109 (1983).
- L. W. Richards *et al.*, *Atmos. Environ.* **17**, 911 (1983).
- J. A. McArdle and M. R. Hoffmann, *J. Phys. Chem.* **87**, 5425 (1983); J. Hoigne, H. Bader, W. R. Haag, J. Staehelin, *Water Res.* **19**, 993 (1985).
- G. L. Kok, S. N. Gitlin, A. L. Lazrus, *J. Geophys. Res.*, in press.
- W. Kerp, *Arch. Kreis. Gesundh.* **421**, 180 (1904).
- L. H. Donally, *Ind. Eng. Chem. Anal. Ed.* **5**, 91 (1933).
- U. Deister, R. Neeb, G. Helas, P. Warneck, *J. Phys. Chem.*, in press.
- The initial formation of HMSA can be expressed in terms of gas-phase concentrations as
 
$$\frac{d[\text{HMSA}]}{dt} = H_1 H_t P_{\text{SO}_2} P_{\text{CH}_2\text{O}} \frac{1}{(1 + K_h)} \times \left( \frac{k_1 K_{a1}}{[\text{H}^+]} + \frac{k_2 K_{a1} K_{a2}}{[\text{H}^+]^2} \right)$$
- Values for the Henry's law constants for SO<sub>2</sub> and CH<sub>2</sub>O at 298 K are  $H_1 = 1.245 \text{M atm}^{-1}$  and  $H_t = 6.3 \times 10^3 \text{M atm}^{-1}$  (in terms of hydrated CH<sub>2</sub>O).  $P_i$  is the partial pressure of species  $i$ . The acidity constants for S(IV) are  $K_{a1} = 1.29 \times 10^{-2} \text{M}$  and  $K_{a2} = 6.01 \times 10^{-8} \text{M}$ . The hydration constant for CH<sub>2</sub>O is  $K_h = 2.53 \times 10^3$ . The original references and enthalpy data are given by Munger *et al.* (1). The rate constants are  $k_1 = 7.9 \times 10^2 \text{M}^{-1} \text{sec}^{-1}$  (activation energy = 5.9 kcal mol<sup>-1</sup>);  $k_2 = 2.48 \times 10^2 \text{M} \text{sec}^{-1}$  (activation energy = 4.8 kcal mol<sup>-1</sup>) [S. D. Boyce and M. R. Hoffmann, *J. Phys. Chem.* **88**, 4740 (1984)].
- D. J. Jacob and M. R. Hoffmann, *J. Geophys. Res.* **88**, 6611 (1983); Y. G. Adewuyi, S.-Y. Cho, R.-P. Tsay, G. R. Carmichael, *Atmos. Environ.* **18**, 2413 (1984).
- P. Warneck, W. Klippel, G. K. Moortgat, *Ber. Bunsenges. Phys. Chem.* **82**, 1136 (1978); W. Klippel and P. Warneck, *Atmos. Environ.* **14**, 809 (1980).
- J. R. Snider and G. A. Dawson, *J. Geophys. Res.* **90**, 3797 (1985).
- D. J. Jacob, J. M. Waldman, J. W. Munger, M. R. Hoffmann, *Tellus* **36B**, 272 (1984); D. J. Jacob, thesis, California Institute of Technology, Pasadena (1985).
- During December 1984 and January 1985 fog water was collected at a site adjacent to the Bakersfield Airport and in Buttonwillow. Sampling commenced at the onset of fog formation and continued until the fog dissipated. Major oil fields are located within 5 km of the Bakersfield Airport in the northeast quadrant. Buttonwillow is located near the center of the valley, at least 15 km southeast of oil fields on the west side of the valley. Complete results and site descriptions are given by J. M. Waldman [thesis, California Institute of Technology, Pasadena (1985)].
- The collector is described in D. J. Jacob, R.-F. T. Wang, R. C. Flagan, *Environ. Sci. Technol.* **18**, 827 (1984).
- Total S(IV) was determined in an aliquot of sample that was preserved with CH<sub>2</sub>O immediately after collection. Analysis was by the pararosaniline method [P. K. Dasgupta, K. DeCesare, J. C. Ullrey, *Anal. Chem.* **52**, 1912 (1980); P. K. Dasgupta, *ibid.* **53**, 2084 (1981)]. Standards made from Na<sub>2</sub>SO<sub>3</sub> or NaCH<sub>2</sub>OHSO<sub>3</sub> gave identical results. Analysis was complete within a week of collection; no loss of S(IV) was observed in preserved aliquots or stan-
- dard solutions. Analytical error was within 5 percent.
- Total CH<sub>2</sub>O was determined in a separate aliquot of sample to which Nash reagent was added immediately after collection [T. Nash, *Biochem. J.* **55**, 416 (1953)]. Prior to color determination, I<sub>2</sub> was added to destroy the S(IV) in the sample [R. V. Smith and P. W. Erhardt, *Anal. Chem.* **47**, 2462 (1975)]. Recovery of NaCH<sub>2</sub>OHSO<sub>3</sub> standards was 90 to 100 percent compared to CH<sub>2</sub>O standards. Minimal losses of CH<sub>2</sub>O were observed during storage. Analytical error was less than 5 percent.
- HMSA was determined by ion-pairing chromatography on a polystyrene divinylbenzene column (Dionex MPIC) followed by a suppressor column containing cation-exchange resin in the Ag<sup>+</sup> form (Dionex ISR), and a conductivity detector. The mobile phase contained 2 mM tetrabutylammonium chloride, 5 percent (by volume) CH<sub>3</sub>OH, and  $2 \times 10^{-3} \text{M}$  HCl. Analytical error was less than 5 percent. Samples to be analyzed for sulfonic acids were refrigerated, but no preservatives were used.
- California Air Resources Board, unpublished data.
- D. D. Reible, F. H. Shair, T. B. Smith, D. E. Lehman, *Atmos. Environ.*, in press.
- Supported by the California Air Resources Board (contract AA-075-32) and a summer undergraduate research fellowship from California Institute of Technology (C.T.). We thank D. Jacob, J. Waldman, D. Bucholz, and S. Hawes for their contributions to this work.

30 September 1985; accepted 30 October 1985